2-14-2014

NEW GENERATION POLYMER CONCRETE INCORPORATING CARBON NANOTUBES

Sherif Daghash

SHERIF M. DAGHASH
Candidate

CIVIL ENGINEERING
Department

This thesis is approved, and it is acceptable in quality and form for publication:

Approved by the Thesis Committee:

Dr. Mahmoud Reda Taha , Chairperson

Dr. Arup Maji

Dr. John Stormont

Dr. David Fowler

NEW GENERATION POLYMER CONCRETE INCORPORATING CARBON NANOTUBES

by

SHERIF M. DAGHASH

B.S. CIVIL ENGINEERING, ALEXANDRIA UNIVERSITY, EGYPT, 2009

THESIS

Submitted in Partial Fulfillment of the

Requirements for the Degree of

Master of Science

Civil Engineering

The University of New Mexico

Albuquerque, New Mexico

December, 2013

NEW GENERATION POLYMER CONCRETE INCORPORATING CARBON NANOTUBES

By

Sherif M. Daghash

B.S., Civil Engineering, Alexandria University, Egypt, 2009

M.S., Civil Engineering, University of New Mexico, USA, 2013

ABSTRACT

Polymer Concrete (PC) is one of three types of polymers in concrete that was introduced in the 1950s and has had many successful civil engineering applications. PC is recognized in the industry as a mix of aggregate and polymer resin with no Portland cement. PC has been favoured over conventional Portland cement concrete when special characteristics such as low permeability, high adhesion, and/or high durability for service in aggressive (e.g. chemical) environments are required.

In this research, a new generation of PC incorporating Multi-Walled Carbon Nano-Tubes (MWCNTs) was produced and its mechanical properties were investigated. Four mixes of PC with 0.0 (neat), 0.5, 1.0, and 1.5% MWCNTs, respectively, were prepared using low modulus polysulfide epoxy mixed with fine and coarse aggregate, or fine aggregate only. PC incorporated fine and coarse aggregate in the mixes, while PC overlays incorporated fine aggregate only. Test protocols included investigating the mechanical properties of PC, examining the bond strength of the PC overlays with steel and microstructural characterization of epoxy-MWCNTs nanocomposite.

Investigation of the static mechanical properties of PC included identifying the effect of MWCNTs on compressive strength, flexural strength, and shear strength, as well as creep behavior of PC under axial sustained loads. We also examined the dynamic response of PC using Charpy impact and low-velocity impact tests. Furthermore, the bond strength between steel plates and PC overlays was evaluated. This included performing the pull-off and slant shear tests. Moreover, four-point bending fatigue test was performed to examine the fatigue strength of PC overlays under cyclic traffic loads. Finally, microstructural and thermal stability of epoxy incorporating MWCNTs was evaluated using Scanning Electron Microscope (SEM), Fourier Transform Infrared Spectroscopy (FTIR), Thermal Gravimetric Analysis (TGA), and Differential Scanning Calorimetry (DSC). The test results emphasized that MWCNTs altered the microstructure of the epoxy and increased the crosslinking between epoxy groups significantly. This lead to improving the mechanical properties of PC and PC overlays. Significant improvements were also observed in bond strength with steel, impact strength and fatigue strength. It is believed that using MWCNTs can produce a new generation of PC with much improved performance for bridge deck overlays and for panels used for blast protection.

DEDICATION

I dedicate this thesis to my parents, Azza Zalat and Magdy Daghash, and to my sister Engy. Thank you for your support.

ACKNOWLEDMENTS

No words are enough to thank my advisor Dr. Mahmoud Reda Taha for his guidance, encouragement, patience and trust throughout this research and throughout my graduate program. Thank you Dr. Arup Maji, Dr. John Stormont and Dr. David Fowler for your valuable comments and suggestions during this thesis defense. I would also like to thank Mr. Kenny Martinez for helping me to solve set-ups issues for my experiments and making my life easier in the laboratory.

Thanks to my friends Dr. Eslam Soliman and Mr. Sherif Aboubakr for their encouragement and help throughout this research, and thanks to all of my friends for their help and support.

Finally, this research was supported by STC.UNM and Department of Energy (DOE). This support is gratefully acknowledged.

TABLE OF CONTENTS

LIST OF FIGURES ..... **x**

LIST OF TABLES ..... **xiv**

Chapter 1 Introduction **1**

1.1 Background 1

1.2 Motivation and objectives 2

1.3 Scope of work 3

1.4 Thesis outline 5

Chapter 2 Literature Review **6**

2.1 Introduction 6

2.2 Polymer concrete 6

2.2.1 Definition of polymer concrete 6

2.2.2 Historic prospective on polymer concrete 6

2.3 Synthesis of polymer concrete 8

2.3.1 Binder systems and aggregate 8

2.3.2 Additives 10

2.4 Mechanical properties and applications of polymer concrete 14

2.4.1 Mechanical properties of PC 14

2.4.2 Applications of PC 23

2.5 Conclusion 26

Chapter 3 Experimental Methods **27**

3.1 Introduction 27

3.2 Materials properties and mixes preparation 27

3.2.1 Epoxy 27

3.2.2 Multi-Walled Carbon Nano-Tubes (MWCNTs) 28

3.2.3 MWCNTs-epoxy resin Nano-composite 28
3.2.4 Mix preparation 30
3.3 Fresh properties and mechanical characterization of Polymer Concrete mixes 31
3.3.1 Flowability test 31
3.3.2 Compressive strength test 32
3.3.3 Flexural strength test 33
3.3.4 Shear strength test 34
3.3.5 Creep behaviour test 35
3.3.6 Charpy impact test 38
3.3.7 Low-velocity impact test 38
3.4 Fresh properties and bond strength of Polymer concrete overlay mixes 40
3.4.1 Flowability test 40
3.4.2 Pull-off test 40
3.4.3 Slant shear test 45
3.4.4 Four-point bending fatigue test 48
3.5 Microstructural characterization of epoxy-MWCNTs Nano-composite 52
3.5.1 Scanning Electron Microscope (SEM) 52
3.5.2 Fourier Transform Infrared Spectroscopy (FTIR) 53
3.5.3 Thermal characterization 54
Chapter 4 Results and Discussion 55
4.1 Introduction 55
4.2 Fresh properties and mechanical characterization of Polymer Concrete mixes 55
4.2.1 Flowability test 55
4.2.2 Static mechanical response 56
4.2.3 Dynamic mechanical response 76
4.3 Fresh properties and bond strength of Polymer concrete overlay mixes 82
4.3.1 Flowability test 82

4.3.2 Bond strength between Polymer Concrete overlays and steel substrates 83
4.3.3 Time dependant mechanical response of PC overlays 96
4.4 Microstructural characterization of epoxy-MWCNTs Nano-composite 102
4.4.1 Scanning Electron Microscope (SEM) 102
4.4.2 Fourier Transform Infrared Spectroscopy (FTIR) 104
4.4.3 Thermal characterization 107
4.4.4 Discussion of the characterization of epoxy-MWCNTs Nano-composite 110
Chapter 5 Conclusions 111
5.1 Summary 111
5.2 Conclusions 112
5.3 Recommended future research 115
References 116

LIST OF FIGURES

Figure 1.1: Schematic of thesis scope of work for investigating a new generation of polymer concrete incorporating multi-walled carbon nanotubes. 4
Figure 2.1: Schematic drawing of epoxy resin, epoxy hardener, and neat epoxy *(Soliman 2011).*. 9
Figure 2.2: CNTs grown by CVD method *(Melo et al. 2011).* 13
Figure 2.3: Effect of binder on the compressive strength of PC. 15
Figure 2.4: Variation of flexural strength of PC made of different binders. 17
Figure 2.5: Effect of test temperature on PC specific creep strain. *(ACI 548.6R 1996)* 18
Figure 2.6: Effect of fly ash on PC creep compliance *(Rebeiz et al. 2004).* 19
Figure 2.7: Definition of adhesive (bond) strength and cohesive strength. 21
Figure 2.8: Damage in overlays under cyclic traffic loads. 22
Figure 3.1: (a) Mechanical stirrer, (b) Ultra-sonicator. 29
Figure 3.2: (a) Neat epoxy resin, (b) MWCNTs-epoxy resin nano-composite. 29
Figure 3.3: Flow table, flow cones, and test calliper. 31
Figure 3.4: (a) Filling of flow cone by fresh PC mix, (b) Measuring flowability percentage using test calliper. 32
Figure 3.5: Compression test setup for cylinders. 32
Figure 3.6: (a) Schematic of PC prisms tested in flexure, (b) flexure test setup with 2 LVDTs. .. 33
Figure 3.7: (a) Shear test specimen dimensions, (b) Shear test setup. 34
Figure 3.8: Specimen deformation in shear zone. 35
Figure 3.9: One creep test specimen with 3 strain gauges. 36
Figure 3.10: Creep test frame loaded with test specimen. 36
Figure 3.11: CR1000 data acquisition system with AM 16/32 multiplexer. 37
Figure 3.12: (a) Charpy impact test schematic, (b) charpy impact test setup. 38
Figure 3.13: Test machine of Low-velocity impact test: (a) test chamber, and (b) turret. 39
Figure 3.14: (a) Low-velocity impact test schematic, and (b) one test specimen. 39
Figure 3.15: Pull off test schematic. 41
Figure 3.16: (a) Pull off test apparatus, (b) Sandblasted steel plate with white metal blast cleaning profile 41
Figure 3.17: (a) Test setup of the first stage in the pull off test, (b) 54mm core drilling. 42
Figure 3.18: (a) Second stage test setup, (b) 57mm Cores drilling. 43
Figure 3.19: (a) Fourth stage PC overlay mixes, (b) 25 mm core drilling. 44
Figure 3.20: Fifth stage of pull off test setup. 44

Figure 3.21: Slant shear test schematic. 45
Figure 3.22: (a) Steel part dimensions, (b) Sandblasted half steel cylinder. 46
Figure 3.23: Composite cylinder test specimen of PC overlay on steel. 47
Figure 3.24: Slant shear test setup. 47
Figure 3.25: Schematic of stresses in substrate and overlay under traffic loads. 48
Figure 3.26: Design drawings of new fatigue test fixture. 49
Figure 3.27: Four-point bending fatigue test schematic. 50
Figure 3.28: Four-point bending fatigue test setup. 51
Figure 3.29: Hitachi S-5200 Nano SEM apparatus. 52
Figure 3.30: Nicolet Nexus 670 FTIR apparatus. 53
Figure 3.31: TGA/DSC SDT Q600 apparatus, and specimen holder. 54
Figure 4.1: Variation of flowability of PC mixes with varying MWCNTs content. 56
Figure 4.2: Compression stress-strain curves of PC mixes incorporating varying contents of MWCNTs 56
Figure 4.3: Compression Young's modulus of elasticity of PC with varying MWCNTs content. 57
Figure 4.4: Compressive strength of PC with varying contents of MWCNTs. 58
Figure 4.5: Compressive failure strain of PC with varying contents of MWCNTs. 59
Figure 4.6: Toughness of PC with varying contents of MWCNTs. 59
Figure 4.7: Different failure modes of Compressive strength test. 60
Figure 4.8: Crushing of PC specimens at failure under axial compression loads. 60
Figure 4.9: Stress-strain curves of flexure test of PC with varying MWCNTs content. 61
Figure 4.10: Flexural Young's Modulus of Elasticity of PC with varying MWCNTs content. 62
Figure 4.11: Ultimate flexural strength of PC with varying MWCNTs content. 63
Figure 4.12: Flexural failure strain of PC with varying MWCNTs content. 63
Figure 4.13: Variation of PC flexural toughness with varying MWCNTs content. 64
Figure 4.14: Shear stress-strain curves and failure mode for PC with varying MWCNTs content. 65
Figure 4.15: Variation of shear modulus of PC mixes with varying MWCNTs content. 66
Figure 4.16: Ultimate shear strength of PC mixes with varying MWCNTs content. 67
Figure 4.17: Shear strain at failure of PC mixes with varying MWCNTs content. 67
Figure 4.18: Shear toughness of PC mixes with varying MWCNTs content. 68
Figure 4.19: Total strain of PC specimens with varying contents of MWCNTs under sustained axial load. 69
Figure 4.20: Creep compliance of PC specimens with varying contents of MWCNTs. 69

Figure 4.21: Failure creep compliance of PC specimens with varying contents of MWCNTs. 71
Figure 4.22: Failure time of PC specimens with varying contents of MWCNTs under sustained axial load. 71
Figure 4.23: Crushing of PC specimens at failure under sustained axial loads. 72
Figure 4.24: Schematic drawing of the reaction between functionalized MWCNTs and epoxy groups *(Soliman 2011)*. 73
Figure 4.25: Cohesive shear failure under axial loading in the case of 1.5% MWCNTs. 75
Figure 4.26: Schematic of failure mechanism of PC with varying content of MWCNTs in compression and creep tests. 75
Figure 4.27: Results of Charpy impact test. 76
Figure 4.28: Failure mode of Charpy impact test of PC specimens. 77
Figure 4.29: Effect of MWCNTs in decreasing the drop in PC resistance to impact loads. The significant increase in the residual strength after the main impact event (peak force) in PC with MWCNTs specimens reflect the ability of PC incorporating MWCNTs to dissipate and absorb energy compared with neat PC. 78
Figure 4.30: Variation of PC maximum impact resistance in low-velocity impact test with varying MWCNTs content. 78
Figure 4.31: Effect of MWCNTs on slowing down impact target and reducing penetration velocity after impact. 79
Figure 4.32: Variation of maximum absorbed energy in low-velocity impact test. The figure shows the increase of number of cracking lines in PC incorporating MWCNTs compared with neat PC. 80
Figure 4.33: Variation of the flowability of PC overlay mixes incorporating varying contents of MWCNTs 82
Figure 4.34: All possible failure patterns in the Pull-off test. 84
Figure 4.35: Failure patterns observed in the first stage. 85
Figure 4.36: Variation of the bond strength of PC overlays tested in stage I. 85
Figure 4.37: Second stage failure patterns, invalid pattern I on the left and valid result on the right (pattern III). 86
Figure 4.38: Variation of the bond strength of PC overlays tested in stage II. 86
Figure 4.39: Variation of the bond strength of PC overlays tested in stage III. 87
Figure 4.40: Fourth stage failure pattern IV. 88
Figure 4.41: Variation of the bond strength of PC overlays tested in stage IV. 88
Figure 4.42: Fifth stage failure pattern IV. 89

Figure 4.43: Bond strength of polymer layers with and without MWCNTs in stage V of the pull-off test. 89
Figure 4.44: Load-displacement curves of slant shear test for PC overlays incorporating varying amounts of MWCNTs. 90
Figure 4.45: Variation of the bond strength between PC overlays and steel with varying amount of MWCNTs. 91
Figure 4.46: Variation of failure displacement of PC overlay mixes incorporating different contents of MWCNTs. 92
Figure 4.47: Increased number of overlay parts on steel at failure in the case of MWCNTs. 93
Figure 4.48: Schematic comparison between cohesion and adhesion strengths as explained by slant shear and pull-off tests. 95
Figure 4.49: Variation of the fatigue strength represented by number of cycles to failure for PC overlays with varying MWCNTs content (* no failure up to 50,000 cycles). 96
Figure 4.50: Mean damage evolution of PC prisms under fatigue loading. 98
Figure 4.51: Variation of number of cycles to total failure for PC overlays incorporating varying amount of MWCNTs. 98
Figure 4.52: Fracture of some fatigue specimens. 99
Figure 4.53: SEM image of epoxy incorporating 1.0% MWCNTs. 102
Figure 4.54: SEM images of epoxy incorporating 1.0% MWCNTs. 103
Figure 4.55: SEM images of epoxy incorporating 1.0% MWCNTs. 103
Figure 4.56: FTIR curves of reflected waves for neat epoxy and epoxy with MWCNTs. 104
Figure 4.57: Taller 1511 cm^{-1} peak in the case of epoxy with MWCNTs. 105
Figure 4.58: Increase of 39% at the C-O bonds peak in the case of epoxy with MWCNTs. 105
Figure 4.59: Very slight shift toward higher wavenumbers at 1250 cm^{-1} and 1610 cm^{-1}. 106
Figure 4.60: Relatively large shift at O-H bonds in the case of epoxy with MWCNTs. 107
Figure 4.61: TGA results of neat epoxy and epoxy incorporating MWCNTs. 108
Figure 4.62: DSC curves of neat epoxy and epoxy incorporating MWCNTs. 109
Figure 4.63: Obtaining T_g from glass transition zone. 110

LIST OF TABLES

Table 3.1: Properties of MWCNTs (Cheaptubes, Inc.)..... 28
Table 3.2: Mix proportions by weight kg/m^3 (lb/ft^3). 30
Table 4.1: Mix proportions by weight (kg/m^3) 101

Chapter 1 Introduction

1.1 Background

The construction field is always looking for new materials with superior performance criteria such as long service life and good mechanical properties that are inexpensive to produce. In the last few decades, polymers and polymer-based materials have been one of these new materials that can achieve the previously mentioned requirements. Polymer-based materials and especially Polymer Concrete (PC) has been attracting increased attention in the construction field due to their attractive properties compared with other conventional concretes.

PC was one of three types of polymers in concrete introduced to the construction industry. It was first commercially used in the 1950s to produce architectural facade panels *(Prusinski 1987)*. PC is similar to conventional concrete when the binder system is used to bind the coarse and fine aggregate in order to obtain the required strength. However, PC's binder system is not cement and water. In PC, a few polymers such as epoxy, acrylics, polyester and phenolic are used to form the matrix binder. Using polymers as binders provides rapid setting properties, very low permeability, enhanced chemical resistance and high durability *(ACI 548.6R 1996)*.

The early use of PC in the construction field was limited to repair applications. With the increase in manufacturing facilities and the availability of better production technologies, PC is now used in structural applications such as bridge deck overlays *(Lopez-Anido et al. 1998)* and concrete pavement rapid repair *(Wang et al. 2003)*, utility structures *(ACI 548.6R 1996)* and as lining for sewer lines *(ACI 548.6R 1996)*.

1.2 Motivation and objectives

Mechanical and chemical properties of PC mixes depend mainly on the type of polymer used to form the binder. Thermoset polymers are typically mixed with fine and coarse aggregate to produce structural PC. Most of the thermoset polymers are rigid and can provide PC with good mechanical properties. However, limited fatigue life, potential debonding and relatively low energy absorption (due to brittleness) are a few limitations of the current PC *(ACI 548)*. These limitations prevent the widespread of PC in structural applications.

The objective of this thesis is to develop a new generation of PC with enhanced mechanical properties. The new generation PC is produced by incorporating Multi-Walled Carbon Nano Tubes (MWCNTs) in the polymer mix binder. However, the enhanced mechanical properties of PC cannot be achieved if the MWCNTs do not bond chemically with the polymer groups. MWCNTs will work as impurities inside the polymer mix binder and might have an adverse effect on the mechanical properties. MWCNTs are a tabular structure made from concentrically rolled multiple graphite sheets. MWCNTs are synthesized at a relatively low temperature of 450 ^{o}C using the chemical vapor deposition (CVD) method. Because of this relatively low temperature, MWCNTs are considered an inexpensive alternative of CNTs with good mechanical properties compared with Single-walled Carbon Nano Tubes (SWCNTs) which are synthesized at a much higher temperature of 700 ^{o}C and are also much more expensive.

Our hypothesis is that when MWCNTs are used as binder additives they are expected to alter the polymer binder microstructure and hence improve limitations of the

PC by providing higher bond strength and improved fatigue life and energy absorption compared with conventional PC.

1.3 Scope of work

This thesis is focused on the investigation of the mechanical properties of PC mixes incorporating different contents of MWCNTs represented as the weight ratio of the epoxy resin. The mixes are made from low modulus polysulfide epoxy typically used to produce PC and PC overlays for bridge decks. In order to ensure the chemical bond between the MWCNTs and the epoxy, MWCNTs functionalized with carboxyl groups (COOH) were used. Moreover, preparation of the MWCNTs-epoxy resin nanocomposite included the use of high temperature stirring and sonication in order to reduce the epoxy resin viscosity and improve the dispersion of the MWCNTs.

The investigation was divided into three parts. The first part aimed at investigating the mechanical behavior of PC including compressive, flexural, shear strengths, creep behavior, and impact resistance. The second part included investigation of bond strength and fatigue behaviour of PC overlays incorporating MWCNTs. Testing the significance of adding MWCNTs on the flowability of both PC and PC overlays was also investigated. The investigation of bond strength was performed using the pull-off test. However, the required failure mode was never achieved. Therefore, the bond strength was further investigated by performing the slant shear test. Moreover, a new test setup was designed and produced to investigate PC fatigue behavior. This new setup follows AASHTO specification and is typically used in testing asphalt pavements. The final part of the investigation involved microstructural characterization of neat epoxy and

epoxy incorporating MWCNTs. Figure 1.1 represents a schematic plan of the scope of work.

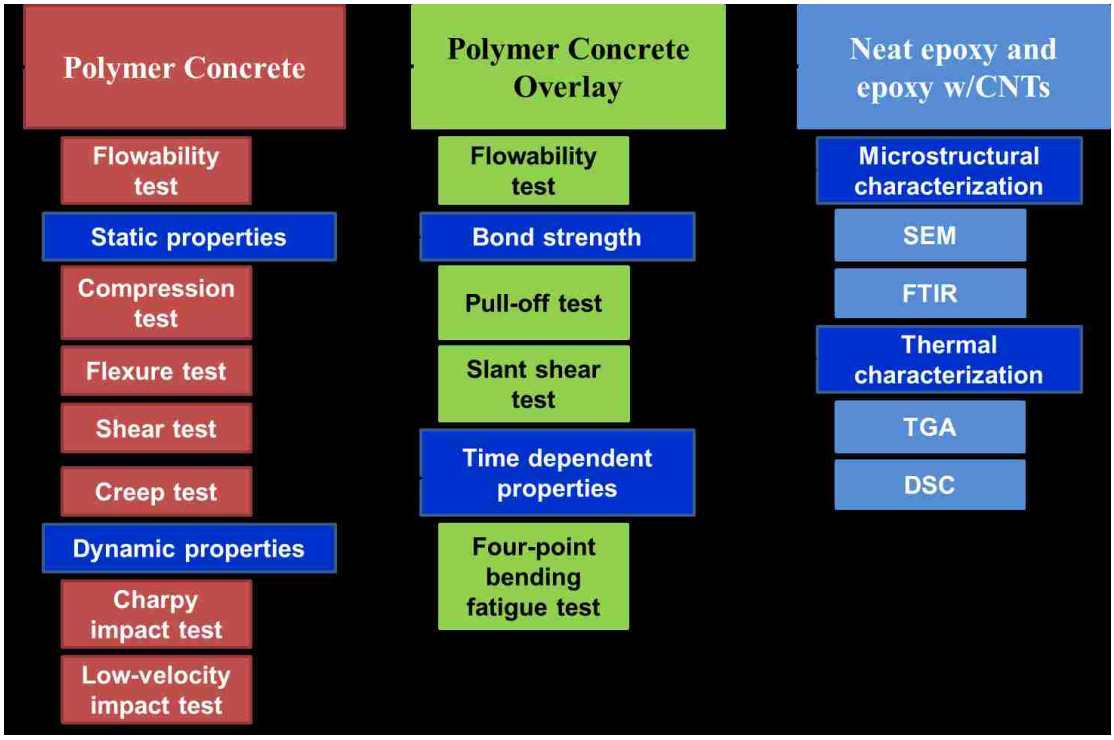

Figure 1.1: Schematic of thesis scope of work for investigating a new generation of polymer concrete incorporating multi-walled carbon nanotubes.

From the tests results, it was obvious that adding MWCNTs to PC improved the compressive, flexural, shear and impact strengths. MWCNTs also enhanced the adhesion strength between PC overlays and steel, limited bond failure strain, and enhanced significantly the damage evolution in PC overlays under cyclic loading. Moreover, adding MWCNTs made the nanocomposite more thermally stable with higher decomposition temperature compared with the neat polymer. These improvements prove that the addition of MWCNTs fibers bridged the PC micro-cracks and significantly enhanced the PC's energy absorption, durability and resistance to crack propagation.

1.4 Thesis outline

Chapter 2 of this thesis represents the literature review of PC including definition of PC, its historic prospective, PC mechanical properties, and its applications. Chapter 3 explains properties of the materials used, fabrication methods, test procedures and setups, and data analysis. Chapter 4 presents test results and observations with discussion about the effect of incorporating MWCNTs in polymer concrete mixes. Finally, Chapter 5 summarizes and concludes the research work with recommendations for future work.

Chapter 2 Literature Review

2.1 Introduction

This chapter is a background study of polymer concrete. The first part of this chapter starts with definitions of polymer concrete. It also provides information about the evolution of polymer concrete. In the second part, information about polymer concrete materials is reviewed. The chapter ends with the third part which is an overview on the mechanical properties of polymer concrete and its recent applications.

2.2 Polymer concrete

2.2.1 Definition of polymer concrete

Polymer concrete (PC) is defined as a hardened composite produced by mixing resins or monomers with aggregates without adding any Portland cement. The mix is hardened by a process called polymerization initiated after placement of fresh concrete. Polymer concrete (PC) has advantages of easy placement, fast curing, and rapid setting properties. PC has also gained remarkable acceptance over the last 15 years due to its enhanced mechanical and chemical properties compared with conventional concrete.

2.2.2 Historic prospective on polymer concrete

Polymer concrete (PC) was first introduced in the United States through three polymers in concrete categories. The categories included polymer impregnated concrete (PIC), polymer modified concrete (PMC), and polymer concrete (PC). In the 1950s, PC was first commercially used in the United Stated in order to produce synthetic marble and to manufacture architectural facing panels. The use of PC was developed by the mid-1970s to be a repair material for cement concrete structures. Through the 1970s and the 1980s, The U.S. Federal Highway Administration, the Bureau of Reclamation, the

Department of Energy, and chemical companies in US performed intensive research on the properties of the materials included in PC manufacturing process. This research resulted in enhancing and developing many polymers used in PC and made it available for PC commercial production. As a result, the American Concrete Institute (ACI) 548 committee of Polymers in Concrete was formed in 1971. The committee published "Polymers in Concrete—State-of-the-Art Report" (ACI 548R), "Guide for the Use of Polymers in Concrete" (ACI 548.1R), and proceedings of ACI symposia considering the materials and production of PC. In 1975, the first International Congress on Polymers in Concrete (ICPIC) was held in England and published technical reports considering PC materials and applications. Subsequently, ICPIC congresses were held in different places and published documents about PC concluding the research work performed all around the world.

2.3 Synthesis of polymer concrete

2.3.1 Binder systems and aggregate

In polymer concrete, polymers form the main binder systems which combine the aggregates together and produce the concrete. These systems are equivalent to the cement and water binder system in conventional concrete. Epoxies, which are type of polymers, usually consist of two individual parts called A/B components, which are mixed together to form the polymer binder system. The (A) component is called the resin and contains polymerization accelerator. The (B) component contains polymerization initiator and called the hardener. As defined earlier, polymerization is the chemical process of transferring the polymer resin and hardener liquids into solid polymer material. During polymerization, original molecules are tied and large molecules are formed. Through the mixing process, fine and coarse aggregates are added in order to form the final PC mixes and provide the required strengths.

Thermoset polymers are typically used to form the binder system of structural PC. Thermoset polymers include aminos, most unsaturated polyesters, alkyds, epoxies, and phenolics. Unsaturated polyesters are the most popular thermoset used to produce PC. Orthophthalate unsaturated polyester (UP) resins are used as binders combined with Methyl Ethyl Ketone Peroxide as initiator *(Soh et al. 1999, San Jose and Ramirez 1999, Ribeiro et al. 2003, and Jo et al. 2008).* Moreover, unsaturated isophatalic polyester resin was observed to be hard, rigid, and can provide hard mechanical properties *(Orak 2000).* PC binder systems were produced from other thermoset polymers including low viscosity vinylester resin *(Czarnecki, and Chmielewska 1999),* polystyrene resins *(Choi and Ohama 2004, and Rai and Singh 2004),* and polyurethane foam made of wood wastes

(Tokushige et al. 2005). Orthophthalate unsaturated polyester could also be mixed with polyurethane forming interpenetrating polymer networks in order to produce new polymer mortars *(Bignozzi et al. 2001).*

Epoxies have been extensively utilized to form the binder systems in order to produce polymer concrete *(Ribeiro et al. 2003, Reis and Ferreira 2004, and Barbuta et al. 2010).* Epoxies consist of two parts, which are epoxy resin and epoxy hardener. While the resin contains epoxy reactive groups (C-O-C) at the two ends of the polymer chain, the hardener contains amino groups (NH_2). Chemical reaction occurs between the two groups in order to tie polymer chains together and form the solid polymer mass. This chemical reaction is called the crosslinking process. Figure 2.1 shows schematic drawing of epoxy resin, epoxy hardener, and neat epoxy after crosslinking of polymer chains.

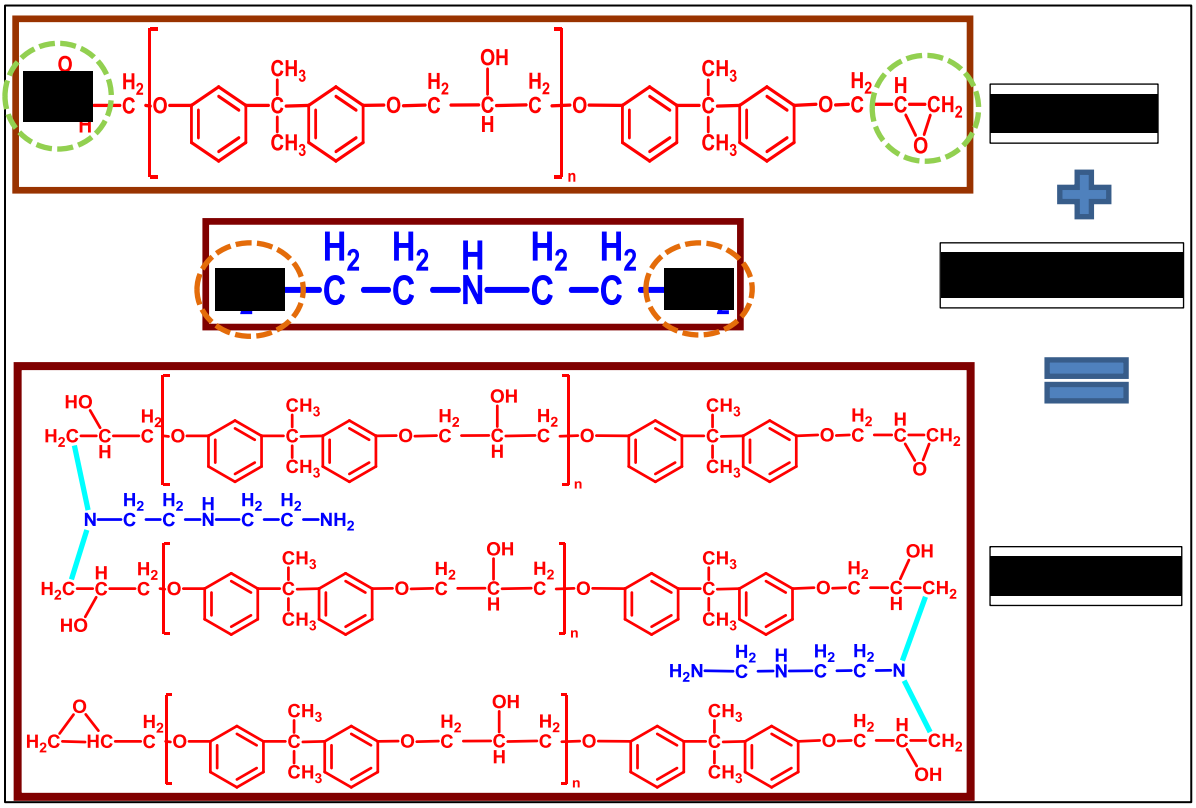

Figure 2.1: Schematic drawing of epoxy resin, epoxy hardener, and neat epoxy *(Soliman 2011).*

In order to produce PC, filler materials combined with fine and coarse aggregates have been used with polymer binder systems. Fillers and aggregates should be dry, clean, and can provide chemical resistance. Silica sand was utilized as inorganic fine aggregate used with calcium carbonate as filler material *(Soh et al. 1999, Bignozzi et al. 2001, and Choi and Ohama 2004)*. Moreover, recycled waste materials and available natural composites could be used as fillers and/or aggregates in order to preserve the environment and reduce the cost. The recycled waste materials include chipped and crumb rubber tire particles *(Reda Taha et al. 2005)*, recycled concrete aggregates *(Jo et al. 2008)*, silica fume *(Barbuta et al. 2010)*, and fly ash *(Barbuta et al. 2010)*; While the natural composites include ophitic aggregate *(San Jose and Ramirez 1999)*, and wood stubs and roots *(Tokushige et al. 2005)*. Maksimov et al. (2003) reported the use of ground limestone (flour), quartz sand, and crushed granite as mineral fillers in a polyester PC.

It is important to differentiate between PC and PC overlays. While PC mixes consist of polymer binder system, filler powder, and coarse aggregate, PC overlays consist of a polymer binder system and filler powder without adding coarse aggregate. Aggregate can be broadcasted on top of the PC overlay to increase the overlay friction necessary for traffic.

2.3.2 Additives

Additives are materials added to the binder system and aggregate of PC to enhance one or more of the mechanical or chemical properties. In some cases, additives can replace part of the fine or coarse aggregate used in the mix. Each material added to the mix should be compatible to react with the binder system and aggregate in order to

obtain the required enhancement. In many cases, polymers were used as additives to PC. Expanded polystyrene (EPS)-based resin melted in styrene monomer (SM) can be added to unsaturated polyester (UP) mortars as a low profile additive in order to reduce the curing shrinkage *(Soh et al. 1999);* Polymeric waste including recycled polyethylene terephthalate from plastic bottles *(Rebeiz and Fowler 1996),* rubbers *(Bignozzi et al. 2000 and 2002),* and electrical cable wastes *(Bignozzi et al. 2000 and 2002)* was added to polymer mortars as polymeric additives to modify its properties. Moreover, recycled textile chopped fibers consisting of cotton, polyester, silk and rayon can be utilized in some polymer concrete systems in order to decrease brittleness in failure of unreinforced PC *(Dos Reis 2009).*

Additives other than polymers were also used to produce new PC and enhance the ductile behavior. Silane coupling agents were added to vinylester mortars and improved the bond and mechanical strengths *(Czarnecki, and Chmielewska 1999, and Chmielewska et al. 2006)*; Cork granulates partially replaced sand to produce lightweight polymer mortar with improved compressive ductility *(Novoa et al. 2004)*; and finally fly ash was added to sulfur polymer system and sand in order to manufacture new sulfur polymer concrete with improved compressive strength and chemical properties *(Mohamed and Gamal 2009).*

Nano-scale inorganic particles such as nanoclay, carbon nanotubes, and carbon nanofibers are added to polymer matrices to manufacture polymer nanocomposites. The dimensions of these nano-scale particles typically range from 1 to 1000 nm. With homogeneous dispersion of the nano-scale particles in polymer matrices, polymer nanocomposites experience improved properties compared with pure polymer matrices.

Jo et al. (2008) reported enhanced mechanical and thermal performance of unsaturated polyester (UP) concrete mixed with montmorillonite (MMT). Moreover, modified nanoclay was added to epoxy concrete and improved some mechanical properties but decreased tensile and flexural strengths *(Shokrieh et al. 2012)*.

As a part of utilizing nano-scale inorganic particles as additives, a new generation of latex modified concrete with enhanced properties can be produced by incorporating Carbon Nano-Tubes (CNTs) in the polymer matrix during PC fabrication *(Reda Taha et al. 2011)*. This thesis further investigates the use of CNTs in producing PC. Carbon Nano-Tubes (CNTs) are tabular structure made from concentrically rolled single or multiple graphite sheets. CNTs produced using the carbon arc-discharge method normally consist of hollow carbon hexagonal networks concentrically arranged around each other and containing multiple inner chambers *(Zhou and Chow 2003)*. CNTs were firstly introduced as single-walled carbon nanotubes (SWCNTs) and proved to have superior mechanical properties, but SWCNTs showed to be significantly expensive. High-purity SWCNTs are synthesized and grown using thermal Chemical Vapor Deposition (CVD) at a growth temperature of and above 700^{o} C *(Sharma and Iqbal 2004, and Ting et al. 2008)*. Multi-walled carbon nanotubes (MWCNTs) appeared later as a cheaper alternative form of CNTs. Using the Chemical Vapor Deposition (CVD) method, MWCNTs are synthesized at a relatively low temperature of 450^{o} C compared to 700^{o} C for SWCNTs *(Sharma and Iqbal 2004)*. Figure 2.2 shows CNTs manufactured by CVD method.

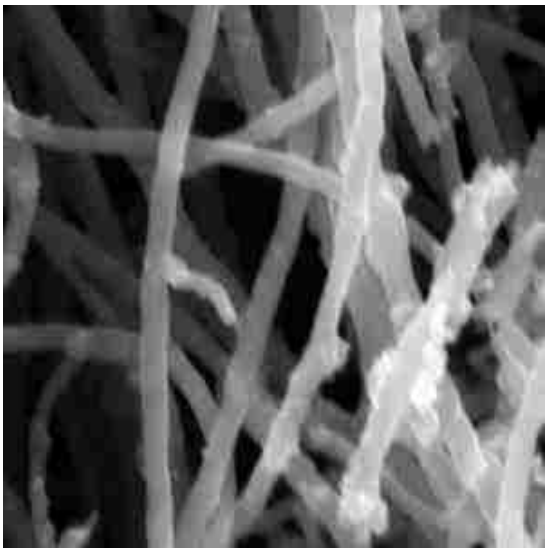

Figure 2.2: CNTs grown by CVD method *(Melo et al. 2011)*.

In many cases and in order to enhance the chemical bond between CNTs and polymer systems, CNTs are functionalized by chemical groups which react with the polymer resin and hardener. (Swain et al. 2012) reported improvement in the electrical properties of unsaturated polyester resin by incorporating allylester functionalized MWCNTs and silane functionalized MWCNTs. Furthermore, wax coated MWCNTs enhanced the electrical conductivity and improved the mechanical properties of High Density Polyethylene system *(Jiang and Drzal 2011)*.

2.4 Mechanical properties and applications of polymer concrete

2.4.1 Mechanical properties of PC

Polymer concrete has superior mechanical properties compared with conventional Portland cement concrete, but still less than structural metals. These mechanical properties depend on the binder system, curing conditions, service parameters, and additives used in the PC mix.

2.4.1.1 Compressive strength

As mentioned before and similar to conventional concrete, the compressive strength of PC is about one order of magnitude of its tensile strength. PC has compressive strength ranging from 60 MPa to 180 MPa (9000 psi to 26000 psi), and a ratio of compressive to tensile strength from 6 to 10 *(ACI 548.6R 1996)*. One of the factors that affects compressive strength is the type of polymer used as a binder as shown in Figure 2.3. Isophtalic polyester PC with concentration of 15-20% of fly ash demonstrated a compressive strength around 95 MPa (14000 psi) *(Rebeiz et al. 2004, and Gorninski et al. 2007)*. Orthophthalic polyester PC reinforced with non-metallic glass reinforced polymer bars showed compressive strength of 102 MPa (14800 psi) *(San Jose et al. 2008)*. Moreover, the compressive strength and strain of a polymer concrete made from rubber solutions were 93.4 MPa (13600 psi) and 6.7%, respectively *(Chung and Hong 2009)*.

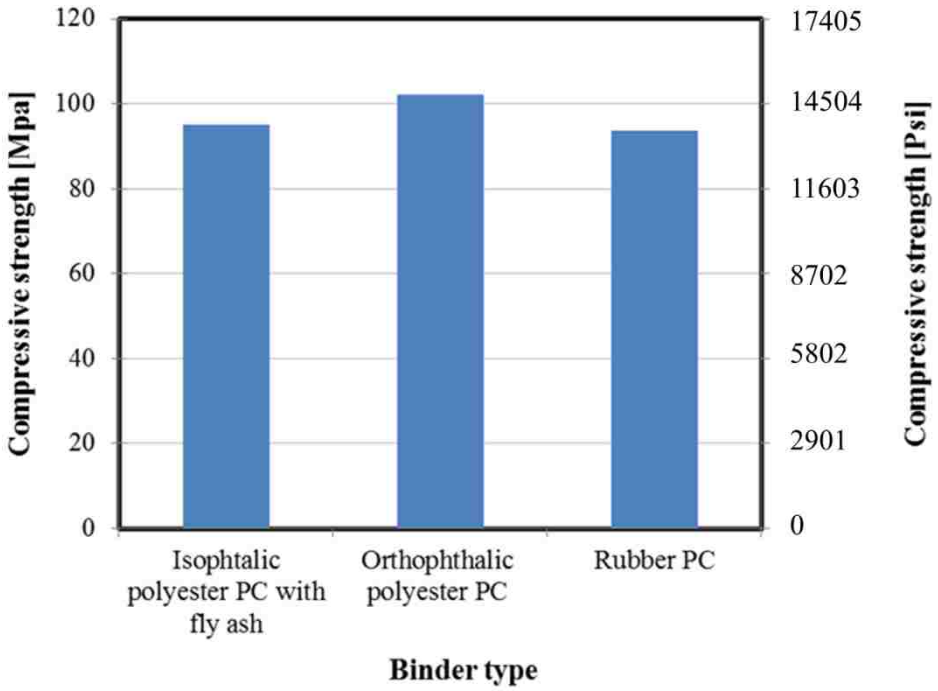

Figure 2.3: Effect of binder on the compressive strength of PC.

In addition, compressive strength of PC is affected by filler and aggregate used in the mix. *Barbuta et al.* (2010) reported epoxy PCs with compressive strengths ranging from 43.47 MPa to 69.82 MPa (6305 psi to 10127 psi) using different dosage of fly ash and silica fume as fillers. Polyester PC with marble of different particle size added as aggregate and submitted to gamma radiation doses reached a compressive strength of 89.1 MPa (13000 psi) *(Martinez-Barrera and Brostow 2010)*. Furthermore, epoxy micro PC was reported to obtain compressive strength of 70 MPa (10150 psi) under different conditions of curing *(Haidar et al. 2011).*

Different mortars made of polymers were also investigated under axial compression. *Soh et al.* (1999) reported unsaturated polyester resin mortar added polystyrene resin with compressive strength of approximately 85 MPa (12000 psi). Moreover, compressive strengths of 128 MPa (18500 psi), 52 MPa (7550 psi), and 28.5

MPa (4100 psi) were obtained from vinylester mortar with silane coupling agents *(Chmielewska et al. 2006)*, epoxy polymer mortar *(Reis 2009)*, and UP mortars manufactured from PET bottles *(Mahdi et al. 2013)*, respectively.

2.4.1.2 Flexural strength

Flexure strength of PC depends mainly on the polymer used to form the binder system. While rigid polymers exhibit higher modulus of elasticity and brittle failure behavior, flexible polymers produce ductile behavior. The flexural strength of unreinforced PC usually ranges between 14 MPa and 28 MPa (2000 psi and 4000 psi), and modulus of elasticity between 4 GPa and 40 GPa (500,000 psi and 5,000,000 psi) *(ACI 548.6R 1996)*. PC made of polyester resin incorporating 15-20% fly ash reported flexure strength around 21 MPa (3050 psi) *(Rebeiz et al. 2004, and Gorninski et al. 2007)*. Beams manufactured of orthophthalic polyester resin reinforced with non-metallic glass reinforced polymer bars demonstrated flexural strength of 26 MPa (3771 psi), modulus of elasticity of 37.9 GPa , and maximum strain of 0.98% *(San Jose et al. 2008)*. Furthermore, *Rebeiz and Fowler* (1996) reported flexure strength of 96 MPa (13977 psi), and failure strain of 0.87% for steel-reinforced polymer concrete beams made of unsaturated polyester resins based on recycled PET. *Reis and Ferreira* (2003) investigated the fracture behavior of chopped glass fiber reinforced epoxy polymer concrete and reported flexural modulus of elasticity of 9.5 GPa (1400 ksi). Figure 2.4 represents comparison between the flexural strength of PC made of different binders.

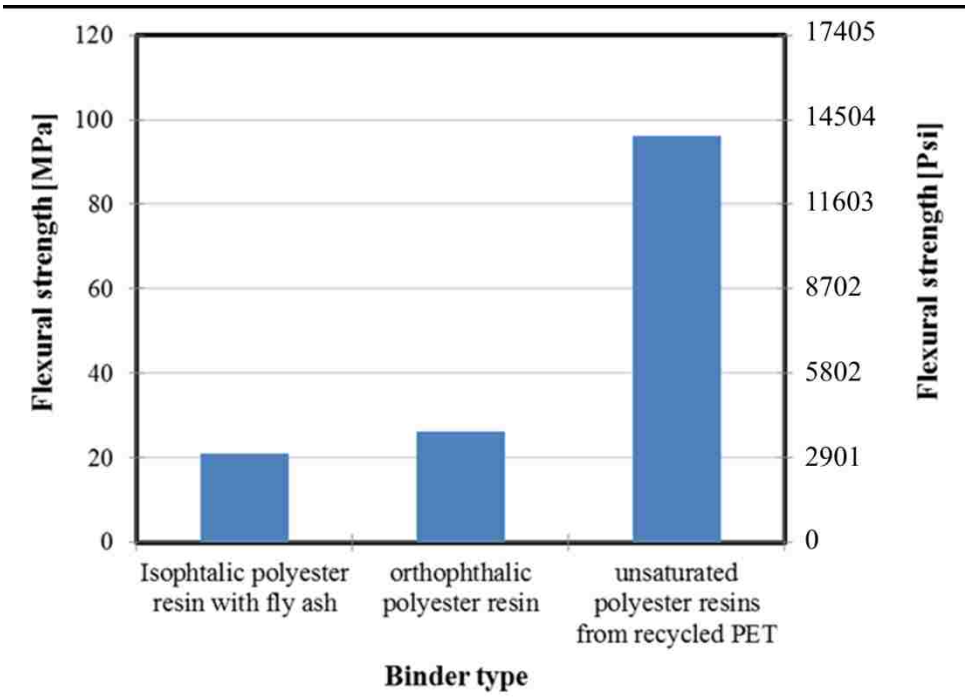

Figure 2.4: Variation of flexural strength of PC made of different binders.

Similar to the compressive strength and other mechanical properties, the filler and aggregate used affect the flexural strength of the mix. Flexural strengths of 21 MPa (3050 psi), 15 MPa (2180 psi), and 28 MPa (4060 psi) were obtained for PC mixes utilizing calcium carbonate and recycled concrete aggregate *(Jo et al. 2008)*, fly ash and silica fume *(Barbuta et al. 2010)*, and graded mixture of coarse and fine sand *(Haidar et al. 2011)*, respectively.

Flexural strength of different polymer mortars was investigated. *Soh et al.* (1999) obtained flexural strength around 26.5 MPa (3770 psi) using unsaturated polyester mortar adding polystyrene resin. Silane coupling agents were mixed with polyester *(Bignozzi et al. 2000)*, and vinylester *(Chmielewska et al. 2006)* mortars demonstrated flexural strengths of 33.9 MPa (4915 psi), and 40.9 MPa (5932 psi), respectively. Moreover, epoxy mortar showed flexure strength of 42.64 MPa (6184 psi) *(Ribeiro et al. 2004)*.

2.4.1.3 Shear Strength

Similar to Portland cement concrete, shear failure in PC beams would happen as diagonal cracks in PC sections due to its reduced tensile strength compared to its compression capacity. Shear strength of PC would vary between 2 MPa and 26 MPa (275 psi and 3700 psi) depending on the material used in the mix *(ACI 548.6R 1996). Rebeiz et al.* (2004) achieved shear strength of 8 MPa (1160 psi) for polyester PC replacing 15% of sand by fly ash. Steel-reinforced PC beams using polyester resin and based on recycled PET demonstrated shear strengths ranging between 0.53 MPa and 19 MPa (77 psi and 2754 psi) *(Rebeiz and Fowler 1996, and Mahdi et al. 2013).*

2.4.1.4 Creep behavior

PC is a material with considerable viscoelasticity given its relatively high polymer content. Under sustained load, PC would experience creep strain until failure depending on the stress/strength ratio applied. Creep of PC is approximately two to three times that of conventional Portland cement concrete *(ACI 548.6R 1996).* The magnitude of creep strain mainly depends on the polymer used to form the polymer binder system. Figure 2.5 shows the effect of temperature on the specific creep strain of PC.

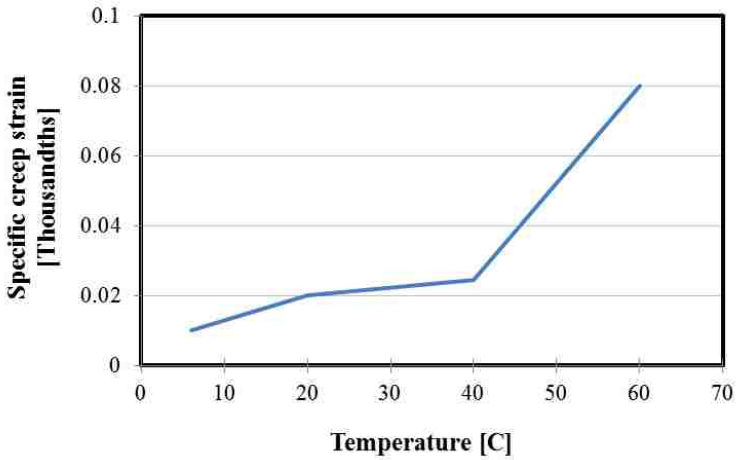

Figure 2.5: Effect of test temperature on PC specific creep strain. *(ACI 548.6R 1996)*

Some additives would increase the cross-linking of the binder system resulting in reducing the slip between the molecules and hence reducing creep strains. Moreover, using fillers and aggregate in the mix was proved to restrict the resin deformation and decrease creep *(Jo et al. 2007)*. Fly ash proved to decrease the creep compliance of PC by about 5% as shown in figure 2.6 *(Rebeiz et al. 2004)*. However, calcium carbonate utilized as filler proved to have better creep behavior than using fly ash *(Jo et al. 2007)*. This could be referred to the relatively large surface area of calcium carbonate compared with fly ash resulting in higher bond area with polymer resin and stronger bond with aggregate than with fly ash. Furthermore, it was suggested that the fineness of fly ash interrupts the bond between the polymer and the aggregate *(Jo et al. 2007)*.

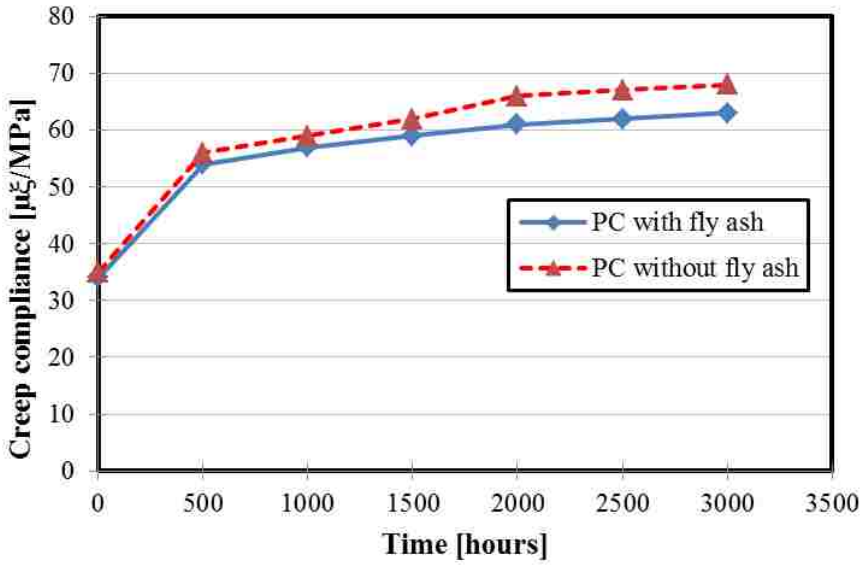

Figure 2.6: Effect of fly ash on PC creep compliance *(Rebeiz et al. 2004)*.

2.4.1.5 Impact resistance

It has been suggested that PC can be used as a protective material for sensitive structures such as military buildings, parking structures and bridges. This might be attributed to the relatively high strain capacity of PC. Energy absorption and dynamic

modulus of elasticity of PC give an indication about its impact properties. Glass fibers proved to enhance the impact and abrasion resistance of isophthalic polyester mortar *(ACI 548.6R 1996)*. The addition of basalt fibers to geopolymer concrete also increased energy absorption capacity and improved deformation at failure *(Li and Xu 2009)*. *Martinez-Barrera and Brostow* (2010) showed an increase in the dynamic modulus of elasticity of polymer concrete adding marble particles with gamma radiation.

2.4.1.6 Bond Strength

Polymer concrete has been utilized as overlays to cover concrete pavements and steel bridge decks. With its low water and acid permeability *(ACI 548.6R 1996)*, PC can protect any substrate, repair damaged Portland cement concrete pavement, and provide high skid resistance. PC also has superior mechanical and durability compared with conventional concrete. This allows using of thin overlays which reduces the structure dead load and minimizes the cost of repair and maintenance. Coarse aggregate is usually broadcast on the overlay upper surface to increase friction between tires and the overlay. One of the main concerns with overlays is the adhesive strength between the overlay and the substrate. In this part, it is important to differentiate between adhesive and cohesion strength and the possible modes of failure. Adhesive strength, usually called the bond strength, can be defined as a measure of the bond between an overlay and its substrate. On the other hand, cohesion strength is defined as a measure of the tensile bond between the overlay layers. Therefore, adhesion or bond strength describes the bond line between the overlay and its substrate, while cohesion strength describes the bond lines inside the overlay itself. Figure 2.7 shows schematic drawing of the definition of bond and cohesion strength. Under traffic loads, failure in the case of overlay and substrate can occur in one

of three modes. The first mode is failure in the substrate and this can happen if the substrate is deteriorated concrete while can rarely happen if the substrate is made of steel. The second mode is cohesion failure inside the overlay which depends on the overlay mechanical properties. The last mode is debonding between the overlay and the substrate indicating bond failure. The bond strength between overlay and substrate can be reduced if the overlay has limited shear strength. Furthermore, this bond strength can be significantly decreased if the structure experiences high temperature variations or significantly different thermal expansion coefficients of the two materials exist. The industry has agreed that bond strength above 1.4-2.0 MPa (200-300 psi) is acceptable for most applications *(ACI 548.5R)*.

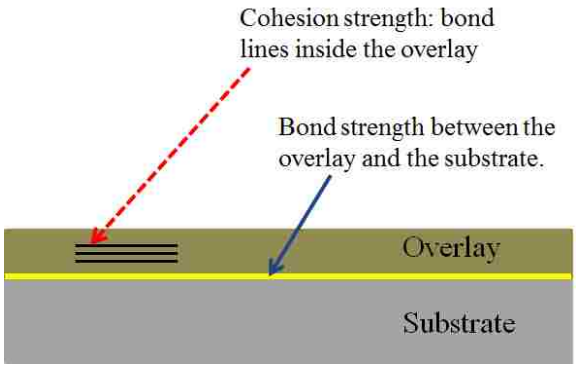

Figure 2.7: Definition of adhesive (bond) strength and cohesive strength.

Low viscosity vinylester mortar modified with silane coupling agent showed bond strength of 2.8 MPa (406 psi) to a wet Portland cement concrete substrate compared with 1.86 MPa (270 psi) for non-modified mortar *(Czarnecki, and Chmielewska 1999)*. *Rebeiz et al.* (2004) reported bond strength of 3.3 MPa (479 psi) between polyester PC modified with fly ash and cement concrete substrate. It is important to state that this bond strength was reduced by more than 45% after 80 thermal cycles.

2.4.1.7 Fatigue behavior

Bridges experience millions of cycles of loading and unloading due to traffic loads. These cycles cause fatigue which expresses the stiffness degradation in the structure that occurs over time. Fatigue can cause failure in some cases. In PC overlays, cracks initiate between the overlay and the substrate due to debonding between the two materials. This might start due to temperature effects. Under continuous cyclic loading, such debonding cracks propagate horizontally resulting in complete debonding between the overlay and the substrate. Moreover, the cracks can propagate vertically through the overlay causing overlay deterioration. Figure 2.8 represents crack propagation in PC overlays under cyclic loading. Fatigue behavior of PC, as in many other materials, depends on the maximum applied stress (σ_{max}) and the stress range ($R = \sigma_{max} - \sigma_{min}$), where σ_{min} is the minimum applied stress *(Dowling 2007)*. Fatigue life decreases with increasing the maximum stress or/and the stress range *(Dowling 2007)*.

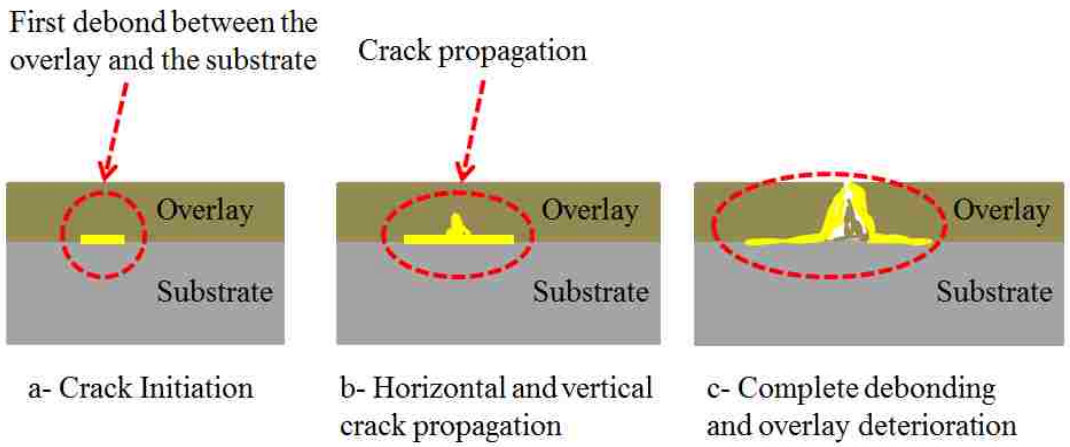

Figure 2.8: Damage in overlays under cyclic traffic loads.

Wheat et al. (1993) investigated the fatigue behavior of beams made of Portland cement concrete overlaid by epoxy PC. The composed beams survived 2 million load

cycles without significant loss of stiffness or delamination. Beams were statically loaded to failure after load cycles and the obtained stiffness was found to be close to the initial stiffness. Therefore, it was concluded that fatigue was not the primary cause of failure. Furthermore, *Tavares et al.* (2001) tested PC prisms reinforced with GFRP rods in three-point bending fatigue test. The PC prisms which were made of epoxy resin lasted for one million cycles without rupture. The observed fatigue strength was attributed to both PC and the GFRP rods.

2.4.2 Applications of PC

Through the development of PC, it had shown to have improved performance properties compared with conventional cement concrete. The improved properties include light unit weight, high resistance to moisture and other chemical elements, and enhanced tensile and compressive strengths. As a result, precast PC elements were intensively used in many architectural and structural commercial applications.

2.4.2.1 Architectural polymer concrete panels

The first architectural application was the precast PC panels in 1958. Polyesters resins and pure silica were used to produce the first precast PC panels. For single skin panels and after performing tests and trials, the best practical thickness was found to be 20 mm (0.75 in) *(Prusinski 1978).* Sandwich panels with 20-mm (0.75-in) facing skin encapsulating polyurethane foam were also manufactured. In order to accommodate wind load requirements, reinforcing material such as fiberglass cloth and steel bars were used to stiffen the panels and allow clear spans of 4.5 m (15 ft). Moreover, aggregate was broadcasted on the exposed faces. Around 1970, single skin polyester PC panels of 15 mm (0.6 in) in thickness and insulating sandwich panels of 100 mm (4.0 in) in thickness

were produced in Netherlands. The panels were reinforced with fiberglass. In 1972, polyester PC panels with different surface finishing were developed by a firm in Quebec, Canada. Afterwards, many examples of using PC panels in the United States and around the world were reported *(Prusinski 1987)*.

Polyester polymer panels were the most popular for this application as it proved to be able to provide the required strength and wind load resistance (*Kaeding and Prusinski 2003)*, and high performance in different climatic conditions *(Wahby and Prusinki 2005)*. Subsequently, high ductility and load bearing capacity polymer mortar panels without and with steel fiber and crimped wire cloth reinforcements were produced *(Bhutta et al. 2011)*. The polymer mortar panels were made of methyl methacrylate (MMA) solution produced of waste expanded polystyrene (EPS).

2.4.2.2 Structural members

Structural members are used to safely transfer the external loads acting on the structure to the foundations and then to ground. Therefore, such members should resist flexure, compression, shear, torsion or any combination of these stresses. Similar to conventional concrete, PC has high compressive strength and relatively low tensile strength *(ACI 548.6R 1996)*. Reinforced PC has been used to manufacture beam elements in order to resist flexural stresses. The flexural failure of reinforced PC beams was observed to occur in a similar manner of beams made of Portland cement concrete. However, reinforced PC beams would have higher strength, more ductility, and require less reinforcement cover *(Rebeiz and Fowler 1996)*. The failure compressive strain of PC was observed to be 0.005. According to experimental data, the equivalent rectangular stress block method for conventional concrete would yield conservative results for

reinforced PC beams. Therefore, a new flexure design equation, developed using statistical analysis of tests results, should be used to calculate the flexural capacity of reinforced PC beams *(Rebeiz and Fowler 1996)*. In addition, an empirical equation to predict the effective moment of inertia of reinforced PC beams was proposed by analyzing the structural behavior of some PC beams *(Park et al. 2010)*.

PC with longitudinal reinforcement has been used to form columns in order to support axial loads and moments. Some columns were made of fly ash-based geopolymer concrete and showed enhanced performance under axial compressive load and uni-axial bending *(Sumajouw et al. 2007)*. The experimental and analytical studies on steel encased polymer concrete under axial compressive load proved the enhanced ductility and increased compressive strength *(Oyawa et al. 2001 and Oyawa 2007)*. The previous results support the use of PC filled steel tubes columns in seismic resistant structures.

The third structural application of PC is the high-speed machines beds. Suh and Lee (2008) studied the design and manufactured a hybrid polymer concrete bed for high-speed milling machine. The hybrid bed, which had welded steel faces and polymer concrete core, provided high damping and high stiffness compared with conventional concrete beds.

2.4.2.3 Repair and retrofit

PC provides the required properties for a repair material of easy installation, fast curing, and high chemical resistance. Polymer mortars were used for structural restoration of deteriorated wooden beams *(Van Gemert et al. 1998)*, concrete pavement rapid repair *(Wang et al. 2003)*, seismic retrofit of concrete structures *(Ono et al.)*, and enhancing shear behavior of reinforced concrete beams *(Ha et al. 2010)*. PC allowed

performing reinforced concrete repairs in aggressive environments. The applications included the use of aggregate-filled epoxy grouts in polymer-encapsulation of concrete piles in marine environment *(Snow 1999)*, and the use of polyester-based polymer concrete coating to protect underground facilities made of cement concrete and clay bricks from sulfuric acid attack *(Liu and Vipulanandan 2001)*. Moreover, a combination of ferrocement and polymeric materials was used to restore the durability of water tanks located in aggressive environment *(Rajamane et al. 2003)*.

2.4.2.4 Transportation

PC has been used in many transportation applications due to its light weight and reduced maintenance cost. New low-smoke, low-styrene, MMA-free flame-retardant polyester resin systems were used for mass transit applications *(Martens and Siegel 1998)*. Many bridge overlays were manufactured of PC. PC overlays can provide high tension elongation, high adhesion to deck surface, and high energy absorption *(Lopez-Anido et al. 1998)*. Moreover, PC has been used to connect bridge barriers made of reinforced Portland cement concrete to FRP composite bridge decks *(Zhao et al. 2004)*. Median barriers and curb facing have been produced form PC for several years.

2.5 Conclusion

The above review showed polymer concrete as a material used extensively as overlays for highway application. While PC overlays have many advantages over overlays made using conventional cement based materials, a few limitations exist for these overlays. The most critical properties of these overlays are their limited bond and fatigue strength with steel substrates. We hypothesize that using nanomaterials such as carbon nanotubes can help overcoming this limitation.

Chapter 3 Experimental Methods

3.1 Introduction

This chapter describes the experimental methods including material properties, mixes and specimens' preparation, tests setups and procedures, and methods used to analyze tests data. The first part of this chapter starts with the properties of the epoxy and the Multi-Walled Carbon Nano-Tubes (MWCNTs) used in this research. Afterwards, it describes how to prepare the MWCNTs-epoxy resin nanocomposite. The second part describes tests performed on polymer concrete. These tests included flowability of fresh polymer concrete, compressive strength, flexural strength, shear strength, creep behavior test, Charpy impact strength, and low-velocity impact strength. In this part, specimens for each test were produced in replicas of three except the compression test, which was produced in replicas of five, and the flowability test which was performed one time for each mix. The third part deals with polymer concrete overlays. Tests in this part were flowability of fresh polymer concrete overlay, pull off test, slant shear test, and four-point bending fatigue test. Specimens in this part were produced for each test in replicas of five except the flowability test which was performed as the second part, one time for each mix. The chapter ends with the fourth part including the micro-structural and thermal characterization of neat epoxy and epoxy incorporating MWCNTs.

3.2 Materials properties and mixes preparation

3.2.1 Epoxy

In this research, low modulus polysulfide epoxy was used. This epoxy is typically used to produce polymer concrete and polymer concrete overlays for bridge decks. The epoxy consists of two components, Bisphenol A/Epichlorohydrin epoxy resin, and Phenol

based epoxy hardener. Epoxy resin and epoxy hardener are mixed by a ratio of 2:1. Neat epoxy was reported to have density of 8.8 Ibs/gal (1054.5 kg/m^3), viscosity of 1200-1600 cps, pot life of 15-30 minutes at 21° C (70° F), compressive strength of 34.5 MPa (5000 psi), tensile adhesion to concrete of 1.7 MPa (250 psi), and tensile strength of 12.4 MPa (1800 psi).

3.2.2 Multi-Walled Carbon Nano-Tubes (MWCNTs)

Functionalized MWCNTs with carboxyl (COOH) groups supplied by Cheap Tubes®, Inc. were used. The MWCNTs were produced using Catalysed Chemical Vapor Deposition (CCVD) technique with purity greater than 95% by weight. Table 3.1 presents the geometrical properties and elemental analysis of the MWCNTs used in this research. The MWCNTs used has 20-30 nm outer diameter and 10-30 μm length.

Table 3.1: Properties of MWCNTs (Cheaptubes, Inc.)

Outer diameter, nm	20-30
Inner diameter, nm	5-10
MWCNTs ash, % wt.	<1.5%
Purity, %	>95%
Length, μm	10-30
Specific surface area, m2/g	110
Bulk density, g/cm3	0.28
Electrical conductivity, S/cm	>100
COOH groups	1.2%

3.2.3 MWCNTs-epoxy resin Nano-composite

In order to prepare the nanocomposite, the desired percentage of MWCNTs was added to the required amount of epoxy resin, and the mix was stirred for 2 hours at 110° C using a mechanical stirrer at 800 rpm. This relatively high mixing temperature was

used to reduce the resin viscosity and improve the dispersion of MWCNTs. The mix was then sonicated for 2 additional hours at 65° C. During the sonication, sound waves are generated from the transducer and radiate through the liquid causing high and low pressures. At the low pressure stage, millions of microscopic bubbles are formed; during high pressure stage, the previous bubbles collapse releasing high amount of energy and improving the dispersion of MWCNTs. The MWCNTs-epoxy resin nanocomposite was left for one hour to reach room temperature, so it could be used to prepare the mixes. Figure 3.1 shows the mechanical stirrer and ultra-sonicator.

(a)  (b) 

Figure 3.1: (a) Mechanical stirrer, (b) Ultra-sonicator.

Figure 3.2 (a) shows the neat epoxy resin, and Figure 3.2 (b) represents the dispersed MWCNTs inside the epoxy resin forming the MWCNTs-epoxy resin nano-composite.

(a)  (b) 

Figure 3.2: (a) Neat epoxy resin, (b) MWCNTs-epoxy resin nano-composite.

3.2.4 Mix preparation

Four mixes were prepared and examined. The mixes were neat polymer concrete (PC) or neat polymer concrete (PC) overlays without MWCNTs; and three other PC or PC overlay mixes incorporating 0.5, 1.0, and 1.5% MWCNTs by weight of the epoxy resin, respectively. In order to prepare the PC mixes, the required amount of either neat epoxy resin or MWCNTs-epoxy resin nanocomposite was mixed with the epoxy hardener for 2-3 minutes using a low speed mixer; then a silica filling powder followed by the required coarse aggregate were added. Mixing continued for 2-3 minutes until the mixture was uniform. The silica filling powder used was crystalline silica (quartz), and ceramic microspheres, while the coarse aggregate used was bauxite-based aggregate with a nominal maximum size of 4.75 mm. Following the same procedure used to make PC mixes, PC overlay mixes were prepared but no coarse aggregate was added. Table 3.2 presents the mix proportions by weight for the four PC and PC overlay mixes. It is important to state that all the specimens, except for the flowability test, were air cured for 7 days in room temperature and relative humidity of 50% RH before testing.

Table 3.2: Mix proportions by weight kg/m^3 (lb/ft^3).

	PC overlay				
Mix Designation	Resin	Hardener	Powder	Coarse Aggregate	MWCNTs
Neat	288 (18)	128 (8)	1570 (98)	320 (20)	–
0.5% MWCNTs	288 (18)	128 (8)	1570 (98)	320 (20)	0.041 (0.09)
1.0% MWCNTs	288 (18)	128 (8)	1570 (98)	320 (20)	0.082 (0.18)
1.5% MWCNTs	288 (18)	128 (8)	1570 (98)	320 (20)	0.123 (0.27)
	Polymer Concrete				

3.3 Fresh properties and mechanical characterization of Polymer Concrete mixes

3.3.1 Flowability test

This test was performed to examine the effect of adding MWCNTs on the flowability of the fresh PC mixes. The test was performed according to ASTM C1437- 07 (2009). In this test, a flow table, flow cone, and standard calliper were used. The cone smaller diameter was 70 mm (2.8 in), larger diameter was 100 mm (4.0 in), and the height was 50 mm (2.0 in). Figure 3.3 shows the apparatus used for flowability test.

Figure 3.3: Flow table, flow cones, and test calliper.

For testing, each mix was prepared and the cone was filled by the fresh PC mix in two layers. Each layer was tapped 20 times to ensure uniform filling of the cone. The cone was lifted in 4 seconds and 25 strikes were applied to the fresh PC in 15 seconds. After the 25 strikes, four perpendicular measurements of the diameter of the fresh PC were recorded. The flowability percentage was considered as the sum of the four readings. Figure 3.4 describes the filling of the flow cone by the fresh PC mix and measuring the flowability percentage using the test calliper.

(a)  (b) 

Figure 3.4: (a) Filling of flow cone by fresh PC mix, (b) Measuring flowability percentage using test calliper.

3.3.2 Compressive strength test

Five 50*100 mm (2.0*4.0 in) cylinders were made from each mix and tested in compression using Instron® testing machine according to ASTM C39/C39M-12a. The cylinders were tested at an age of 7 days to failure with a loading rate of 29400 N/min (6600 lbf/min). Load and displacement were recorded while performing the test using MTS® 793 data acquisition system with a sampling rate of 10 Hz. The compressive strength was estimated to be the failure load divided by the cross-sectional area of 2,027 mm^2 (3.14 in^2). Figure 3.5 shows the compression test setup for cylinders.

Figure 3.5: Compression test setup for cylinders.

3.3.3 Flexural strength test

In order to perform the flexure test, three polymer concrete prisms were fabricated from each mix. The prisms dimensions were 25.4*25.4*116 mm (1*1*5 in). The prisms were tested in a three-point bending test setup at age of 7 days with a loading rate of 300 N/min. (67 Ibf/min.) according to ASTM C78 - 02 (2002). Figure 3.6(a) shows schematic of the test setup and specimen dimensions. The distance between the supports was 96 mm (3.75 in.). Using LVDT supplied by National Instruments ® Corporation, the mid span deflection was recorded simultaneously with the applied force. Figure 3.6(b) shows the LVDTs attached to the flexure test setup. The flexural stress-strain of PC was computed to examine the significance of MWCNTs on the flexural stiffness of PC. The flexure test was performed using MTS® Bionix servo hydraulic system and the measurements were collected by MTS® 793 data acquisition system with a sampling rate of 10 Hz for all experiments.

(a) 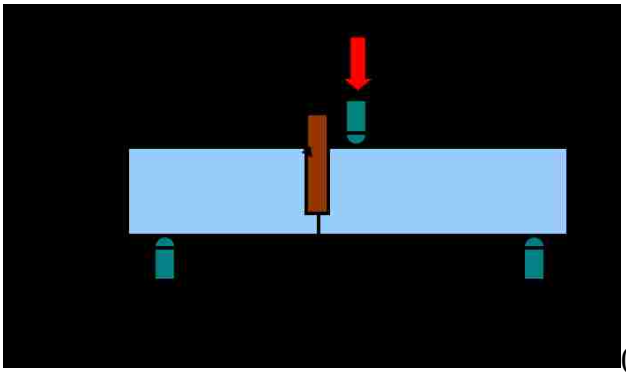 (b) 

Figure 3.6: (a) Schematic of PC prisms tested in flexure, (b) flexure test setup with 2 LVDTs.

In each experiment, the maximum flexural stress at the mid-span and the corresponding maximum strain were calculated using the following equations:

$$\sigma = \frac{3PL}{2bd^2} \tag{3.1}$$

$$\varepsilon = \frac{6\delta d}{L^2} \tag{3.2}$$

where σ is the maximum flexural stress at the mid-span, ε is the corresponding maximum strain, *P* is the applied load, *L* is the span, *b* is the width of the specimen, *d* is the depth of the specimen, and δ is the mid-span deflection.

3.3.4 Shear strength test

The shear test was performed following the guidelines of ASTM D4475-02 (2008) in a flexural shear setup on what is known as short beam setup using three 25.4*25.4*48 mm (1*1*2 in) prisms made from each mix. The prisms were tested in a four-point bending test setup at an age of 7 days. In order to investigate the shear strength of the prisms, the distance between supports was limited to 32 mm (1.25 in.) and the distance between points of loading was set at 24 mm (1.0 in.) such that the distance between each support and the adjacent point of loading was limited to 4 mm (0.15 in.) as shown in Figure 3.7 to enforce shear failure. The rate of loading was 700 N/min (157 Ibf/min). The test and data acquisition were performed using MTS® Bionix servo hydraulic system with a sampling rate of 10 Hz.

(a) 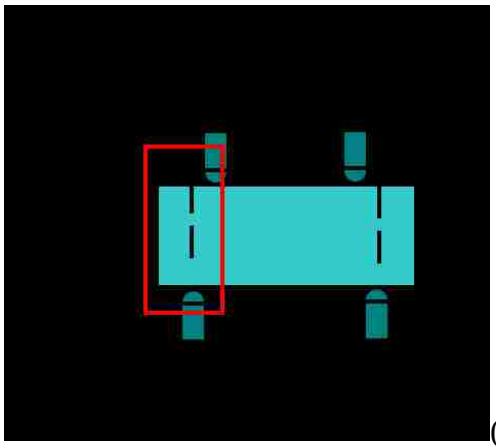 (b) 

Figure 3.7: (a) Shear test specimen dimensions, (b) Shear test setup.

The load at each point of loading and the deflection under that point were recorded during the test as shown in Figure 3.8 and the average shear stress and shear strain were computed as:

$$\tau = \frac{Q}{bd} \tag{3.3}$$

$$\gamma = \frac{\delta}{a} \tag{3.4}$$

where τ is the average shear stress, γ is shear strain, Q is shear force, b is the width of the specimen, d is the depth of the specimen, δ is the deflection under the point of loading, a is the shear span which equals 4 mm.

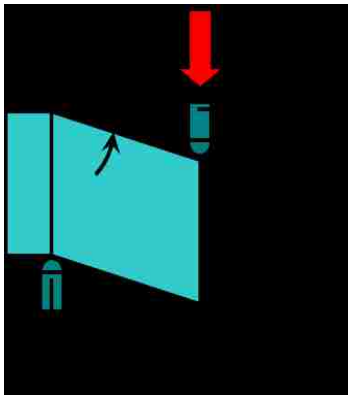

Figure 3.8: Specimen deformation in shear zone.

3.3.5 Creep behaviour test

Creep tests for each mix were performed on three cylinders. The cylinders had a diameter of 50 mm (2.0 in) and a height of 100 mm (4.0 in). At the age of 7 days, specimens of each mix were aligned in a hydraulic spring-loaded creep frame and sustained uniaxial compression load was applied. The applied compression load was taken as 25% of the compressive axial capacity obtained from the compression test performed on the cylinders of each mix (see section 3.3.2). Three 20% elongation strain

gages were bonded on each specimen using high elongation epoxy. The electrical strain gages covered the height and one side of each specimen. Therefore, one strain gage was bonded on each third of the specimen with 45^{o} between each other covering a total angel of 90^{o} as shown in Figure 3.9. Moreover, one strain gage was bonded to a dummy unloaded specimen to correct for temperature and bond adhesive shrinkage deformations. The test was performed in relative humidity of 50% and room temperature of 23^{o} C. Figure 3.10 shows the creep frame with one test specimen.

Figure 3.9: One creep test specimen with 3 strain gauges.

Figure 3.10: Creep test frame loaded with test specimen.

All strain gauges were connected to a CR1000® data acquisition system with an AM 16/32® multiplexer as shown in Figure 3.11. Strain readings were collected every minute using Loggernet® data logger software. Afterwards, uniaxial compression compliance and compliance were calculated as:

$$J(t) = \frac{\varepsilon(t)}{\sigma} \tag{3.5}$$

$$Jc(t) = J(t) - J(0) \tag{3.6}$$

where *J(t)* is the compression compliance at any time interval, ε(t) is the average strain reading obtained from each specimen, σ is the sustained axial stress calculated by dividing the applied load by the specimens cross sectional area, $J_c(t)$ is the creep compliance at any creep time interval, and *J(0)* is the initial compression compliance at zero creep time.

Figure 3.11: CR1000 data acquisition system with AM 16/32 multiplexer.

3.3.6 Charpy impact test

Three prisms were made from each mix to be tested in the Charpy impact test. The prisms dimensions were 25.4*25.4*50.8 mm (1*1*2 in). A notch was produced at the centre of each specimen according to ASTM E23 - 02 (2002). The notch height was 5 mm (0.2 in.) and the width was 3 mm (0.1 in.). The test span was 40 mm (1.5 in.), and that allowed a supporting distance of 5 mm (0.2 in.) in each side. For the test, a hammer struke the notched specimens with a velocity of 5.1 m/s (16.8 ft/s) and the absorbed energy by each specimen was recorded. The test was performed and energy was recorded using standard Tinius Olsen® Charpy impact machine. Figure 3.12 shows schematic drawing for Charpy impact test and the test setup.

(a) 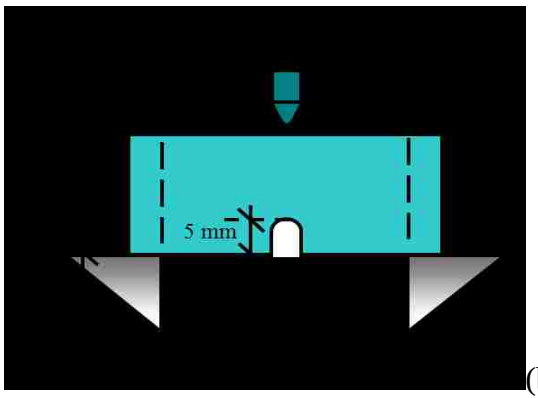

(b) 

Figure 3.12: (a) Charpy impact test schematic, (b) charpy impact test setup.

3.3.7 Low-velocity impact test

The low-velocity impact test was performed on three prisms from each mix using an impact machine by Instron® as shown in Figure 3.13. The prisms for this test were 101.6-mm (4.0-in) square prisms with a thickness of 20 mm (0.75 in). During the test, the specimens were clamped by two rings attached to the test machine of outer diameter of 101.6 mm (4.0 in). Following the guidelines reported by (*Soliman et al. 2012*) for low-velocity impact of thin woven carbon fabric composites, 40 joules of energy were applied

on each specimen. That was achieved using a striker and additional weights of 10 kg making a total weight of 15.46 kg. Using a DAS 8000® data acquisition system, the impact force, absorbed energy, and test velocity were recorded. Figure 3.14 shows a schematic of the test and one test specimen.

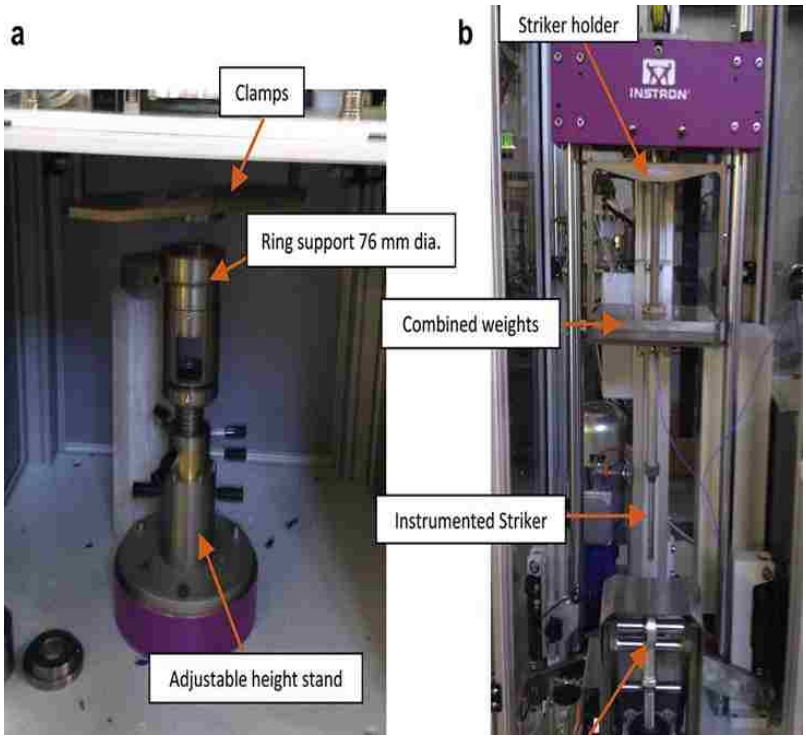

Figure 3.13: Test machine of Low-velocity impact test: (a) test chamber, and (b) turret.

(a)

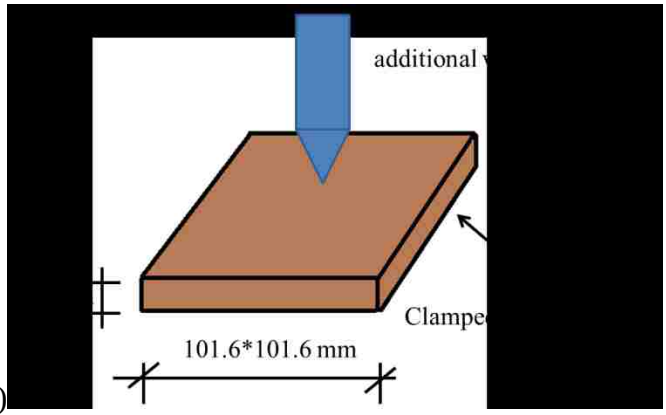

(b)

Figure 3.14: (a) Low-velocity impact test schematic, and (b) one test specimen.

3.4 Fresh properties and bond strength of Polymer concrete overlay mixes

3.4.1 Flowability test

This test was performed to examine the effect of adding MWCNTs on the flowability of the fresh PC overlay mixes. The test was performed according to ASTM C1437- 07 (2009) and following the same procedure of section 3.3.1.

3.4.2 Pull-off test

The pull-off test was performed to determine the bond strength between PC overlays and bridge decks made of steel. In order to present the case of an overlay on a steel bridge deck, a 12.7 mm (0.5 in) A36 steel plate was sandblasted to have minimum roughness of 4.0 Mil and white metal blast cleaning profile according to the NACE No. 1/SSPC-SP5 (1994) standard. Afterwards, 9.5-mm (0.375-in) PC overlays were casted onto the steel plate. Test dollies of either 20 mm (0.8 in) or 50 mm (2.0 in) in diameter were glued to the overlay surface. Cores were drilled around the dollies using core drillers. When the age of the overlays reached 7 days, dollies were tested in tension using a pull-off test apparatus and according to ASTM C1583/C1583M – 04 (2004). The tension rate used was 0.2 MPa/sec (30 psi/sec). The bond strength was defined as the maximum tension stress occurred at the failure between the dollies and the overlay which was obtained from the apparatus. Figure 3.15 is a schematic drawing of the test.

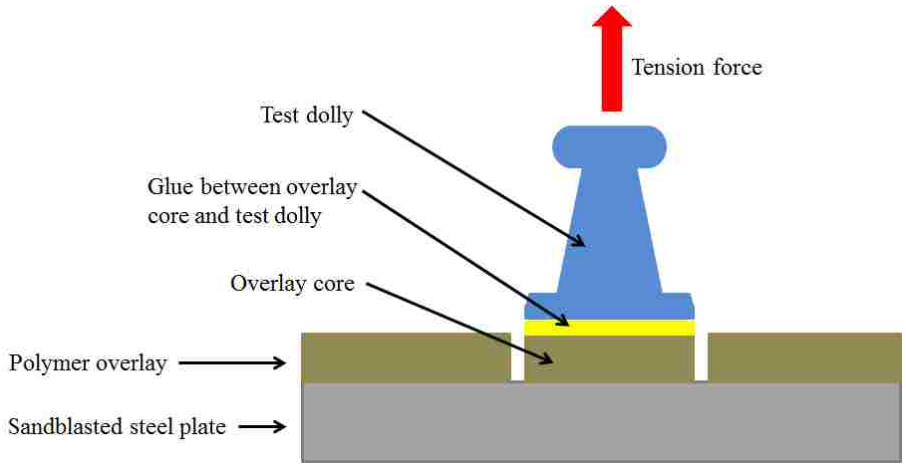

Figure 3.15: Pull off test schematic.

The test was performed using PosiTest AT-A® automatic pull-off adhesion tester with adhesion capacity of 20 MPa (3000 psi) with the 20 mm (0.8 in) test dollies and 3.5 MPa (500 psi) with the 50 mm (2.0 in) test dollies. PosiTest AT-A® test dollies were used. Figure 3.16 shows the pull-off adhesion tester used and a sandblasted steel plate with white metal blast cleaning profile.

(a) 

(b) 

Figure 3.16: (a) Pull off test apparatus, (b) Sandblasted steel plate with white metal blast cleaning profile

The test was performed in five stages. In the first stage, only neat and 0.5% MWCNTs 9.5 mm (0.375 in) PC overlays were casted over the sandblasted steel plates. No aggregate was broadcasted on the overlay surface. Eight 50-mm (2.0-in) test dollies were assigned for each mix and used without sandblasting the dollies' surfaces. In this stage, Loctite® Hysol 608 epoxy glue was used to bond the dollies to the overlay surface. A 54 mm (2.125 in) Morse® hole saw was used to produce the cores around the test dollies. Figure 3.17 shows the first stage test setup and core drilling for this stage.

(a) 

(b) 

Figure 3.17: (a) Test setup of the first stage in the pull off test, (b) 54mm core drilling.

The second stage was performed by casting the neat and the 0.5% MWCNTs 9.5 mm (0.375 in) PC overlays on one sandblasted steel plate. Surface aggregate was broadcasted on the overlays with a rate of 4897.6 gm/m^2 (1.0 Ib/ft^2). Nine 50-mm (2.0-in) test dollies were used for each mix and surfaces were sandblasted to have a minimum roughness of 4.0 Mil. Special epoxy glue used by specialists to test bridge decks in pull-off was used to bond the dollies to the overlay. In order to make the cores, a 57-mm

(2.25-in) concrete core driller was used. Figure 3.18 shows the second stage configurations and core drilling.

(a) 

(b) 

Figure 3.18: (a) Second stage test setup, (b) 57mm Cores drilling.

In the third stage, the same procedures of neat and 0.5% MWCNTs 9.5-mm (0.375-in) PC overlays casting, surface aggregate broadcasting, cores drilling, and using sandblasted 50 mm (2.0 in) test dollies were followed. Four test dollies were used for each mix. In this stage, the epoxy glue was first applied to the overlay cores then test dollies were glued.

For the fourth stage, neat, 0.5%, 1.0%, and 1.5% MWCNTs PC overlays were casted over one sandblasted steel plate. The same procedure of surface aggregate broadcasting was followed. Seven sandblasted 20-mm (0.8-in) test dollies were used for each mix. 25 mm (1.0 in) concrete core driller was used to form the cores. Epoxy glue was first applied to the cores and test dollies were glued afterwards. Figure 3.19 shows the four mixes on the steel plate and core drilling for this stage.

(a) 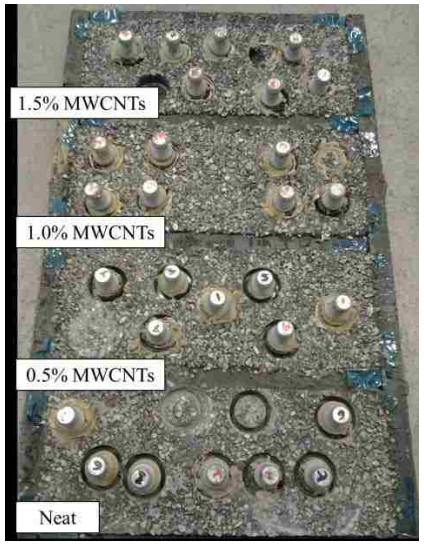

(b) 

Figure 3.19: (a) Fourth stage PC overlay mixes, (b) 25 mm core drilling.

The fifth stage of testing was performed on 4.0-mm (0.16-in) polymer layers without filler, casted on the sandblasted steel plate. No surface aggregate was used. Two mixes of neat polymer and 1.0% MWCNTs polymer were tested using six sandblasted 20-mm (0.8-in) test dollies for each mix. The same procedures from the fourth stage for core drilling, and dolly gluing were followed. Figure 3.20 shows the fifth stage test setup.

Figure 3.20: Fifth stage of pull off test setup.

3.4.3 Slant shear test

As it will be discussed later, failures in the pull-off test never occurred between the overlay and the steel plate. Cohesive rather than adhesive failures took place. This indicated that the test was measuring the cohesion strength of PC overlays rather than the adhesion bond strength between the PC overlays and steel. Therefore, the slant shear test was performed according to ASTM C882/C882M- 12 (2012) to examine the bond strength between polymer nanocomposite overlays and steel. According to ASTM standards, composite cylinders of steel and PC overlay were prepared. The composite cylinders had diameter of 50 mm (2.0 in) and height of 100 mm (4.0 in). The bond line between the two halves of the composite cylinders was inclined by 60° with the horizontal, which maximizes the chance to have adhesion failure between the steel parts and PC overlays rather than comprising the overlay parts. Five composite cylinders for each mix were tested in compression until failure using Instron® testing machine. Figure 3.21 represents slant shear test schematic.

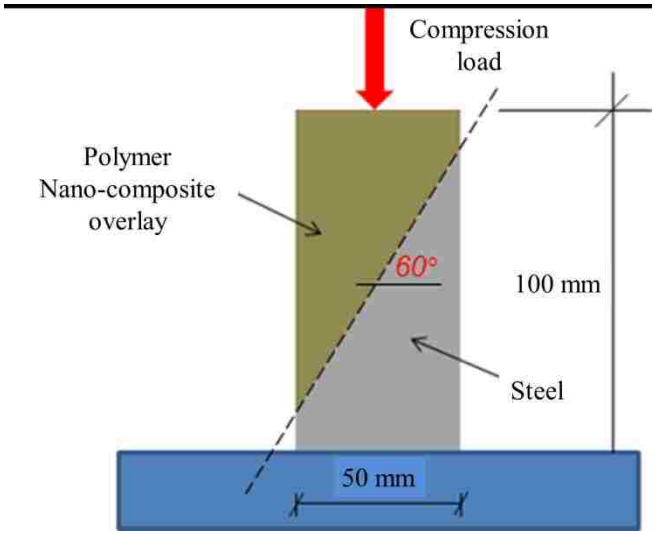

Figure 3.21: Slant shear test schematic.

In order to prepare the steel halves, six cylinder halves were cut from a 50x610 mm (2.0x24.0 in) A36 steel rod and surfaces were sandblasted to have white metal blast cleaning profile with minimum surface roughness of 4.0 Mil. Figure 3.22 shows the dimensions used to produce the steel halves and a sandblasted steel part.

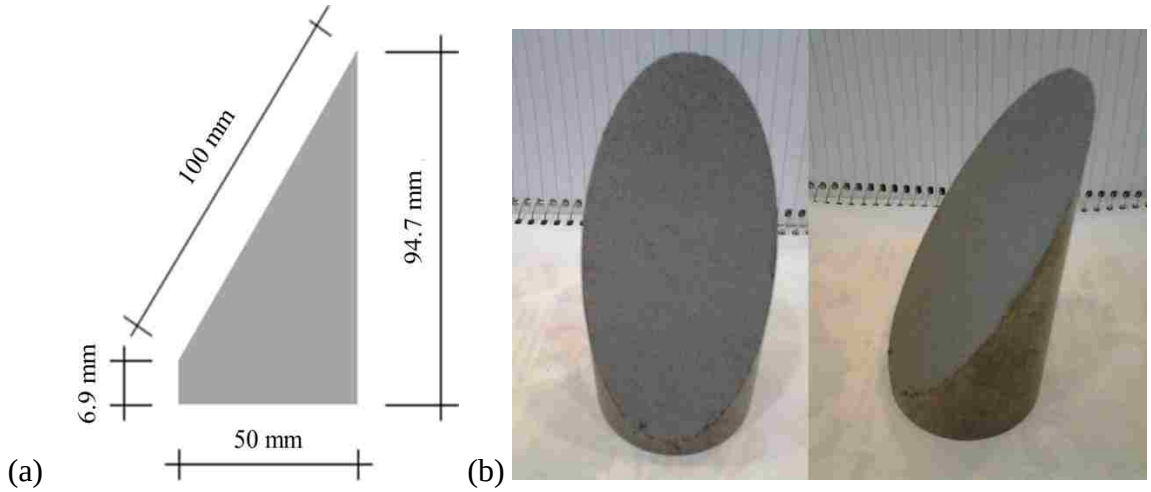

Figure 3.22: (a) Steel part dimensions, (b) Sandblasted half steel cylinder.

In order to determine the test rate in compression, a trial specimen was prepared and trial slant shear test was performed. Specimen preparation was performed by placing the steel half in a 50x100-mm (2.0x4.0-in) mold, and polymer nanocomposite overlay was casted on the steel half in two layers. Each layer was tapped 10 times to ensure uniform filling of the mold, and the surface was leveled. Figure 3.23 shows a ready composite specimen of neat PC overlay on steel. When the trial specimen reached the age of 7 days, the trial slant shear test was performed. The trial test was force controlled with a compression rate of 0.44 kN/sec (0.1 kips/sec). The trial specimen recorded maximum displacement of 3.75 mm (0.15 in) in 104 seconds. As a result of the trial force-controlled test, the steel part of the composite cylinder was damaged at failure of the specimen. Therefore, the test was transferred to be a displacement controlled test for all experiments

with a compression rate of 0.035 mm/sec (0.0014 in/sec) in order to save the steel parts of the composite cylinders. Loads and displacements were recorded using a rate of 10 Hz.

Figure 3.23: Composite cylinder test specimen of PC overlay on steel.

Finally, the bond strength was calculated using the equation:

$$Q = \frac{\mathrm{P}}{\mathrm{A}\prime} \tag{3.7}$$

where Q is the bond strength, P is the maximum axial load, and A' is the inclined cross sectional area ($A' = A/\cos(60^o)$, where A is the horizontal cross sectional area of 2027 mm^2 (3.14 in^2)). Figure 3.24 represents slant shear test setup.

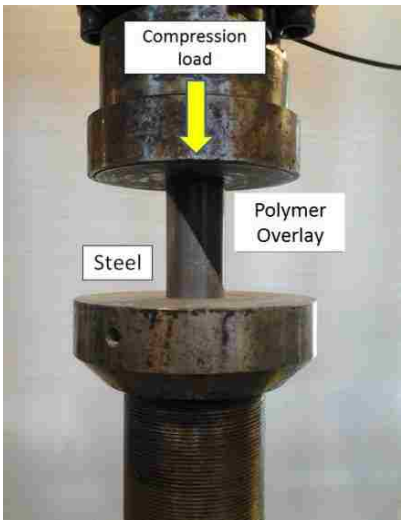

Figure 3.24: Slant shear test setup.

3.4.4 Four-point bending fatigue test

PC overlays are cast over concrete or steel substrates representing bridge decks. Under traffic loads, flexural stresses are generated in both the substrate and the overlay as shown in Figure 3.25. Compared with stresses at the top of the substrate, the stresses in the overlay will be much lower than the stresses in the substrate and can be determined using the modular ratio between the modulus of elasticity of both substrate and overlay as presented in Figure 3.25. This modular ratio is approximately 100 in the case of concrete substrate and 700 in the case of steel substrate. As a result, PC overlays would experience relatively low flexural stresses under traffic loads. Investigating fatigue behavior of the overlay under this level of stresses would take significantly long test duration. Therefore, accelerated flexure fatigue test was performed to study fatigue behavior of PC overlays.

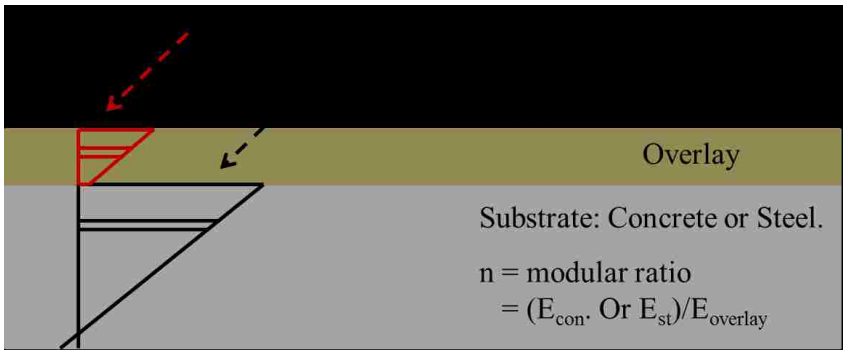

Figure 3.25: Schematic of stresses in substrate and overlay under traffic loads.

The four-point bending fatigue test was performed on nanocomposite overlay prisms prepared from the four mixes. This test was performed in order to determine the significance of adding MWCNTs on the fatigue behavior of bridge decks overlays. Moreover, the test tracked the crack and damage propagation in the overlay under repeated load. The test was performed following the guidelines of determining the fatigue life of compacted hot-mix asphalt subjected to repeated flexural bending, which were

reported in AASHTO T321- 07 (2007) standards. The fatigue test was displacement controlled cyclic test. Therefore, displacement was ramped up from zero to 1.2 mm (0.047 in) in 2 minutes then test specimens were cycled between 0.0 mm (0.0 in) and 1.2 mm (0.047 in) using a sinusoidal waveform with a frequency of 0.5 Hz. From each mix, five prisms with dimensions of 25*25*200 mm (1.0*1.0*8.0 in) were prepared in order to be tested. In order to perform the test using the MTS® Bionix servo hydraulic system, a new test fixture was designed and produced as presented in the design drawings shown in Figure 3.26. A new frame was designed and manufactured to hold 2 LVDTs at the center line of the tested specimen in order to record the displacement. Through the test, time, load, and displacement were recorded using MTS® 793 data acquisition system with a sampling rate of 10 Hz for all experiments. Figure 3.27 shows the schematic drawing of the fatigue test.

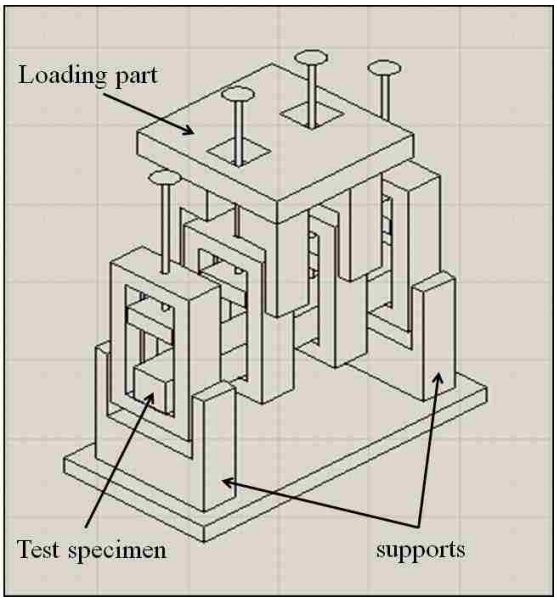

Figure 3.26: Design drawings of new fatigue test fixture.

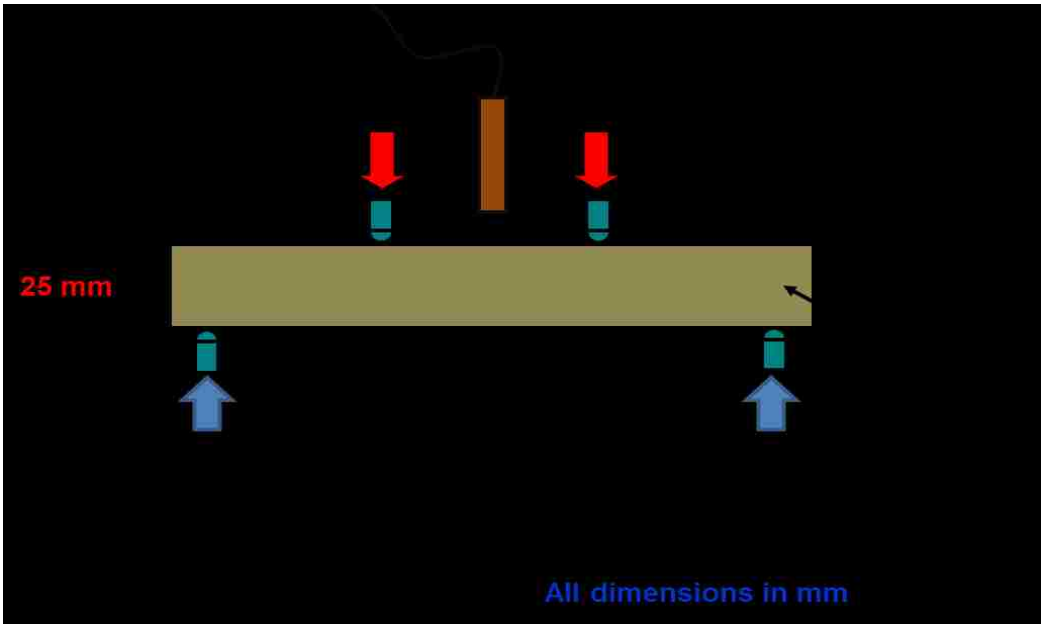

Figure 3.27: Four-point bending fatigue test schematic.

In each experiment, the specimen flexural rigidity and fatigue damage defined as the ratio between the losses in flexural rigidity at any cycle to the initial flexural rigidity were calculated using the following equations for four-point bending setup:

$$EI(i) = \left(\frac{5}{288}\right) * \frac{\Delta\,\mathrm{P(i)}*\mathrm{L\^{}3}}{\Delta\,\delta(\mathrm{i})} \tag{3.8}$$

$$D(i) = 1 - \frac{EI(i)}{EI(0)} \qquad \% \tag{3.9}$$

where *EI(i)* is the specimen flexural rigidity at any cycle, *E* is the modulus of elasticity, *I* is the cross sectional second moment of inertia, $\Delta P(i)$ is the difference between maximum and minimum loads at the same cycle, $\Delta\delta(i)$ is the corresponding difference between displacements, L is the span length of 175 mm (7.0 in.), *D(i)* is the fatigue damage in %, and *EI(0)* is the initial flexural rigidity at the 50th load cycle according to AASHTO standard. Following the AASHTO standard, the failure point was defined as the cycle

that experienced a 50% reduction in the initial flexural rigidity. Finally, Figure 3.28 shows the four-point bending fatigue test setup.

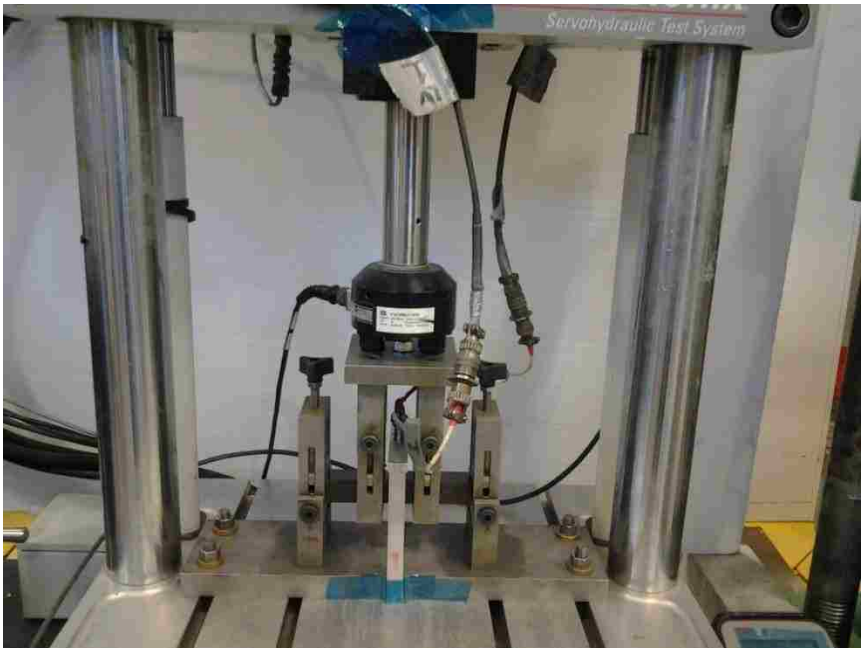

Figure 3.28: Four-point bending fatigue test setup.

3.5 Microstructural characterization of epoxy-MWCNTs Nano-composite

Characterization process of epoxy-MWCNTs nano-composite was performed on two specimens of neat epoxy and epoxy with 1.0% MWCNTs. No filler or aggregate were used in the mixes. The characterization process included microstructural and thermal characterization. This process was performed to investigate the reaction between the functionalized MWCNTs and epoxy group and to investigate the significance of incorporating MWCNTs on the epoxy microstructure.

3.5.1 Scanning Electron Microscope (SEM)

SEM was used in order to investigate the MWCNTs inside epoxy. A Hitachi S-5200 Nano SEM was used as shown in Figure 3.29. The SEM apparatus has magnification rate ranging from 100x to 2,000,000x with a guaranteed resolution of 1.7 nm at 1 Kv and 0.5 nm at 30 Kv. Samples were placed on a specimen holder using double sided tape.

Figure 3.29: Hitachi S-5200 Nano SEM apparatus.

3.5.2 Fourier Transform Infrared Spectroscopy (FTIR)

Samples of neat epoxy and epoxy incorporating MWCNTs were analyzed with biconical reflectance Micro-Fourier Transform Infrared Spectroscopy (Micro-FTIR). The used apparatus, shown in Figure 3.30, was a Nicolet Nexus 670 FTIR and a Continuum microscope with a Globar source, XT-KBr beam splitter and a MCT-A detector over a 100x100 micron area with a 4-cm^{-1} resolution. Spectra were background corrected using a reflective gold slide and converted to absorbance using the Kramers-Kronig equation. This was done to correct the derivative-like nature of the reflectance spectra.

Figure 3.30: Nicolet Nexus 670 FTIR apparatus.

3.5.3 Thermal characterization

Thermal Gravimetric Analysis (TGA) and Differential Scanning Calorimetry (DSC) were performed in order to investigate the thermal stability of epoxy-MWCNTs nanocomposite. Neat epoxy and epoxy with 1.0% MWCNTs samples were tested, and an analysis of weight change and differential heat flow was performed. The used apparatus was TGA/DSC model SDT Q600 as shown in Figure 3.31. The test was performed using a heating rate of 10 ^{o}C/min starting from room temperature to 1000 ^{o}C and purged with nitrogen flow of 60 ml/min. The results recording resolution was 0.001 ^{o}C.

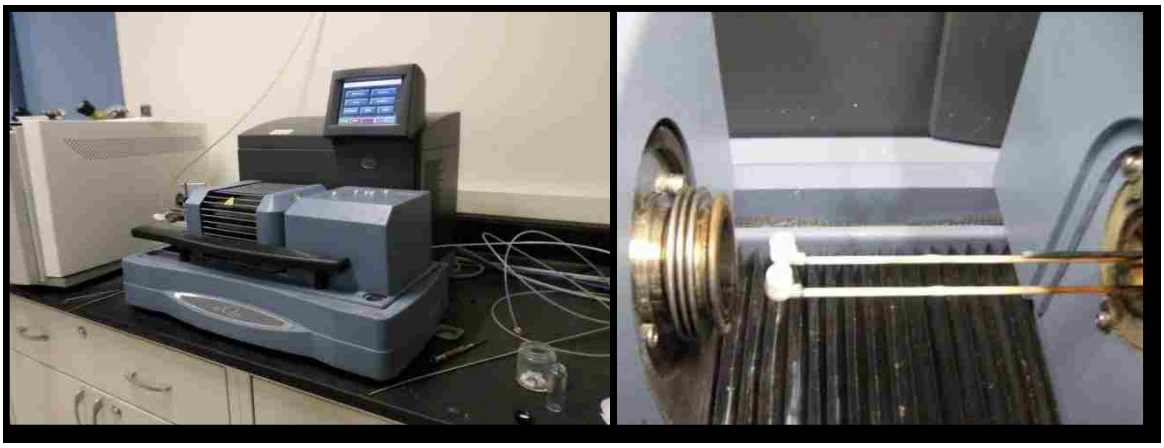

Figure 3.31: TGA/DSC SDT Q600 apparatus, and specimen holder.

Chapter 4 Results and Discussion

4.1 Introduction

This fourth chapter reports the experimental results and statistical analysis for all the experiments reported earlier. The first part of this chapter discusses the results related to tests performed on polymer concrete, while the second part discusses the results of polymer concrete overlays. The third part of the chapter provides discussions on the microstructural and thermal characterization performed.

4.2 Fresh properties and mechanical characterization of Polymer Concrete mixes

4.2.1 Flowability test

Figure 4.1 shows the variation of the flowability of four polymer concrete (PC) mixes due to incorporating MWCNTs. It was obvious that adding MWCNTs affected the flowability. The flowability was decreased by 57, 62, and 66% with the addition of 0.5, 1.0, and 1.5% of MWCNTs, respectively. This reduction in flowability can be explained as the result of the increased viscosity of epoxy when incorporating MWCNTs. it is important to note that in spite of the reduction in flowability of PC with 0.5, 1.0 and 1.5% MWCNTs compared with neat PC, all PC specimen casting was not affected. However, PC specimens incorporating MWCNTs required additional compaction to produce good specimens.

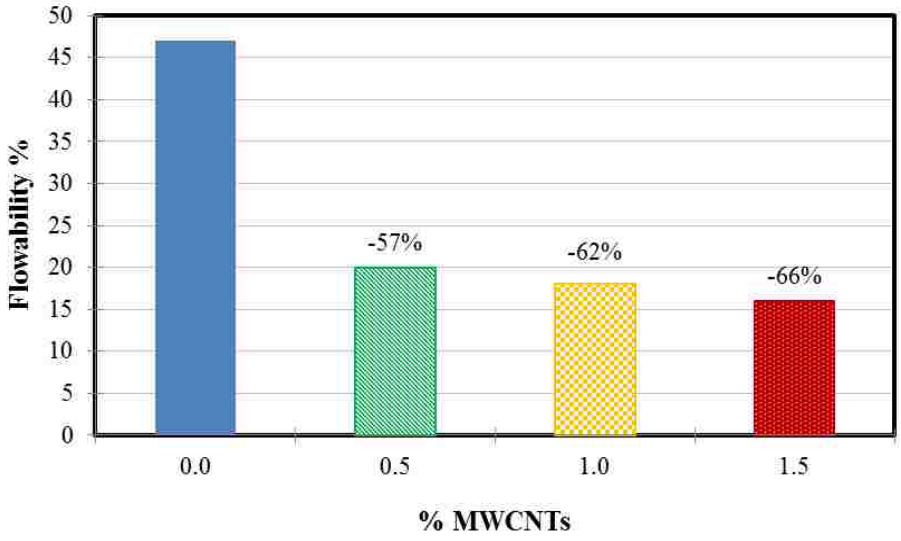

Figure 4.1: Variation of flowability of PC mixes with varying MWCNTs content.

4.2.2 Static mechanical response

4.2.2.1 Compressive strength test

Compression tests were performed on five cylinders for each mix. Figure 4.2 presents the stress-strain curves of test specimens plotted using the recorded loads and displacements.

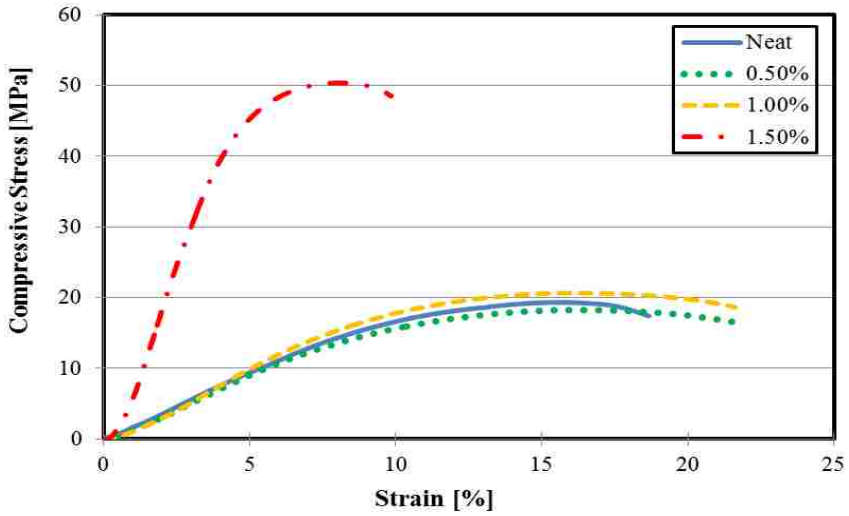

Figure 4.2: Compression stress-strain curves of PC mixes incorporating varying contents of MWCNTs.

Young's modulus of elasticity in compression defined as the initial slope of the stress-strain curve was computed for each mix and the variation of this modulus is presented in Figure 4.3. The modulus of elasticity was decreased by 6.6% by adding 0.5% MWCNTs, increased by 12% with 1.0% MWCNTs and incredibly increased by 539% with 1.5% MWCNTs. Statistical analysis using student *t*-test was performed on the results and proved that no statistical difference was found between Young's modulus of elasticity of PC mixes with 0.5 and 1.0% MWCNTs and neat mixes. However, PC mixes with 1.5% MWCNTs proved to have significantly higher Young's modulus of elasticity compared with neat specimens. Figure 4.4 represents the variation of compressive strength of the tested mixes. The compressive strength was decreased by 6.7% by adding 0.5% MWCNTs, increased by 6.7% with 1.0% MWCNTs and again significantly increased by 153% with 1.5% MWCNTs. Compressive strength of 0.5 and 1.5% MWCNTs specimens were found to be significantly different from neat specimens, while no statistical difference was proven with specimens incorporating 1.0% MWCNTs.

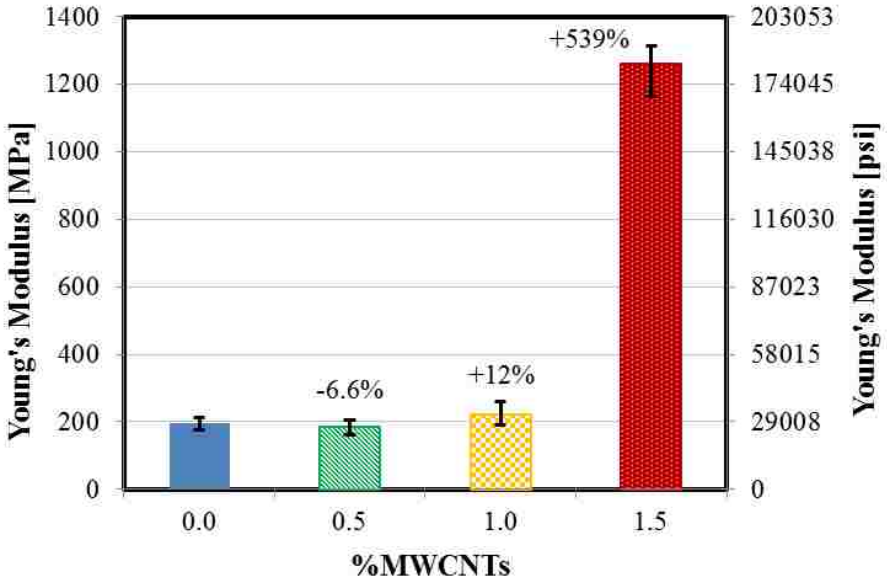

Figure 4.3: Compression Young's modulus of elasticity of PC with varying MWCNTs content.

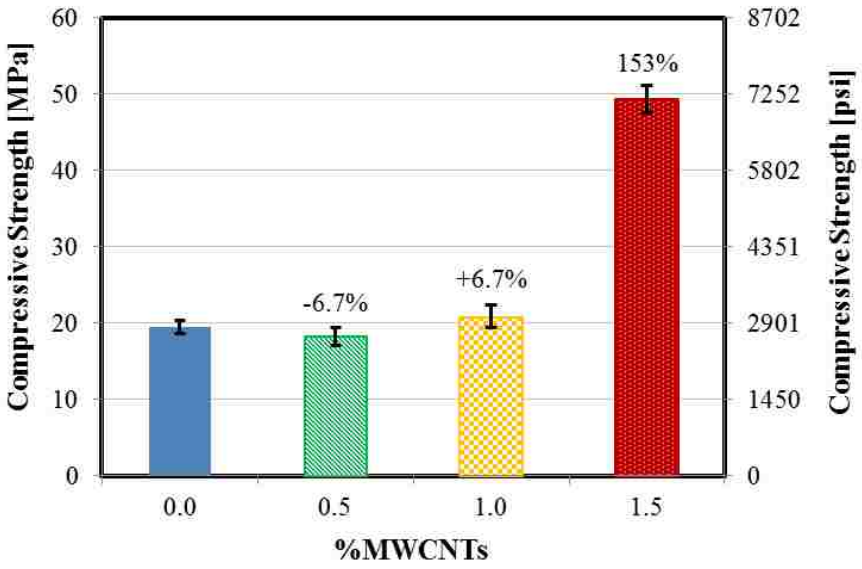

Figure 4.4: Compressive strength of PC with varying contents of MWCNTs.

Failure strain, defined as the strain corresponding to failure stress, was observed for each mix and plotted in Figure 4.5. The strain was reduced by 6.3, 8.8 and 51% by adding 0.5, 1.0 and 1.5% MWCNTs, respectively. Failure strains of all specimens incorporating MWCNTs were proven to be significantly different from the failure strains of neat specimens. Furthermore, Figure 4.6 represents the variation of compressive toughness, defined as the area under stress-strain curve, of the tested mixes. Compressive toughness increased by 12, 27 and 35% by adding 0.5, 1.0 and 1.5% MWCNTs, respectively. Statistical analysis using student *t*-test was performed on the results and proved significant difference between the toughness of specimens incorporating MWCNTs and neat specimens.

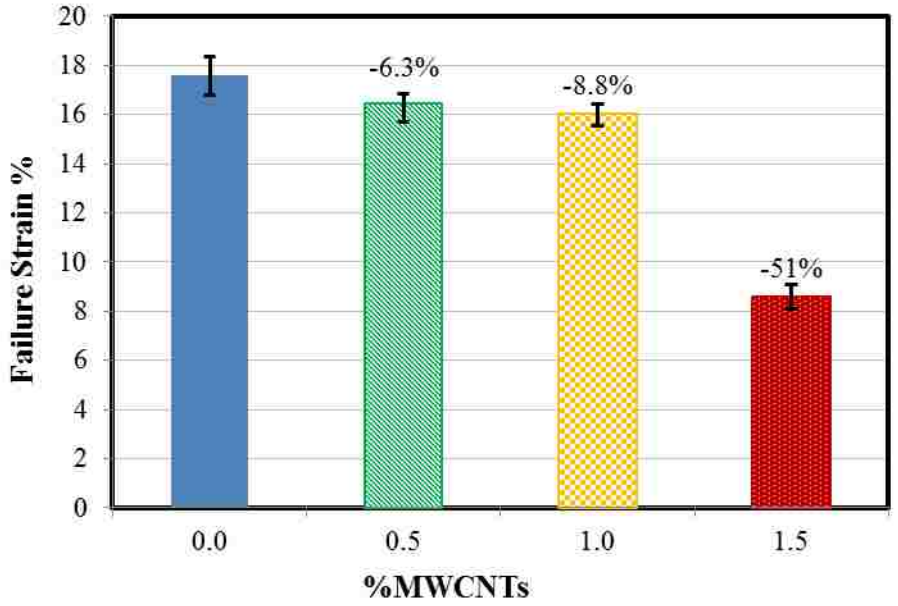

Figure 4.5: Compressive failure strain of PC with varying contents of MWCNTs.

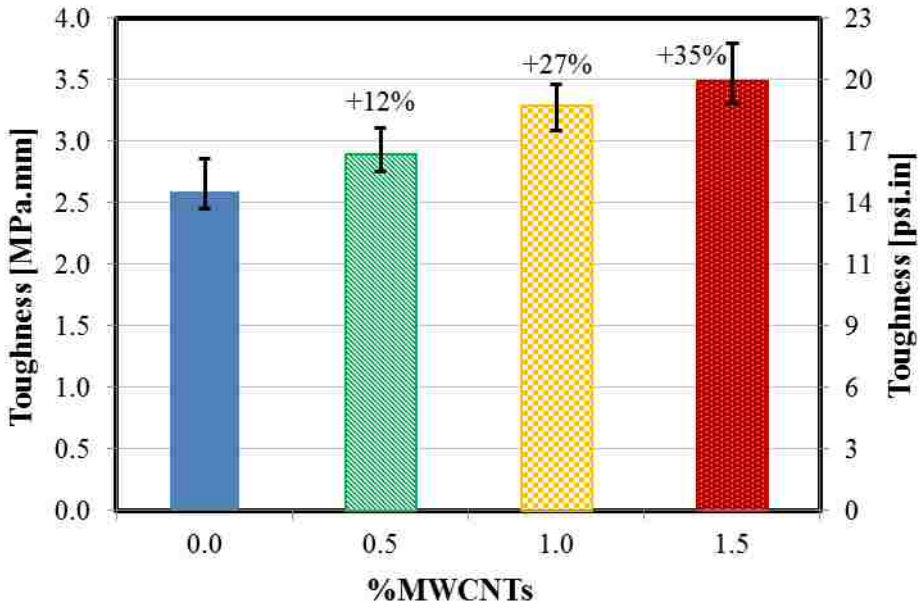

Figure 4.6: Toughness of PC with varying contents of MWCNTs.

Finally, failure mode of neat specimens in compression was different when compared with specimens incorporating MWCNTs. While failure in the neat specimens was observed to happen on inclined failure line inside the specimens, specimens with MWCNTs were observed to take barrel shape prior to failure and fail axially as shown in Figure 4.7. After reaching the compressive strength of each specimen, displacement was increased significantly without increase in load and specimens were crushed as shown in Figure 4.8.

Figure 4.7: Different failure modes of Compressive strength test.

Figure 4.8: Crushing of PC specimens at failure under axial compression loads.

4.2.2.2 Flexural strength test

As mentioned before, the three-point bending flexure test was performed on the four PC mixes in order to investigate the PC flexural behavior. Using the recorded applied forces and mid-span deflections, stress-strain curves were plotted for the tested specimens as presented in Figure 4.9. The figure also shows the fracture pattern of specimens at failure.

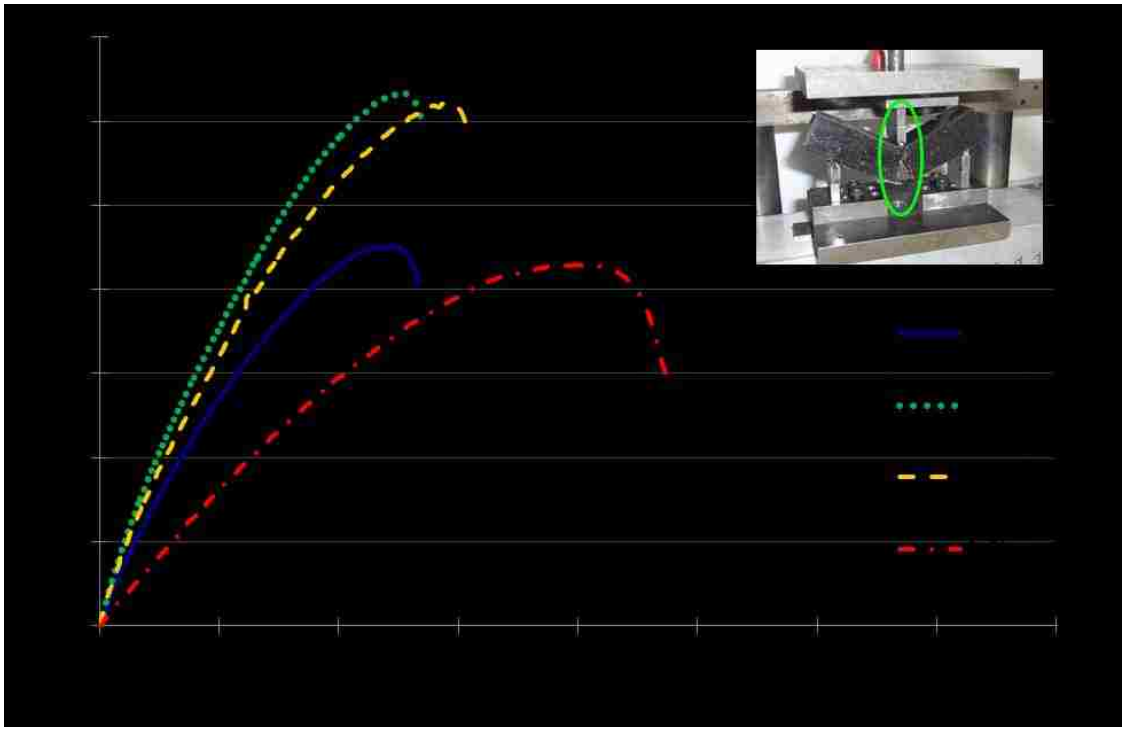

Figure 4.9: Stress-strain curves of flexure test of PC with varying MWCNTs content.

Moreover, the Young's modulus of elasticity in flexure represented by the initial slope of the curve was computed for each mix and the variation of this modulus is shown in Figure 4.10. The modulus of elasticity of PC increased by 15% with adding 0.5% MWCNTs, and decreased by 40% with 1.5% MWCNTs. No change was observed with adding 1.0% MWCNTs. Statistical analysis using student *t*-test proved that there is no

significant statistical difference in the case of 0.5, and 1.0% MWCNTs, but a significant statistical difference with PC incorporating 1.5% MWCNTs.

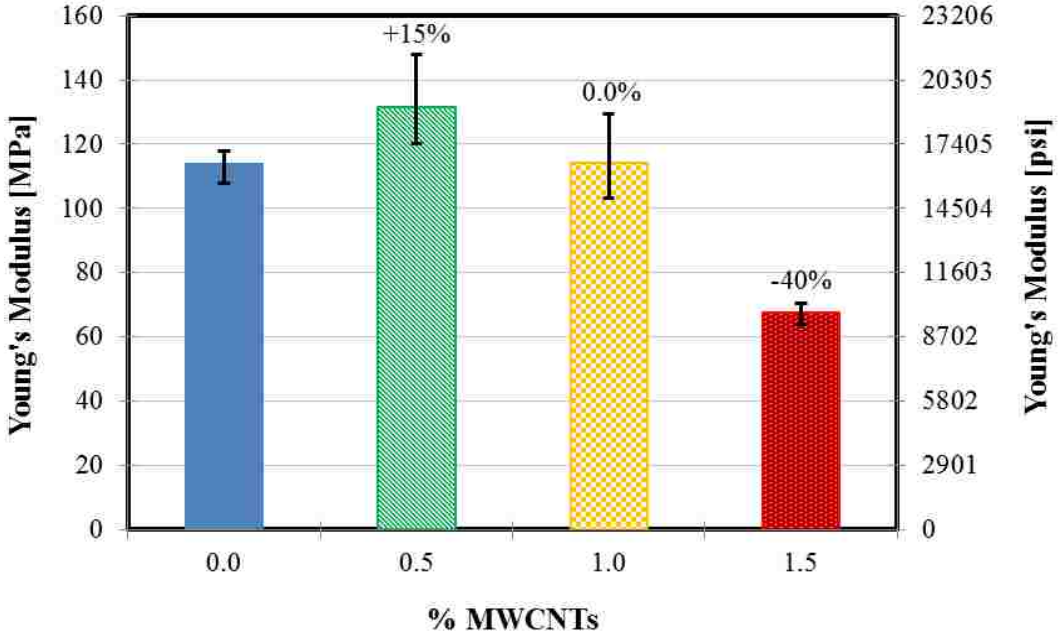

Figure 4.10: Flexural Young's Modulus of Elasticity of PC with varying MWCNTs content.

It is also important to note the change in the ultimate flexural strength and failure strain of the specimens. Figures 4.11 and 4.12 show the effect of adding MWCNTs on the strength and strain capacities of PC, respectively. Incorporating 0.5 and 1.0% MWCNTs in the PC mix increased the ultimate flexural strength by 41 and 26%, respectively, while the 1.5% MWCNTs decreased it by 2%. In the case of 0.5 and 1.0% MWCNTs, significant statistical difference between ultimate flexural strengths was proven by statistical analysis, while no statistical difference was found for 1.5% MWCNTs. Failure strain was increased by 3, 12, and 65% with addition of 0.5, 1.0, 1.5% MWCNTs, respectively. For failure strains, no statistically significant difference was found in the case of 0.5 and 1.0% MWCNTs, while a significant difference was proven with 1.5% MWCNTs.

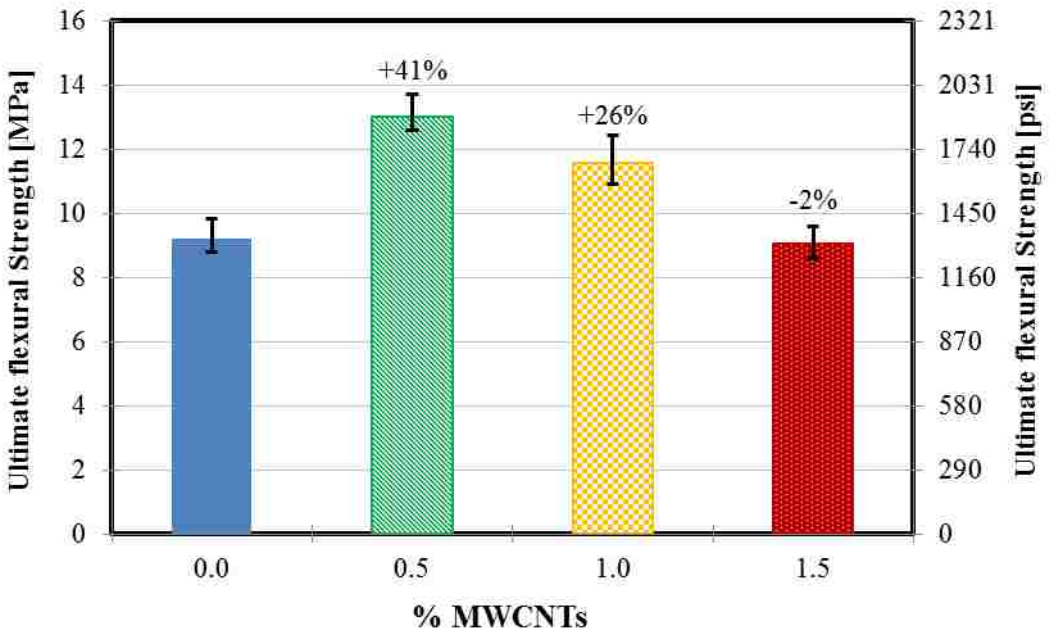

Figure 4.11: Ultimate flexural strength of PC with varying MWCNTs content.

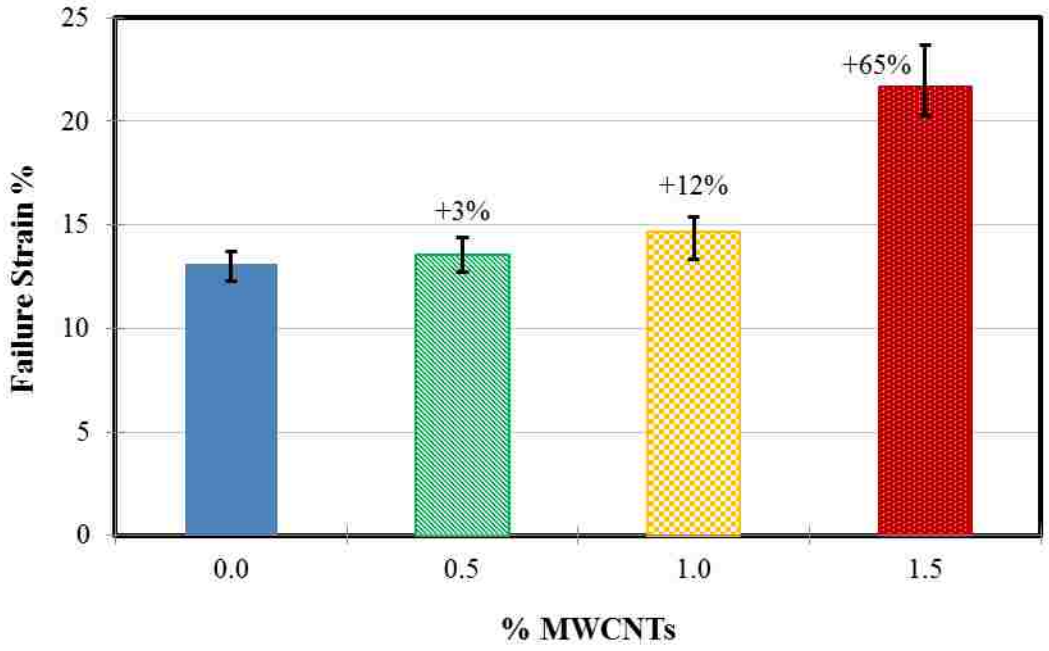

Figure 4.12: Flexural failure strain of PC with varying MWCNTs content.

The area under the flexure stress-strain curves, defined as flexural toughness, was calculated for each mix. The flexural toughness increased by 41, 36, and 54% with adding 0.5, 1.0, and 1.5% MWCNTs, respectively. Statistical analysis proved significant statistical differences between the toughness of the mixes incorporating MWCNTs and the neat mix. Figure 4.13 represents the variation of PC flexural toughness.

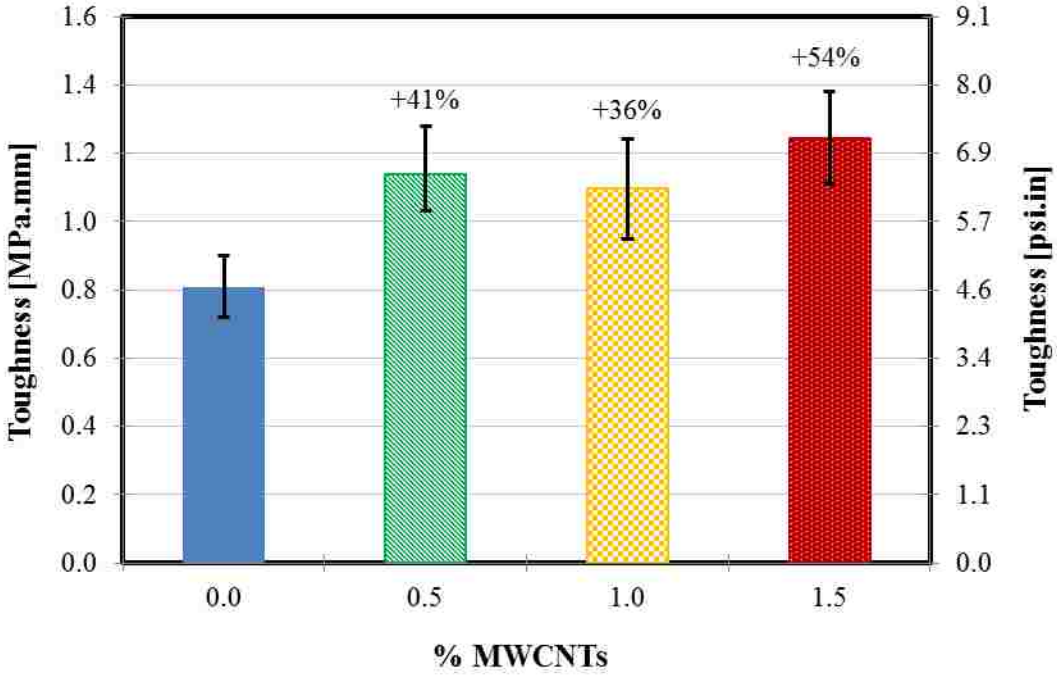

Figure 4.13: Variation of PC flexural toughness with varying MWCNTs content.

4.2.2.3 Shear Strength test

In the shear test, shear stress and strain were calculated at each time interval and stress-strain curves were drawn as shown in Figure 4.14.

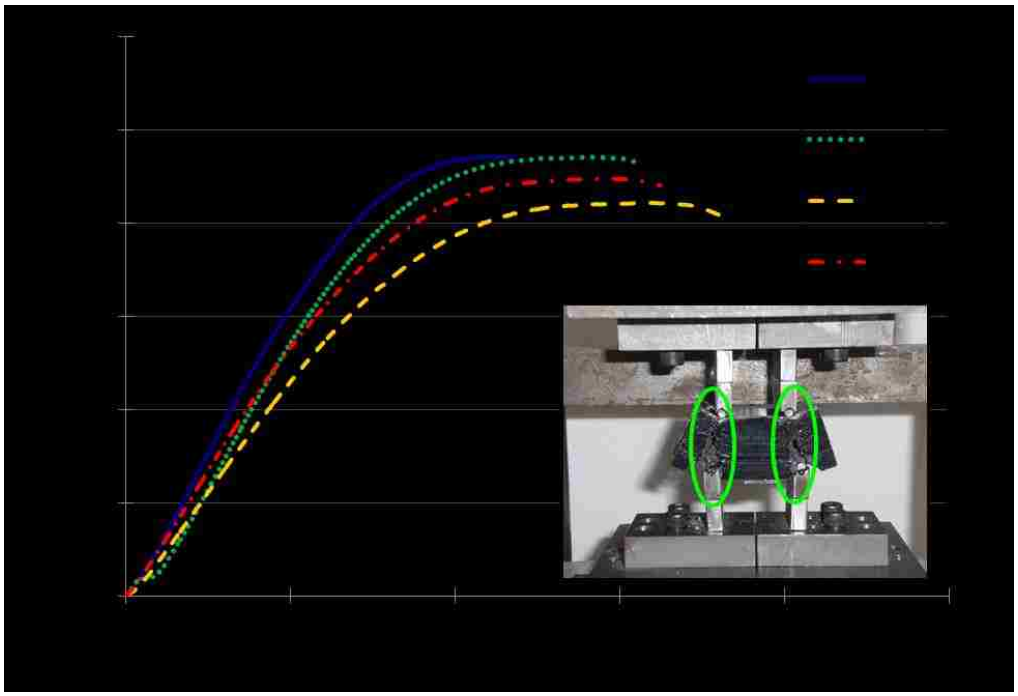

Figure 4.14: Shear stress-strain curves and failure mode for PC with varying MWCNTs content.

The shear modulus was computed from previous curves, and the variation of the elastic modulus was plotted as shown in Figure 4.15. It can be observed that adding MWCNTs decreased the shear modulus of PC. The decrease was 18, 35, and 32% with 0.5, 1.0, and 1.5% MWCNTs, respectively. Significant statistical differences were proved between shear modulus in the cases of 1.0 and 1.5% MWCNTs, while no difference was found in the case of 0.5% MWCNTs.

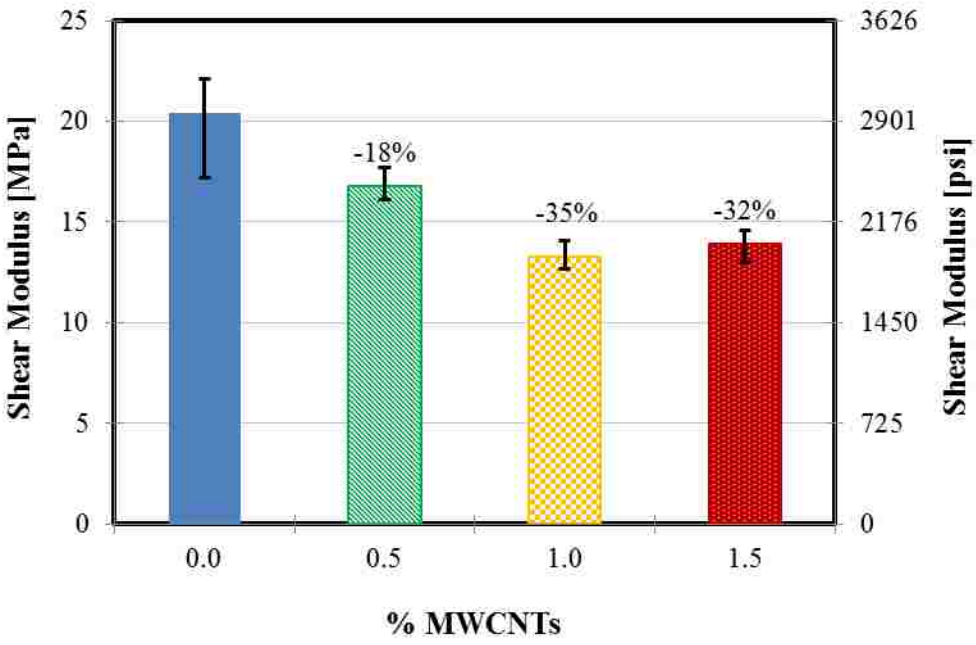

Figure 4.15: Variation of shear modulus of PC mixes with varying MWCNTs content.

Furthermore, Figure 4.16 represents the values of ultimate shear strength for the four mixes. The strength was decreased by 5, 13, 9% for addition of 0.5, 1.0, 1.5% MWCNTs, respectively. Significant statistical difference was found between the neat mix and 1.0% MWCNTs, while no significant difference was proven in the cases of 0.5 and 1.5% MWCNTs. On the other hand, the failure shear strain was significantly increased by adding MWCNTs as shown in Figure 4.17. The increase was 33, 55, and 52% with 0.5, 1.0, 1.5% MWCNTs, respectively. The increase in shear strain was proven to be statistically significant.

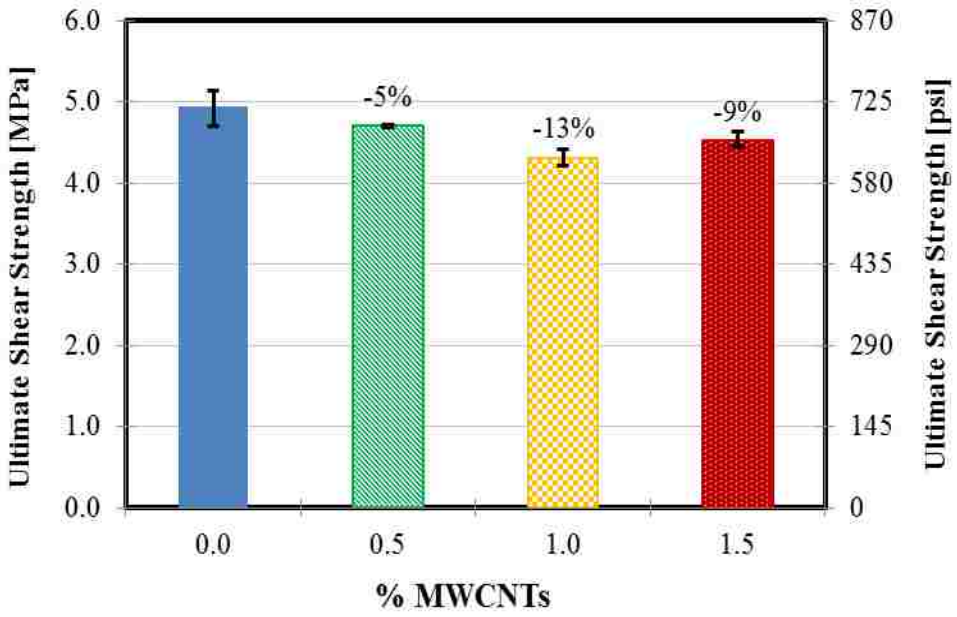

Figure 4.16: Ultimate shear strength of PC mixes with varying MWCNTs content.

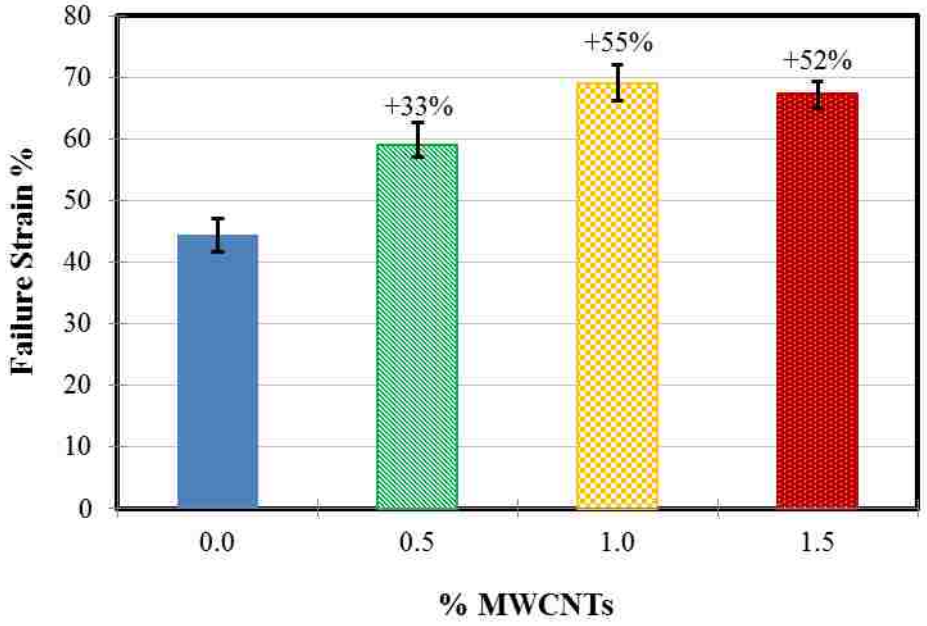

Figure 4.17: Shear strain at failure of PC mixes with varying MWCNTs content.

Shear toughness, defined as the area under shear stress-strain curves, was also calculated. Shear toughness was observed to increase significantly with addition of MWCNTs. The increase was 32, 46, 49% with 0.5, 1.0, 1.5% MWCNTs, respectively as shown in Figure 4.18. This difference was also found to be statistically significant.

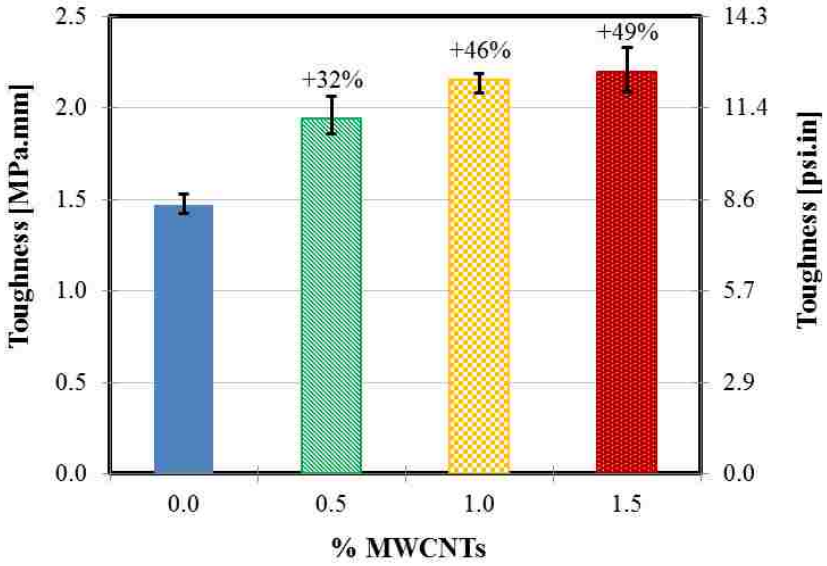

Figure 4.18: Shear toughness of PC mixes with varying MWCNTs content.

4.2.2.4 Creep behaviour test

Three cylinders were tested under sustained axial load taken as a percentage of the compressive strength for each mix. Figure 4.19 represents plots of valid records of total strain at each time interval versus test time for each mix. It is important to state that through the test, some strain gauges were damaged, and the corresponding records were discarded. Creep compliance was calculated at each creep-time interval, and creep compliance versus creep time curves were plotted as shown in Figure 4.20.

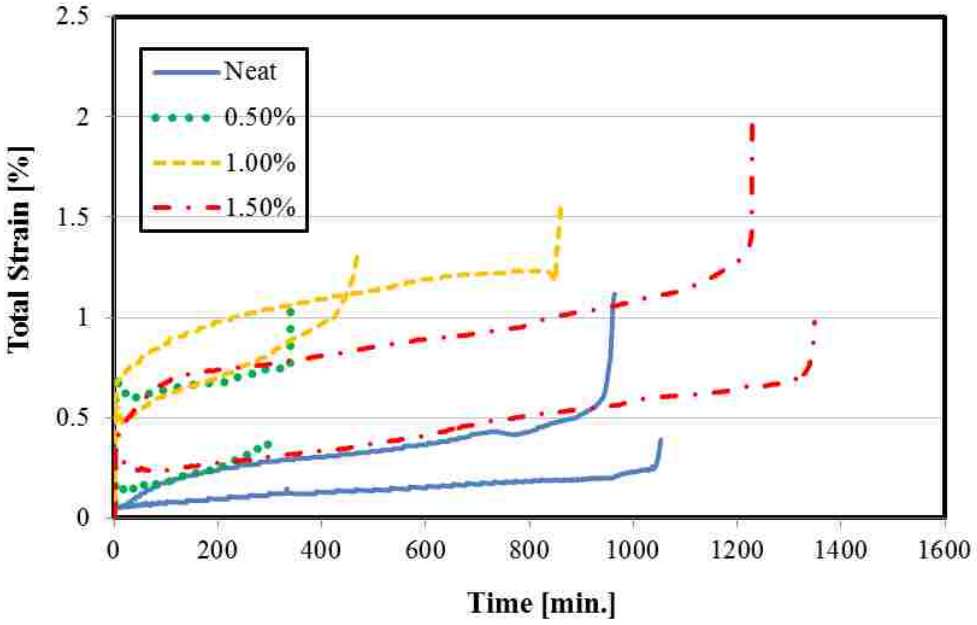

Figure 4.19: Total strain of PC specimens with varying contents of MWCNTs under sustained axial load.

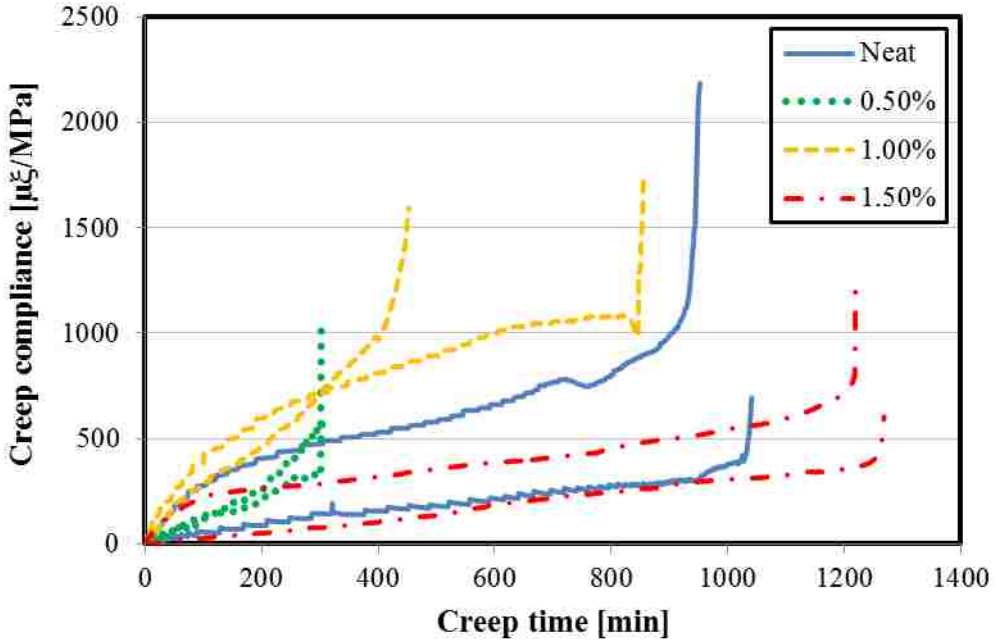

Figure 4.20: Creep compliance of PC specimens with varying contents of MWCNTs.

From Figure 4.20, creep compliance can be divided into three distinct stages. The first stage is the primary creep characterized by logarithmic relationship with high slope. Sometimes this stage was very small or did not exist as shown with the first sample of 1.5% MWCNTs. The second stage is the secondary or steady state creep with a relatively low slope compared with the primary creep slope. This stage usually forms most of the creep time of the specimen. The third stage is the tertiary creep with significantly high slope leading to failure and crushing of the specimen. It is obvious from the figure that the highest creep compliance over time was specimens of 1.0% MWCNTs, while the lowest creep compliance over time was specimens of 1.5% MWCNTs. It is also important to note that tertiary creep started very early in specimens of 0.5% MWCNTs (after 250 minutes), while started after 400-800 minutes for 1.0% MWCNTs specimens. Tertiary creep of 1.5% MWCNTs specimens started after 1200 minutes and were compared with tertiary creep of neat specimens, which started after approximately 9500 minutes of starting the test. Moreover, the creep compliance at failure was calculated, and the variation of this compliance was plotted in Figure 4.21. The creep compliance at failure was decreased by 68, 7 and 35% by incorporating 0.5, 1.0 and 1.5% MWCNTs, respectively. Statistical analysis using student *t*-test was performed on the valid results and proved no difference. This can be attributed to the large variation in results obtained from each mix as shown in Figure 4.21 and the lack of valid records. It is important to state that the creep compliance at failure of specimens from each mix did not occur at the same time. Therefore, Figure 4.22 represents the variation of failure time of PC mixes under sustained axial loads. Failure was accelerated by 68 and 34% with 0.5 and 1.0% MWCNTs, respectively, and delayed by 28% in the case of 1.5% MWCNTs. No

statistical difference was proven in the case of 1.0 and 1.5% MWCNTs, while statistical analysis of failure time of specimens with 0.5% MWCNTs proved to be significantly different from neat specimens.

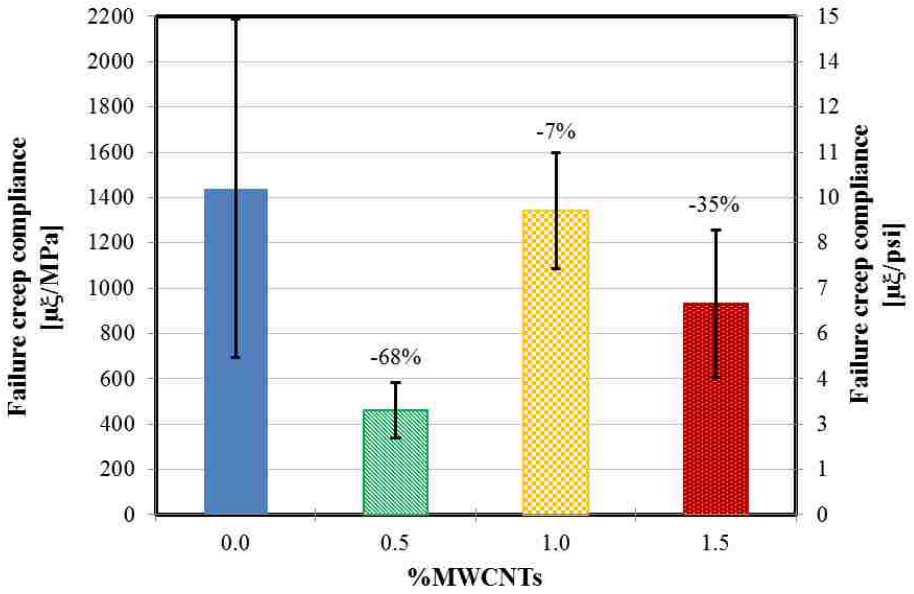

Figure 4.21: Failure creep compliance of PC specimens with varying contents of MWCNTs.

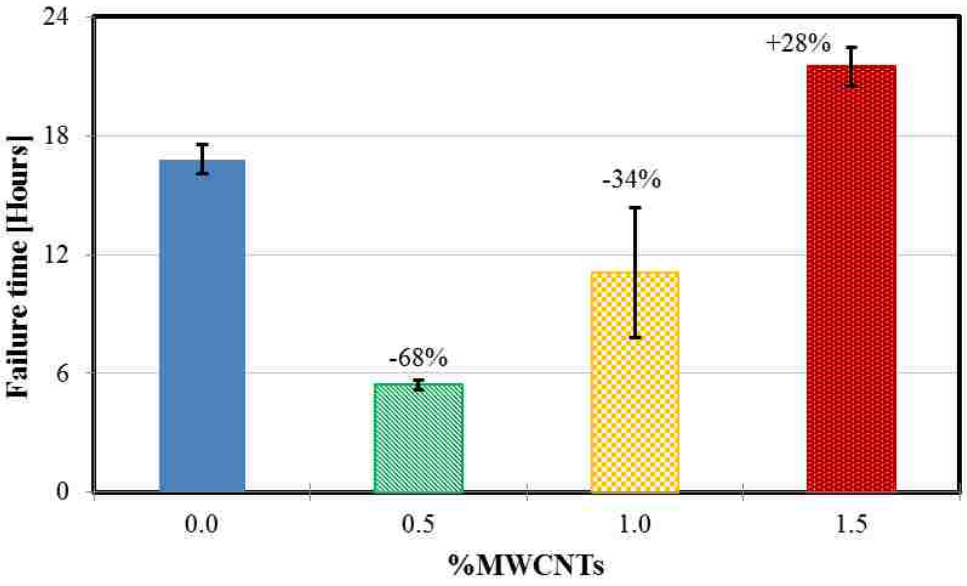

Figure 4.22: Failure time of PC specimens with varying contents of MWCNTs under sustained axial load.

Finally, creep failure occurred in similar mode to that observed in the compression test. Neat specimens experienced failure through inclined failure lines followed by crushing, while specimens with MWCNTs formed the barrel shape and then axial crushing took place as shown in Figure 4.23.

Figure 4.23: Crushing of PC specimens at failure under sustained axial loads.

4.2.2.5 Static mechanical response discussion

Observing the behaviour of PC with MWCNTs under flexure and shear stresses, it is obvious that addition of MWCNTs modified the microstructure of PC significantly and altered its mechanical performance. MWCNTs modification enhanced the flexural strength and had no significant effect on the shear strength. On the other hand, it improved the flexural failure strain and made a significant improvement in the shear failure strain as well. Furthermore, it significantly enhanced the flexural and shear toughness. These enhancements in toughness and failure strain imply improvement in PC crack resistance and durability. It also indicates improvement in the flexibility (failure strain). This significant effect with low content of MWCNTs, <1.0%, might be attributed

to the ability of the MWCNTs to produce a new epoxy-MWCNTs nanocomposite with improved mechanical properties specifically the flexural strength and strain as well as the shear strain. Our observations are supported by observations of other researchers *(Ganguli et al. 2005, and Soliman et al. 2012)* that showed functionalized MWCNTs to act as micro fibers (each individual fiber is 10-20 nm diameter and 10-30 µm long) so as to bridge microcracks. Moreover, the functionalization of MWCNTs also allows the MWCNTs to chemically bond to the epoxy matrix as shown in Figure 4.24 and thus alter the strength, failure strains and stiffness of PC incorporating MWCNTs. However, high MWCNTs content (1.5%) did not show the same effect of low content of MWCNTs (<1.0%) on PC flexure and shear properties except significantly increasing flexure and shear failure strains and toughness. This can be attributed to the reduced flowability (reduced viscosity) of the nanocomposite leading to air entrapment and lower level than optimal compaction.

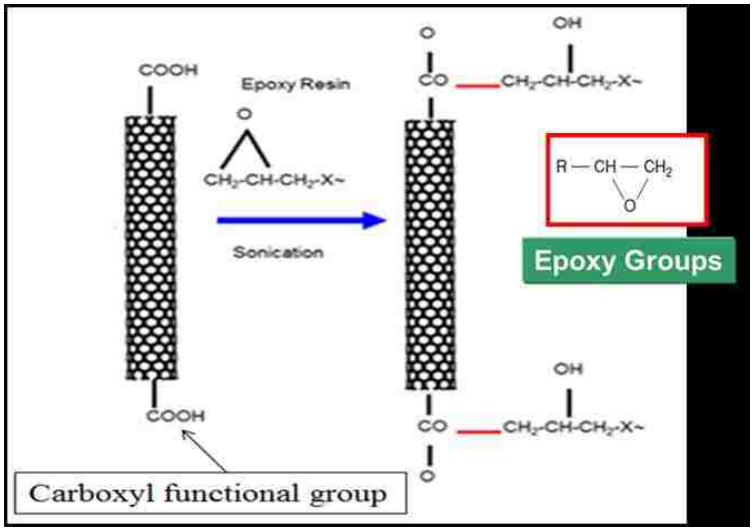

Figure 4.24: Schematic drawing of the reaction between functionalized MWCNTs and epoxy groups *(Soliman 2011).*

Observing the behaviour of PC with MWCNTs under compression and consequently under axial creep, we can conclude that neat PC fabricated of this type of epoxy and same PC with MWCNTs are not suitable for structural applications under axial loading. Neat PC reported relatively low compressive strength compared with conventional concrete. Moreover, creep failure of PC took place in a very short time (less than 18 hours). This can be attributed to the relatively high binder content (18% of total weight) in the used PC mixes compared with the conventional binder content (8-10% of total weight) typically used in overlays. Under axial compressive loading, PC would experience two types of indirect stresses. These stresses are the shear stresses generated at 45^{o} inclined planes as explained by Mohr's cycle, and the lateral tensile stresses at the outer fibers of the specimen generated from the barrel shape extension of the material due to Poisson's effect. In neat specimens under axial loads, the shear strength was weaker than the tensile strength of the material. Therefore, failure occurred in these specimens on inclined planes as shown in Figure 4.7. With low content of MWCNTs (<1.0%), two factors took place. First, adding MWCNTs succeeded to increase Poisson's ratio and thus allow for higher lateral deformation (lateral flexibility). This increased the lateral tensile stresses developed in the specimens under axial loads. As the low content of MWCNTs did not increase the tensile strength proportionally, the higher lateral tensile stresses resulted in premature failure of PC by axial cracks then crushing as in the case of 0.5% MWCNTs. Second, increasing the MWCNTs content allowed the material to have higher resistance to lateral tensile stresses and therefore fail at a slightly higher compressive strength than the case with 0.5% MWCNTs as observed in the case of 1.0% MWCNTs.

Also the 0.5 and 1.0% MWCNTs obviously increased the shear strength of PC, so tension strength rather than shear strength governed the fracture in these cases.

In the case of 1.5% MWCNTs (relatively high content of MWCNTs) under compression, Poisson's ratio and hence lateral deformation further increased but the material tensile strength was significantly enhanced. This improvement in tensile strength is also accompanied by improvement in shear strength which contradicts the results from the shear test. Since the tensile stresses did not exceed the tensile strength, the shear strength governed fracture in this case. Therefore, failure took place on inclined lines as shown in Figure 4.25 indicating shear cohesive failure but at a significantly higher strength than neat specimens. This mechanism is schematically shown in Figure 4.26.

Figure 4.25: Cohesive shear failure under axial loading in the case of 1.5% MWCNTs.

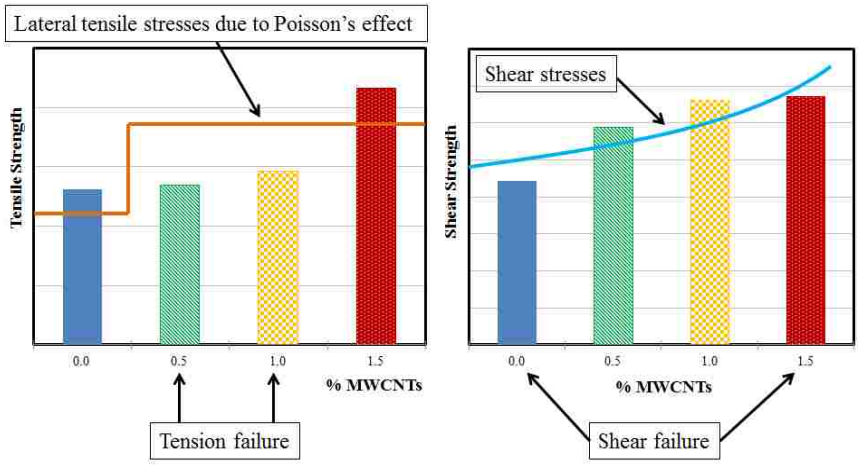

Figure 4.26: Schematic of failure mechanism of PC with varying content of MWCNTs in compression and creep tests.

Finally, the effect of workability of high content of MWCNTs (1.5%) might have not been significant in compression and creep which was dominated by the effect of lateral strain and limited shear capacity. Moreover, flexural behavior under this content of MWCNTs is difficult to explain because of its combined effect of tension, compression and shear stresses.

4.2.3 Dynamic mechanical response

4.2.3.1 Charpy impact test

Figure 4.27 shows the variation of the recorded energy during Charpy impact testing for the four PC mixes. The impact energy increased by 8, and 17% with adding 0.5, and 1.0% MWCNTs, respectively, while was decreased by 8% with 1.5% MWCNTs. Statistical analysis showed all the results to be non-different at all MWCNTs levels. However, the failure mode showed combined flexure and shear fracture in all specimens as shown in Figure 4.28.

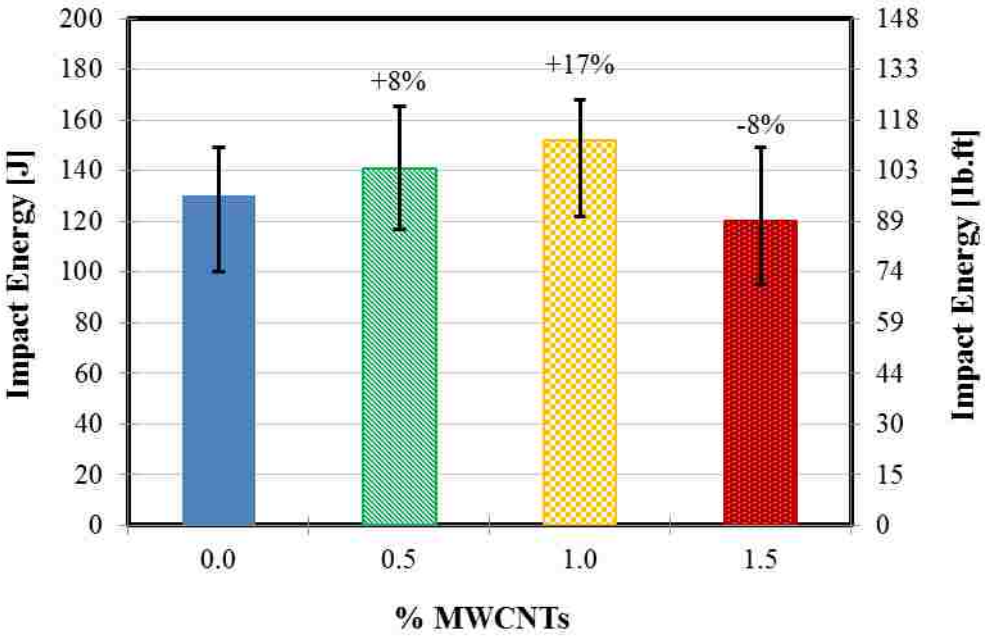

Figure 4.27: Results of Charpy impact test.

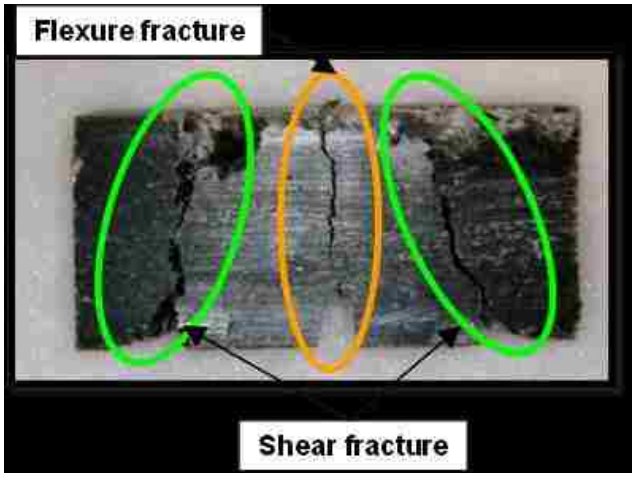

Figure 4.28: Failure mode of Charpy impact test of PC specimens.

4.2.3.2 Low-velocity impact test

In the low-velocity impact test, the impact force and the absorbed energy were recorded. The recorded results showed that adding MWCNTs decreased the sudden drop in PC resistance to impact forces as shown in Figure 4.29. This drop typically happens as the impact target breaks the concrete and starts to penetrate the specimen. Figure 4.30 shows values of the maximum force required to break specimens made of the four mixes. The maximum force increased by 9% with adding 1.0% MWCNTs, while the decrease approached 4 and 3% by adding 0.5, and 1.5% MWCNTs, respectively. No significant difference was found in the impact force in PC specimens with and without MWCNTs.

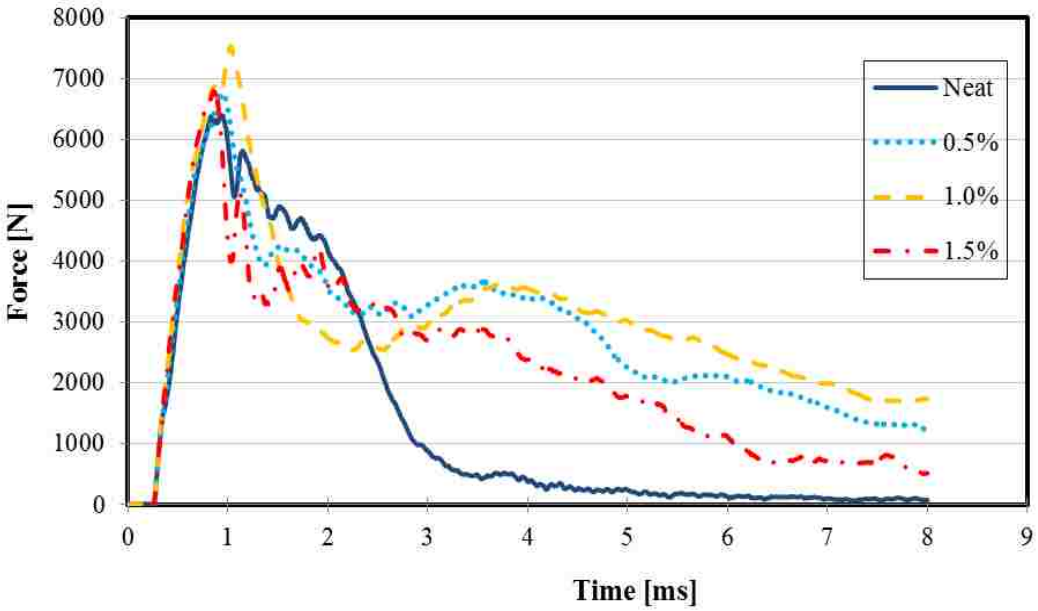

Figure 4.29: Effect of MWCNTs in decreasing the drop in PC resistance to impact loads. The significant increase in the residual strength after the main impact event (peak force) in PC with MWCNTs specimens reflect the ability of PC incorporating MWCNTs to dissipate and absorb energy compared with neat PC.

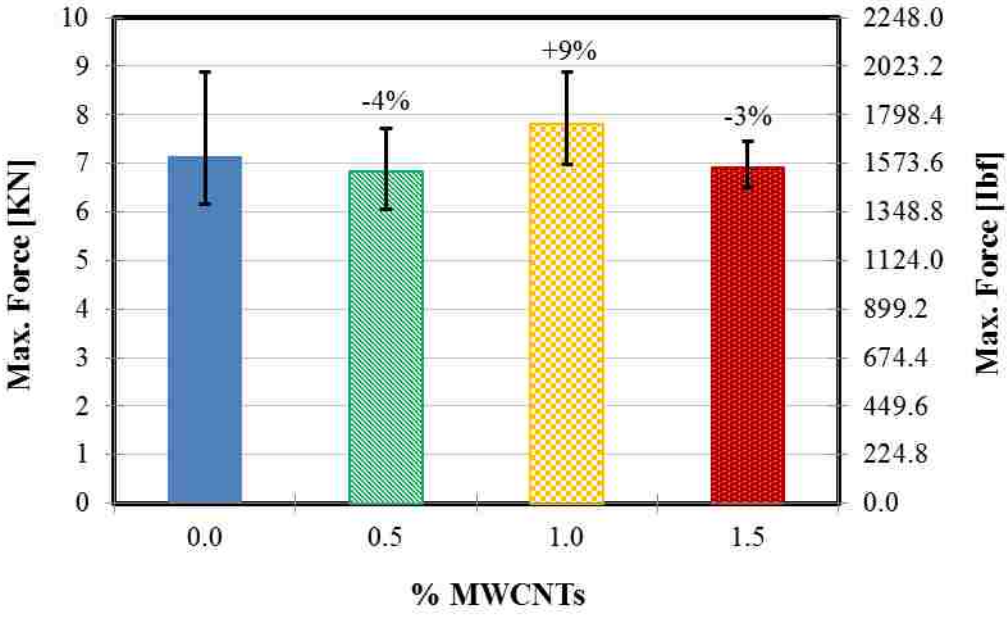

Figure 4.30: Variation of PC maximum impact resistance in low-velocity impact test with varying MWCNTs content.

This observation is also confined by observing the change of target velocity in Figure 4.31. It is obvious that the MWCNTs increased the difference between the initial velocity and the final velocity. The significant reduction of penetration velocity (i.e. slowdown of the impact target inside the PC matrix) incorporating 0.5 and 1.0% MWCNTs is shown in Figure 4.31 and the inset figure.

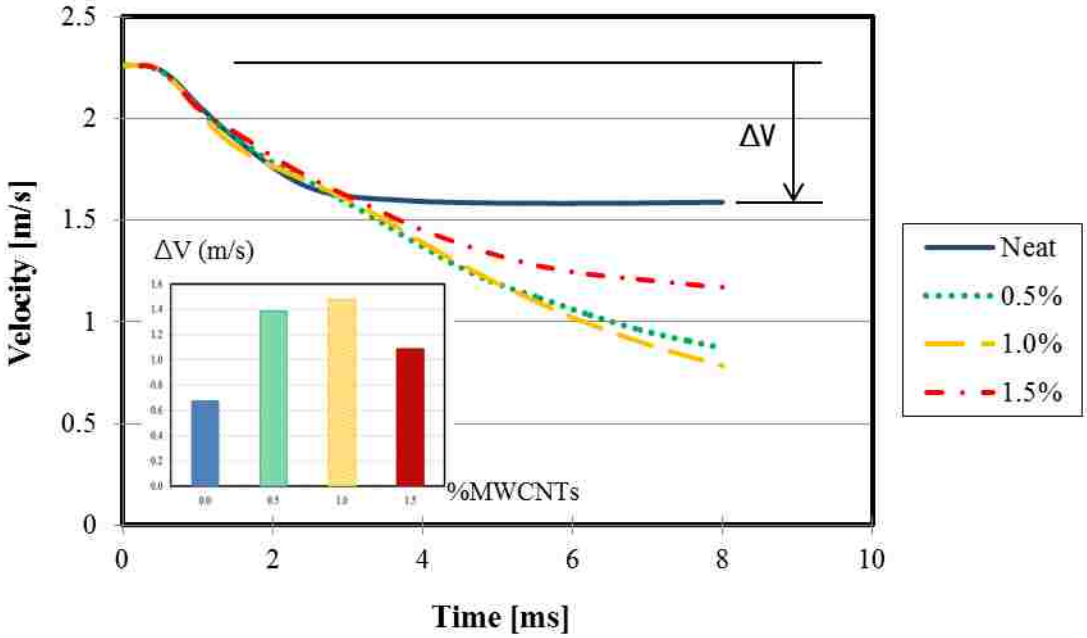

Figure 4.31: Effect of MWCNTs on slowing down impact target and reducing penetration velocity after impact.

Furthermore, Figure 4.32 shows the absorbed energy recorded in the four mixes. It also shows a comparison between the cracking patterns of impact specimens of PC incorporating MWCNTs and neat PC specimens. The absorbed energy increased by 29, 36, and 19% in the case of 0.5, 1.0, 1.5% MWCNTs, respectively. A statistical analysis using student *t*-test was performed and proved that the difference between the impact energy for PC mixes with 0.5% and 1.0% MWCNTs to be significantly higher than that of neat PC. No significant difference was observed for PC with 1.5% MWCNTs.

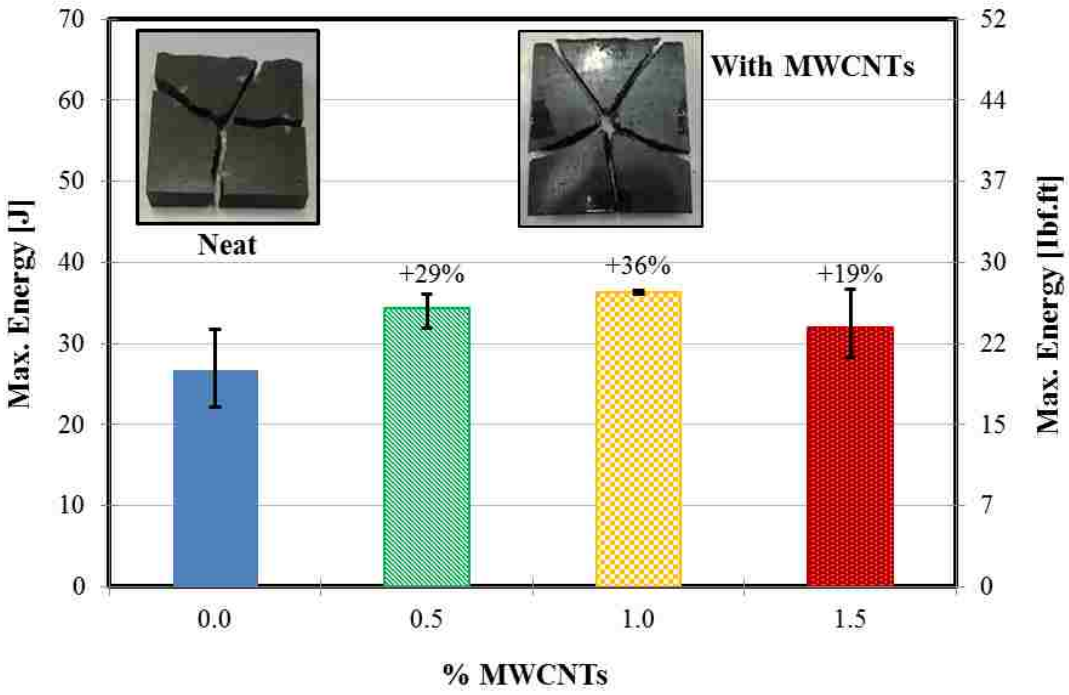

Figure 4.32: Variation of maximum absorbed energy in low-velocity impact test. The figure shows the increase of number of cracking lines in PC incorporating MWCNTs compared with neat PC.

4.2.3.3 Dynamic mechanical response discussion

In the Charpy impact test, no statistical difference was obtained with the recorded test energy. This insignificance might be attributed to the relatively very high impact energy used with the Charpy test that is typically suitable for metals. Therefore, the Charpy test might not be a suitable method to judge the energy absorption of concrete.

On the other hand, a significant reduction of penetration velocity which indicates slowdown of the impact target inside the PC matrix was observed in the low-velocity impact test with MWCNTs specimens. Such impact target slow down implies that MWCNTs make a significant effect on PC resistance to crack propagation. The slowdown of the impact target means that PC incorporating MWCNTs were able to better

dissipate the impact energy applied to the specimen compared with neat PC. That was further evident by observing the cracking pattern of impact specimens of PC incorporating MWCNTs compared with neat PC specimens. Samples of these specimens are shown in Figure 4.32. In all impact specimens of PC incorporating MWCNTs, five or more fracture lines were formed compared with four fracture lines formed in neat PC. The formation of additional fracture lines represents a material ability to further dissipate energy. However, no significant difference was obtained with impact force resistance. This insignificant improvement of the impact force might be explained using the hypothesis provided early in this chapter. It is obvious that low content of MWCNTs can provide little improvement to PC strength by reinforcing the polymers. Nevertheless, this reinforcement mechanism provides significant improvement to cracking and strain capacity, deformability and thus to energy absorption.

The low-velocity impact test proved that adding well dispersed MWCNTs improved impact energy absorption and energy dissipation in PC. The improved energy dissipation proves the ability of the MWCNTs fibres to bridge micro-cracks in the polymer matrix of PC and thus improves the failure strain under different loading mechanisms.

4.3 Fresh properties and bond strength of Polymer concrete overlay mixes

4.3.1 Flowability test

In order to further investigate the flowability issue, flowability test was performed on PC overlay mixes where filler materials with no aggregate were used. The results showed that adding 0.5, 1.0 and 1.5% MWCNTs reduced the flowability of PC overlays as shown in Figure 4.33 by 18, 22, and 26%, respectively.

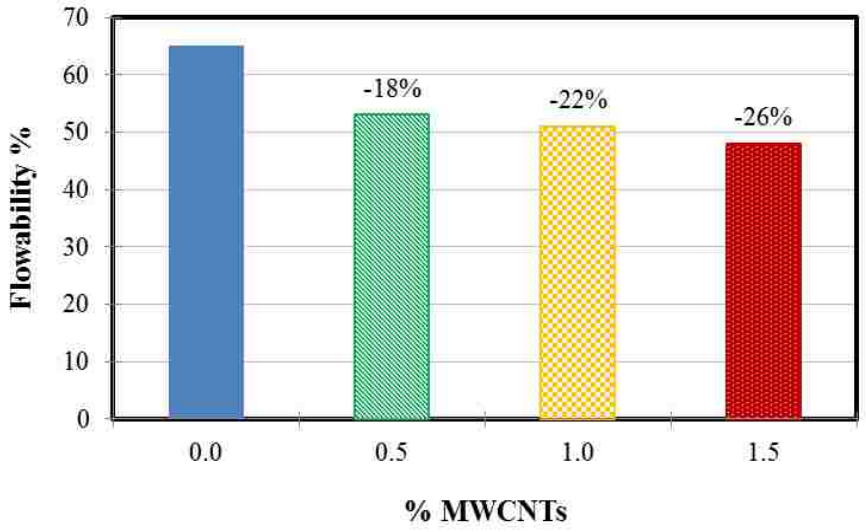

Figure 4.33: Variation of the flowability of PC overlay mixes incorporating varying contents of MWCNTs.

Comparing the results of the flowability of PC concrete mixes with the previous results explains the fact that the reduction in flowability was not only due to the decreased viscosity of epoxy when incorporating MWCNTs, but due to the interaction of the MWCNTs-epoxy nanocomposite with aggregate. This is an important finding as many PC applications do not incorporate aggregate but only combine fillers with the polymer matrix (e.g. bridge deck overlays).

4.3.2 Bond strength between Polymer Concrete overlays and steel substrates

4.3.2.1 Pull-off test

As mentioned earlier, the pull-off test was performed through five stages in order to investigate the significance of MWCNTs on the bond strength between PC overlays and steel substrates. The first four stages included testing of PC overlay mixes; while the fifth stage was performed on polymer layers without filler. Test techniques in each stage can be summarized as:

- Stage I: 50 mm (2.0 in) test dollies were used with smooth surfaces (not sandblasted), normal epoxy glue was used to glue the dollies and no aggregate was broadcasted on the overlay surface.
- Stage II: Test dollies were sandblasted, surface aggregate was broadcasted on the overlay and special (stronger) epoxy glue was used.
- Stage III: 50 mm (2.0 in) sandblasted test dollies with the same special epoxy glue and surface aggregate were used. The epoxy glue was first applied to the overlay cores then test dollies were glued.
- Stage IV: 20 mm (0.8 in) sandblasted test dollies with the same special epoxy glue, gluing technique in stage III and surface aggregate were used.
- Stage V: 20 mm (0.8 in) sandblasted test dollies with the same special epoxy glue were used. No aggregate was broadcasted on the polymer layer surface.

Moreover, Figure 4.34 summarizes all the possible failure patterns that could happen in the pull-off test.

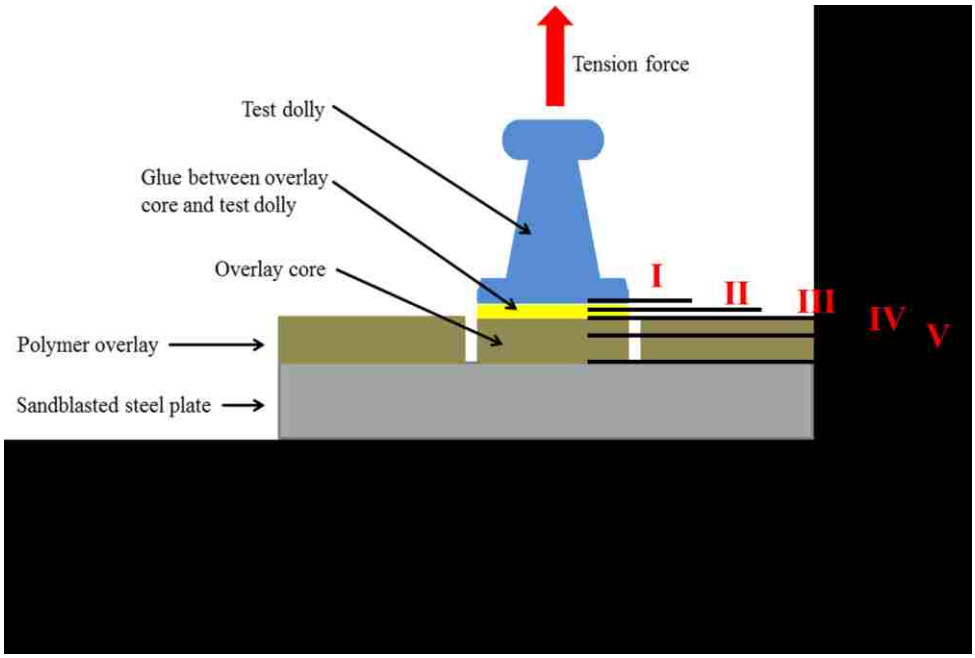

Figure 4.34: All possible failure patterns in the Pull-off test.

Figure 4.35 shows the failure modes occurred in stage I of the test which can be defined as a combination between failure patterns I and III. For some test dollies, failure was observed to happen as pattern I between the test dolly and the glue as shown in the middle dolly in Figure 4.35. The previous failure mode was considered as invalid test result. All other failures occurred as pattern III between the glue and upper surface of the PC overlay. Thin layer of PC overlay was observed to be attached on the failed glue surfaces as shown in Figure 4.35. However, the expected failure mode at the interface between the PC overlay and steel plate was never observed.

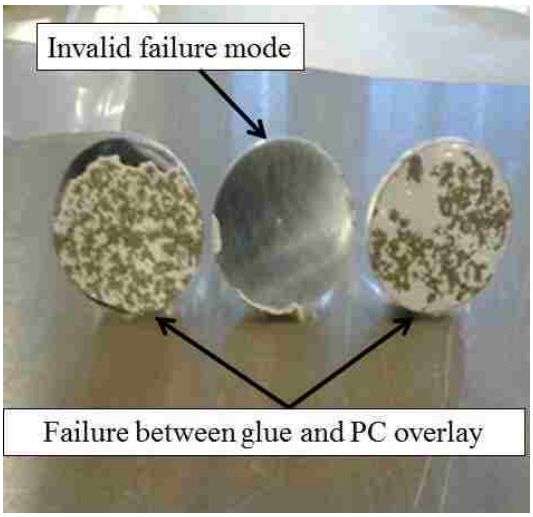

Figure 4.35: Failure patterns observed in the first stage.

The valid test results proved that adding 0.5% MWCNTs increased the strength by 30% as shown in Figure 4.36. Statistical analysis using student *t*-test was performed on the valid test results and statistical difference between the two mixes was found.

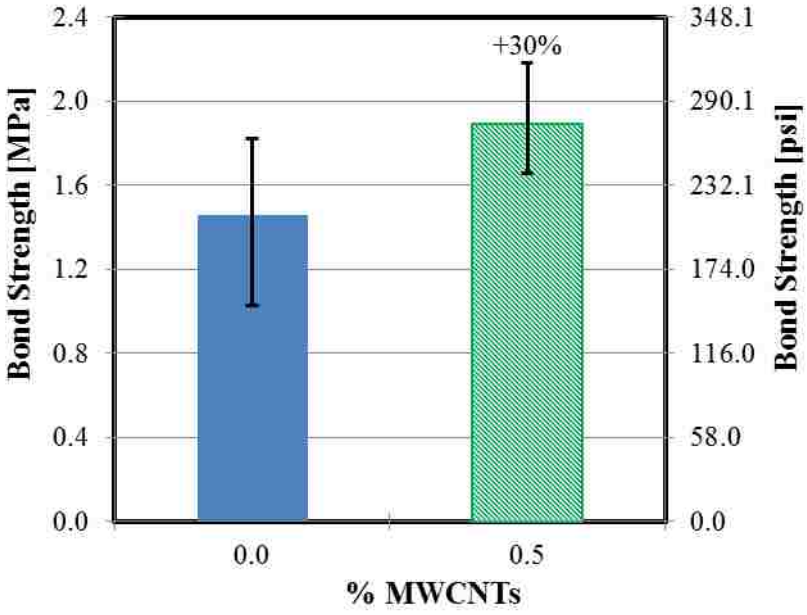

Figure 4.36: Variation of the bond strength of PC overlays tested in stage I.

In stage II, same failure patterns of the first stage were observed as shown in Figure 4.37. The strength was increased by 15% with adding 0.5% MWCNTs, but no significant different was proven between the two mixes. Figure 4.38 represents the variation of the strength reported in the second stage.

Figure 4.37: Second stage failure patterns, invalid pattern I on the left and valid result on the right (pattern III).

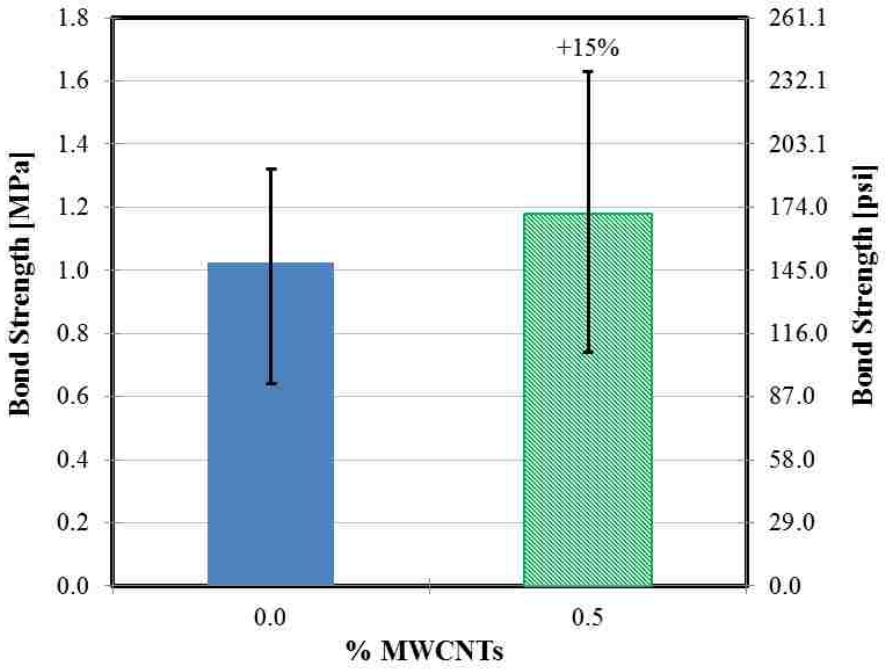

Figure 4.38: Variation of the bond strength of PC overlays tested in stage II.

As shown in Figure 4.39, the strength in stage III increased by 32% with adding 0.5% MWCNTs and all failure patterns were valid. However, no statistical difference was proved between the two mixes.

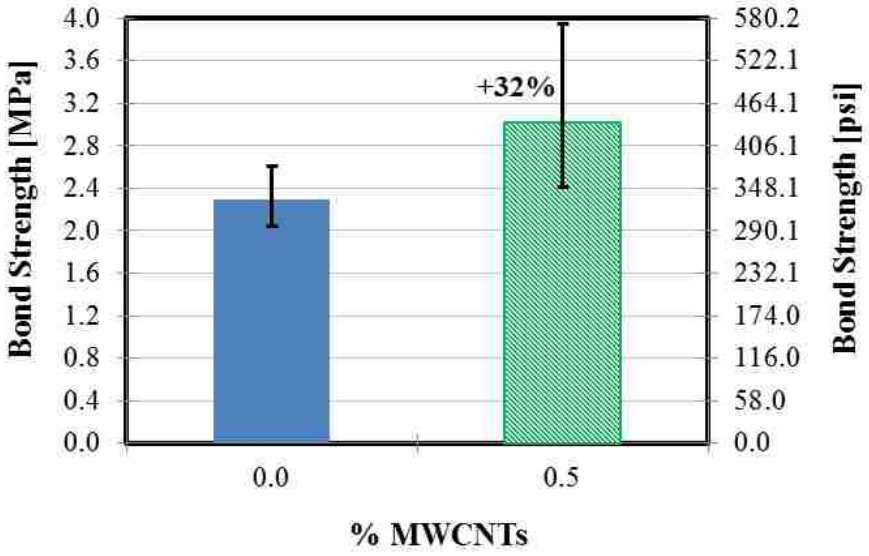

Figure 4.39: Variation of the bond strength of PC overlays tested in stage III.

In stage IV, all failures occurred at the interface between the glue and the overlay as pattern IV with thick layer of overlay attached to the glue surface as shown in Figure 4.40. Figure 4.41 represents an increase in the pull-off bond strength by 15, 30, and 24% by incorporating 0.5, 1.0, and 1.5% MWCNTs, respectively. Significant statistical difference was proved between strengths in the case of 1.0 and 1.5% MWCNTs, while no difference was found in the case of 0.5% MWCNTs.

Figure 4.40: Fourth stage failure pattern IV.

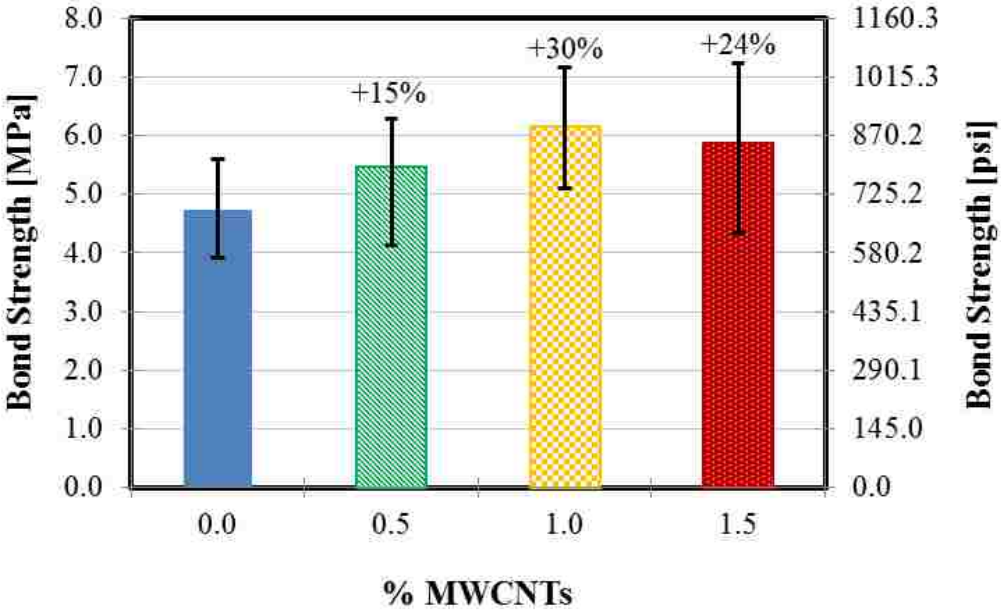

Figure 4.41: Variation of the bond strength of PC overlays tested in stage IV.

In stage V, all specimens' failure occurred between the glue and epoxy layer as shown in Figure 4.42. The strength increased by 42% by adding 1.0% MWCNTs and results were statistically different. Figure 4.43 represents the pull-off bond of polymer layers with and without MWCNTs.

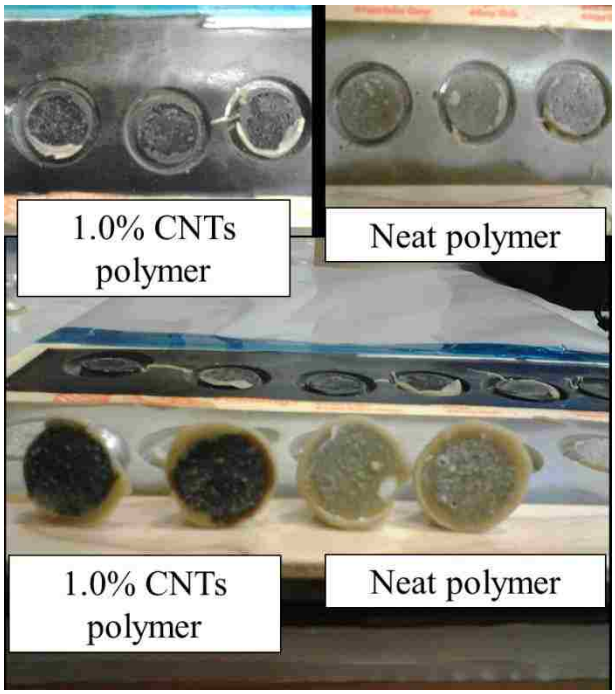

Figure 4.42: Fifth stage failure pattern IV.

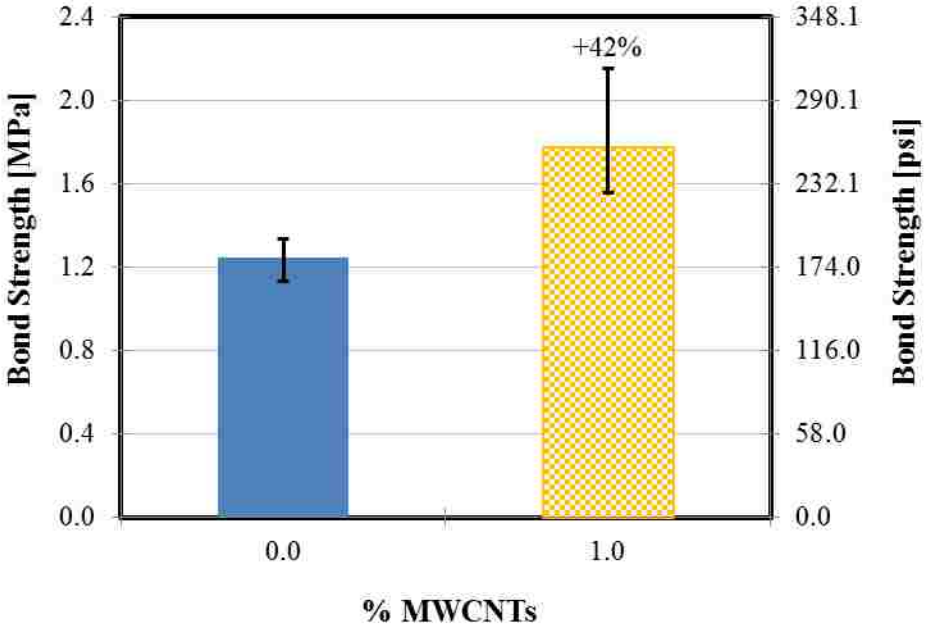

Figure 4.43: Bond strength of polymer layers with and without MWCNTs in stage V of the pull-off test.

4.3.2.2 Slant shear test

In the slant shear test, load and displacement were recorded at each time interval. Load-displacement curves were plotted for the four PC overlay mixes as presented in Figure 4.44. It was observed that these curves have increasing slopes until a displacement of 1.27 mm (0.05 in) took place. A "*toe*" like region appears in the start of these load-displacement curves which is a well-known response for polymers due to non-straighten polymer chains. This region indicates that the polymer response in compression dictates the slant shear behavior. After this relatively small displacement of 1.27mm (0.05 in.), the load-displacement curves start to be linear indicating shear interaction between the overlay and the steel part.

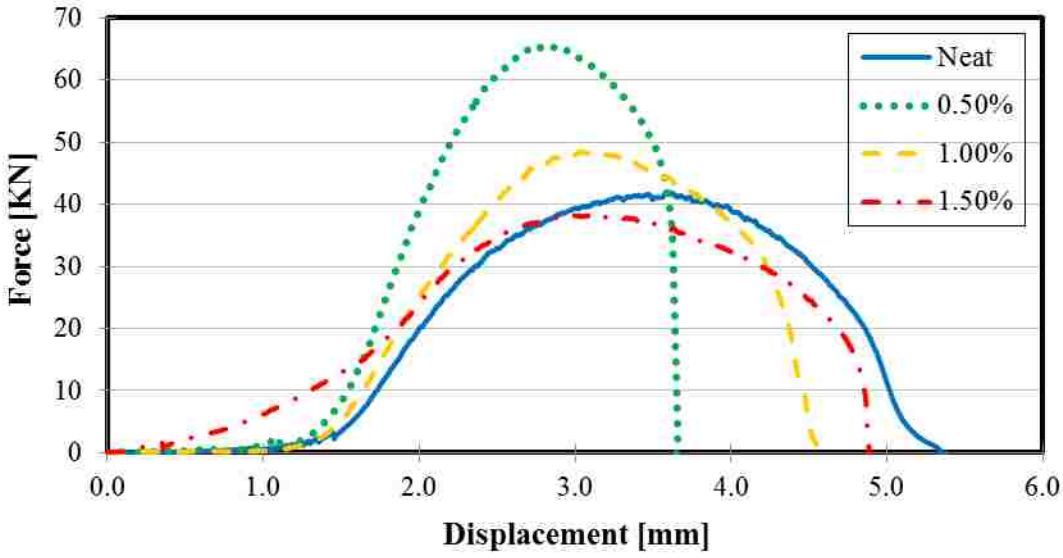

Figure 4.44: Load-displacement curves of slant shear test for PC overlays incorporating varying amounts of MWCNTs.

Using the recorded force and equation (3.7), bond strength between PC overlays and the steel substrate was calculated. Figure 4.45 represents the variation of the bond strength of the four PC overlay mixes for varying amount of MWCNTs. It can be

observed that adding 0.5 and 1.0% MWCNTs increased the bond strength by 56 and 17%, respectively, while adding 1.5% MWCNTs decreased the bond strength by 5.3%. Statistical analysis proved significant difference between the neat mix and 0.5% and 1.0% MWCNTs, while no difference was found between the 1.5% MWCNTs mix and the neat overlay.

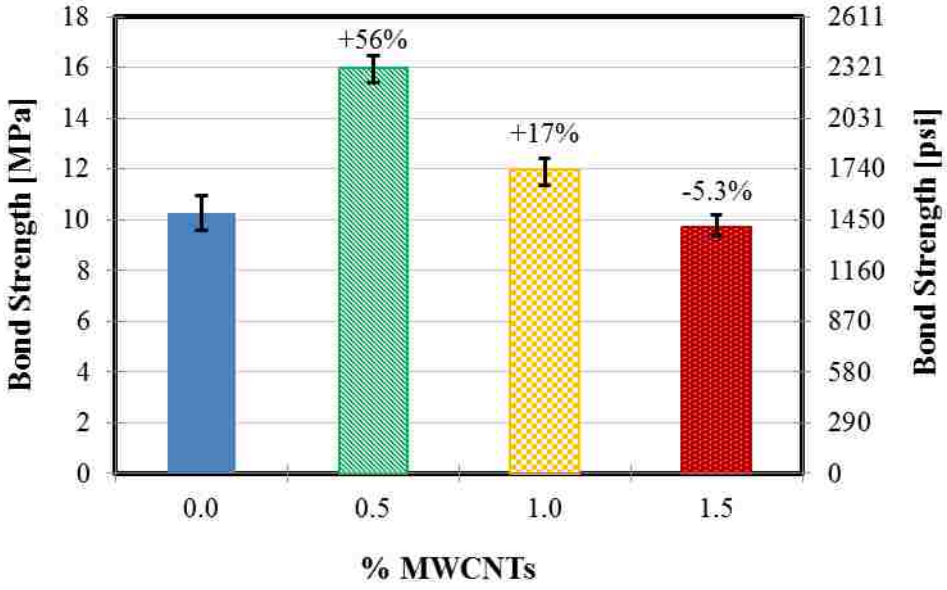

Figure 4.45: Variation of the bond strength between PC overlays and steel with varying amount of MWCNTs.

Moreover, failure displacement, defined as the displacement corresponding to the maximum load, was plotted for the four PC overlay mixes as shown in Figure 4.46. The displacement was decreased by 21, 12, and 5.5% with 0.5, 1.0, and 1.5% MWCNTs, respectively. While the 0.5 and 1.0% MWCNTs mixes were statistically different than the neat mix, no difference was found in the 1.5% MWCNTs case.

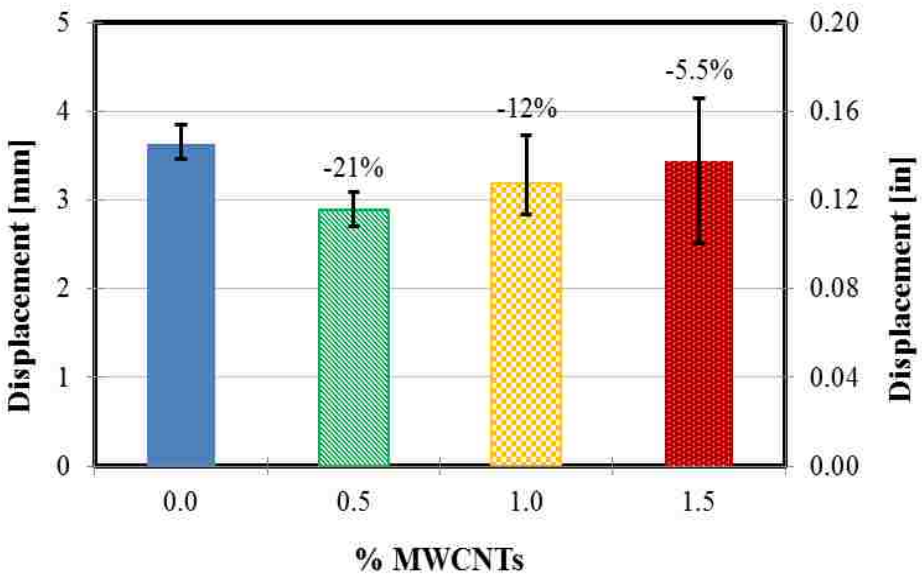

Figure 4.46: Variation of failure displacement of PC overlay mixes incorporating different contents of MWCNTs.

Furthermore, it is important to state that failure in all specimens of slant shear test was observed to occur as adhesion failure at the bond line between the overlay and the steel part. No failure occurred inside the overlay; we therefore state that all slant shear tests resulted in adhesion failure. No cohesion failure was observed. Figure 4.47 shows the failure mode in slant shear test specimens. It can be observed that specimens with MWCNTs have more overlay spots on the steel surface at failure than neat specimens. This indicates higher bond between the polymer overlay and steel when MWCNTs were incorporated.

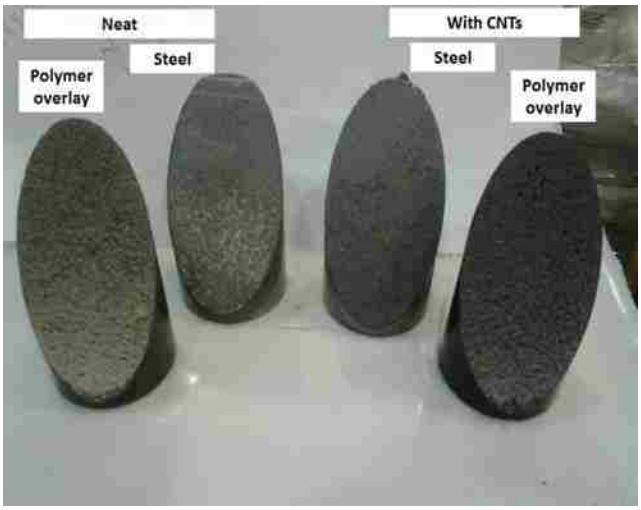

Figure 4.47: Increased number of overlay parts on steel at failure in the case of MWCNTs.

4.3.2.3 Bond strength tests discussion

Regarding the pull-off test, the target adhesion failure patterns at the bond line between PC overlays and steel plate never occurred. Instead, all valid failures took place as cohesion failure at the overlay upper surfaces indicating failure inside the overlay itself. This mode of failure proves that the cohesion strength of the overlays was weaker than the tension adhesion strength between PC overlays and the steel substrate. Therefore, failure occurred inside the overlay when test tensile force reached the cohesion strength of the overlay. However, observing the test results, it can also be concluded that incorporating MWCNTs in PC overlays significantly enhanced the cohesion strength of PC overlays. This can be attributed to the microstructural modification of PC overlay by MWCNTs. This modification was supported and proven by the static mechanical improvements in previous PC tests. As seen earlier, MWCNTs can enhance toughness and flexibility of PC and as a result can resist crack initiation and propagation in PC overlays. Moreover, MWCNTs can bridge the micro-cracks initiated

inside the overlay under tensile forces and therefore improve the cohesion strength as seen in test results.

On the other hand, all failures in the slant shear test occurred at the bond line between PC overlays and steel indicating adhesion failure. This change in failure mode from the cohesion failure mode of the pull-off test to adhesion failure mode indicates that PC overlay cohesion strength was stronger than the shear adhesion strength between the PC overlay and steel. Therefore, failure was forced to happen at the bond line. Figure 4.48 shows a schematic representation comparing tension cohesion and adhesion and shear cohesion and adhesion. It is obvious that adding MWCNTs significantly enhanced both adhesion strength between PC overlays and steel and cohesion strength of PC overlays. The enhancement of adhesion strength can be attributed to one of two possibilities. The first possibility is that the MWCNTs would react with the silane in epoxy, which already bonds epoxy to steel. Consequently, adding MWCNTs improves bond strength through the better bond between silane and steel. The other possibility is that MWCNTs do not react with silane but react with steel surface connecting the epoxy group to steel and therefore improving the bond strength between epoxy and steel. It is important to note that the MWCNTs are functionalized with carboxyl groups (COOH) that might favor bond of MWCNTs to steel directly. MWCNTs might also have a mechanical effect in filling the roughened groves on steel surface and therefore enhancing the bond strength mechanically in addition to the mentioned chemical effects. The microscale length of MWCNTs (10-30 μm) shall allow this effect. Finally, limiting failure strain can be explained by increasing the friction between PC overlay surfaces and

steel through incorporating MWCNTs. This increase would limit slippage of PC overlays and results in limiting the strain.

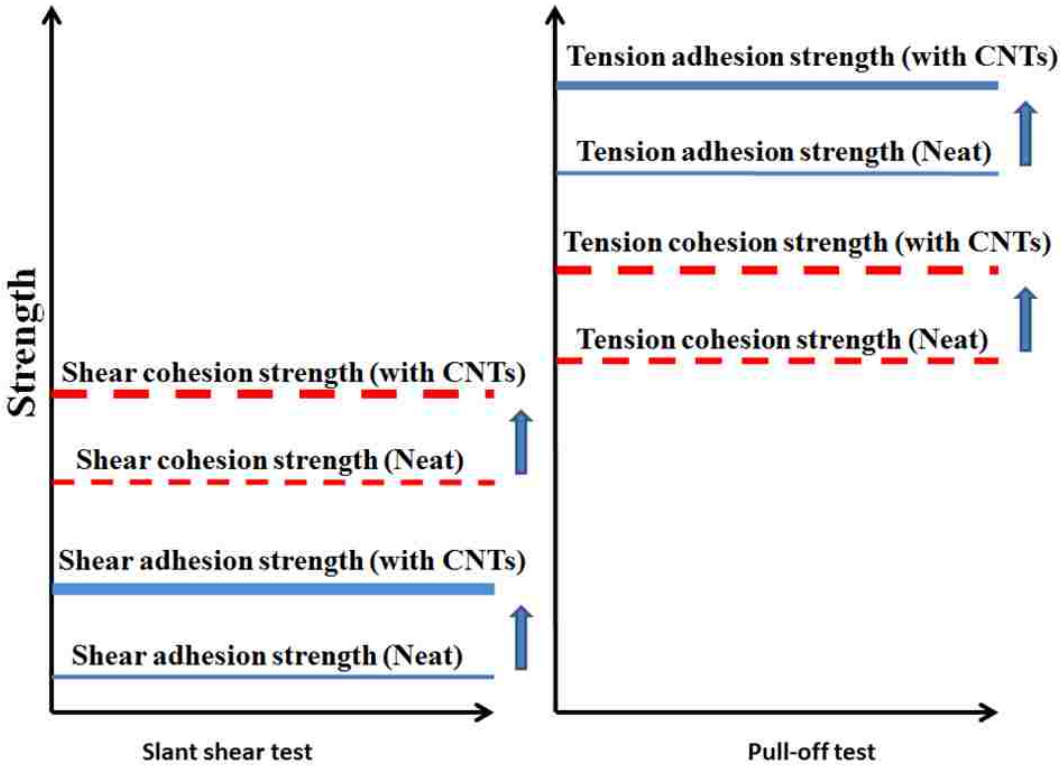

Figure 4.48: Schematic comparison between cohesion and adhesion strengths as explained by slant shear and pull-off tests.

4.3.3 Time dependant mechanical response of PC overlays

4.3.3.1 Flexure fatigue test

Five specimens of each PC overlay mix were tested in the four-point flexure fatigue test. As mentioned earlier, force and mid-span displacement were recorded. Figure 4.49 shows the variation of the number of cycles to failure for the four mixes. Failure is defined as in AASHTO specifications as 50% reduction from initial stiffness. While the mean failure of neat specimens occurred at 8,064 cycles, the 0.5 and 1.0% MWCNTs specimens recorded mean failure at 12,985 and 16,129 cycles with increase of 61 and 100%, respectively. The 1.5% MWCNTs specimens reached 50,000 cycles without failure recording mean increase in fatigue number of cycles to failure in excess of 520%. Statistical analysis proved all the improvement to be significantly different.

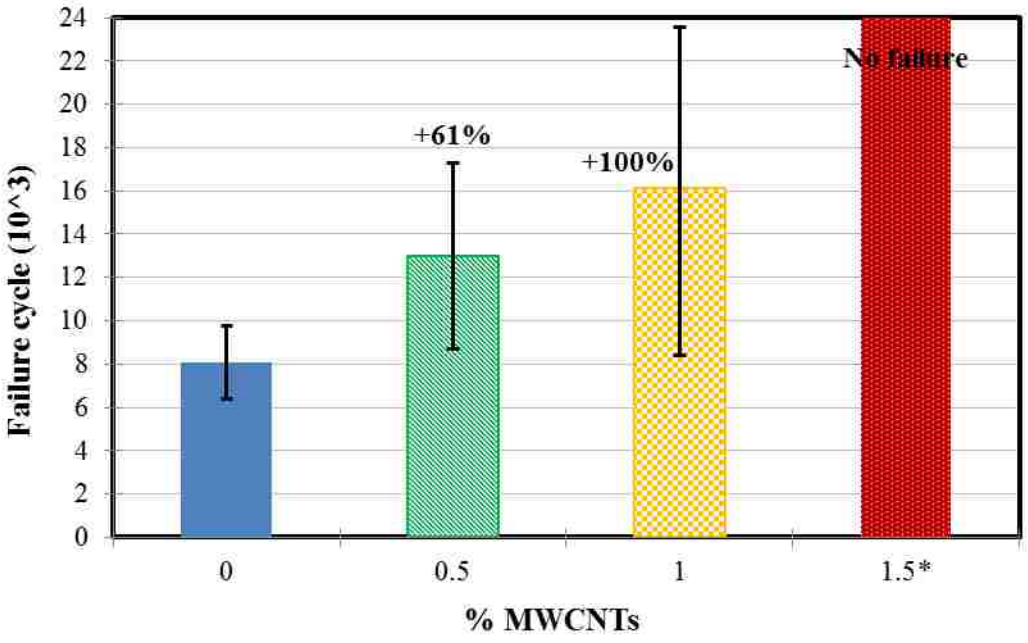

Figure 4.49: Variation of the fatigue strength represented by number of cycles to failure for PC overlays with varying MWCNTs content (* no failure up to 50,000 cycles).

Moreover, fatigue damage due to cyclic loading of PC prisms was also estimated. Figure 4.50 represents the mean damage evolution of PC prisms tested in fatigue. From the figure, damage evolution can be divided into three distinct stages. The first stage is the primary damage stage characterized by a linear (or logarithmic) relationship with high slope. The second stage is the secondary or steady state damage with a relatively low slope compared with the primary damage slope and the third stage is the tertiary damage with significantly high slope leading to damage and fracture. It can be observed that the primary damage extended to approximately 23, 25, and 32% in the cases of 0.5, 1.0, and 1.5% MWCNTs compared with 20% for neat specimens. Moreover, the steady state damage extended to approximately 13,000 and 20,000 cycles in the case of 0.5 and 1.0% MWCNTs, respectively compared with approximately 10,000 cycles for the neat specimens. Furthermore, higher level of final damage, 95% in the case of 0.5 and 1.0% MWCNTs, was observed compared with 82% damage in neat specimens. While this final damage took place after 10,000 cycles for neat specimens, it occurred after 15,000 and 23,000 cycles with 0.5 and 1.0% MWCNTs, respectively. In the case of 1.5% MWCNTs, the total damage was limited to approximately 35% up to 38,000 cycles and to approximately 40% up to 50,000 cycles. It is important to state that no tertiary damage was experienced and no failure was observed up to 50,000 cycles. Figure 4.51 represents the variation of the cycle of total failure, defined as total damage of approximately 100%, for the four mixes. Total failure cycle number was increased by 26 and 97% with 0.5 and 1.0% MWCNTs, respectively. No total failure was experienced in the case of 1.5% MWCNTs. The statistical analysis showed significant improvement in fatigue strength

between 1.0, 1.5% MWCNTs and neat specimens and no difference in the case of 0.5% MWCNTs.

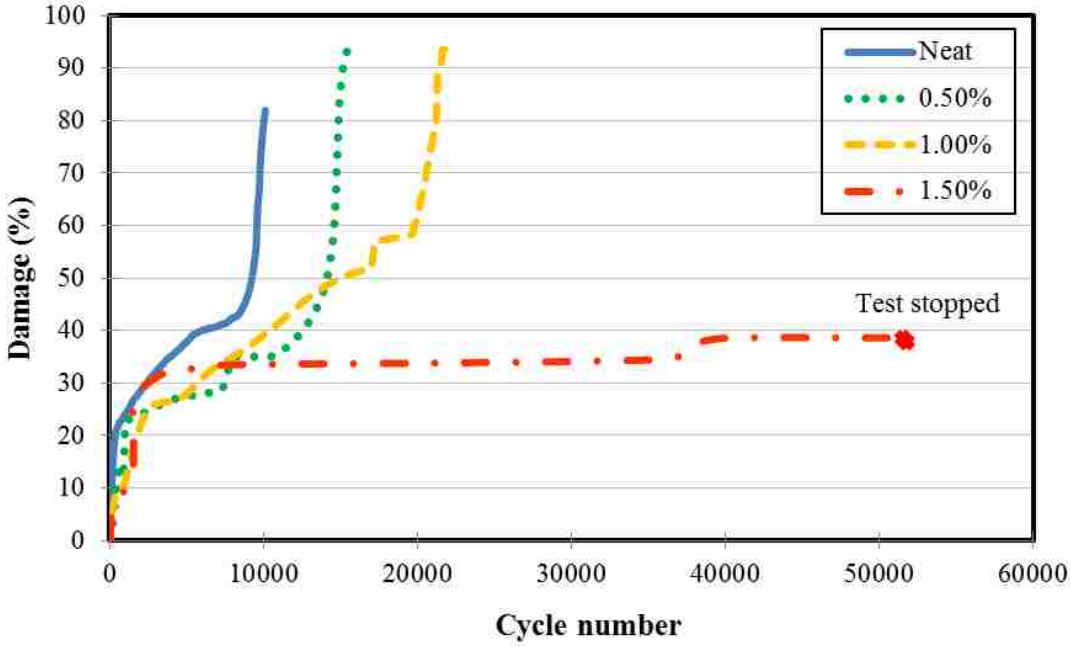

Figure 4.50: Mean damage evolution of PC prisms under fatigue loading.

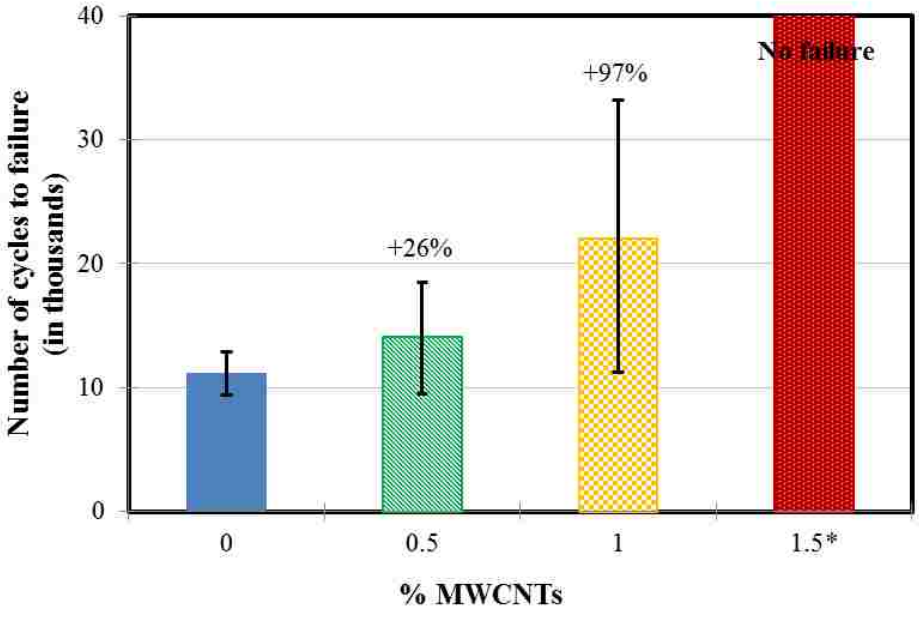

Figure 4.51: Variation of number of cycles to total failure for PC overlays incorporating varying amount of MWCNTs.

It was also observed that some specimens were ruptured in the middle part as shown in Figure 4.52. This rupture was observed to start with small crack initiated in the middle area where maximum moment and hence maximum stresses take place. Under cyclic loads, the crack starts to propagate vertically inside the specimen up to total rupture.

Figure 4.52: Fracture of some fatigue specimens.

4.3.3.2 Discussion of flexure fatigue test

It was obvious from the fatigue test results that incorporating MWCNTs significantly shifted the 50% reduction of stiffness and enhanced the damage evolution under cyclic loading of PC overlays significantly. We define damage here as the onset of loss of stiffness that takes place prior to crack initiation. The evolution of damage in fatigue specimens can be related to two factors. First is the ability of PC overlays to resist cracks initiation. This factor is usually related to primary and steady state damage. The second factor is the ability of PC overlays to resist cracks propagation inside the overlay which is related to the tertiary damage. Under cyclic loading, damage would accumulate in the specimen through primary and steady state damage zones. At the end of the steady state damage zone, microcracks would be initiated. In the tertiary damage zone, these cracks would propagate inside the overlay resulting in degradation of the section moment

of inertia and therefore degradation of the section flexural rigidity. This degradation in flexural rigidity usually leads to fracture of the overlay.

From static tests results, incorporating MWCNTs proved to enhance the toughness and flexibility of PC. The previous enhancements would improve the PC overlay resistance of cracks initiation under cyclic loading. The hypothesis of enhancing the crack initiation resistance of PC overlays can be proved by comparing the extended steady state damage zones of specimens with MWCNTs with the limited steady state damage zone of neat specimens in Figure 4.50. Moreover, the previously mentioned bridging effect of PC overlays micro-cracks by MWCNTs enhanced the resistance of cracks propagation in the overlay and therefore extended the tertiary damage zone as observed in 0.5 and 1.0% MWCNTs specimens. This results in higher number of cycles to failure as shown in Figure 4.51. As a result, the improvement in PC overlays fatigue behaviour can be attributed to the ability of MWCNTs in PC overlays to delay microcracks initiation and propagation. Moreover and although PC proved not to be suitable for applications under axial and axial creep loading, creep would enhance the behaviour of PC overlays under sustained shrinkage and thermal stresses. As explained in Figure 3.25, the reduction of the effective modulus of elasticity of PC because of creep will result in lowering the overlays' stresses and hence improving PC overlay resistance to temperature variation and shrinkage.

4.3.3.3 Cost analysis

In this section, we provide an estimate of the cost of producing PC incorporating 1.0% MWCNTs. We selected 1.0% MWCNTs as the ratio resulted in the highest improvement in PC properties. The analysis is based on cost estimation of $50/gallon

($13208.6/m^3) for epoxy with a density of 8.8 lbs/gal (1054.5 kg/m^3), $32/ton for filler, $26/ton for coarse aggregate and $9/gm for COOH functionalized MWCNTs. Table 4.1 presents the mix proportions by weight for PC and PC overlay mixes.

Table 4.1: Mix proportions by weight (kg/m^3)

	PC overlay				
Mix Designation	Resin	Hardener	Powder	Coarse Aggregate	MWCNTs
Neat	288	128	1570	320	–
1.0% MWCNTs	288	128	1570	320	0.082
	Polymer Concrete				

$$\text{Cost of epoxy} = \frac{288+128}{1054.5} * 13208.6 = 5210.8\ \$/m^3 \quad (4.1)$$

$$\text{Cost of powder} = \frac{1570}{1000} * 32 = 50.24\ \$/m^3 \quad (4.2)$$

$$\text{Cost of coarse aggregate} = \frac{320}{1000} * 26 = 8.32\ \$/m^3 \quad (4.3)$$

$$\text{Cost of MWCNTs} = 82 * 9 = 738\ \$/m^3 \quad (4.4)$$

$$\therefore \text{Total cost of PC mix} = 5210.8 + 50.24 + 8.32 = 5269.36\ \$/m^3 \quad (4.5)$$

$$\therefore \text{Total cost of PC with 1.0\% MWCNTs} = 5269.36 + 738 = 6007.36\ \$/m^3 \quad (4.6)$$

As a result:

$$\text{Additional cost of 1.0\% MWCNTs} = \frac{738}{5269.36} * 100 = 14\% \text{ for PC mix} \quad (4.7)$$

Therefore, there is 15% increase in materials cost. Additional costs shall be considered to produce the new generation of polymer concrete mixes with MWCNTs on

large scale for industrial use. These additional costs include using special large volume mechanical stirrers, such as homogenizers, and sonicators with high efficiency.

4.4 Microstructural characterization of epoxy-MWCNTs Nano-composite

4.4.1 Scanning Electron Microscope (SEM)

Fracture surfaces of epoxy sample incorporating 1.0% MWCNTs were investigated by SEM as shown in Figures 4.53, 4.54, and 4.55. SEM images were able to show clear pictures of MWCNTs well dispersed in the epoxy matrix. The SEM images show the MWCNTs (indicated by yellow arrows) as longitudinal tubular particles bridging epoxy fracture surfaces and connecting epoxy parts together. The figures show this feature at micro and nano scales.

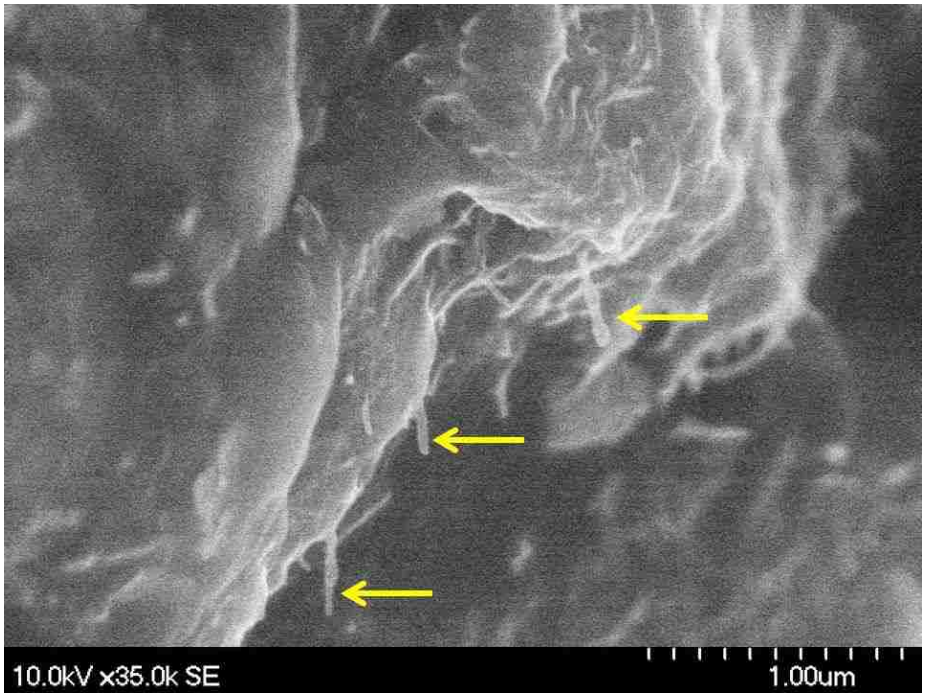

Figure 4.53: SEM image of epoxy incorporating 1.0% MWCNTs.

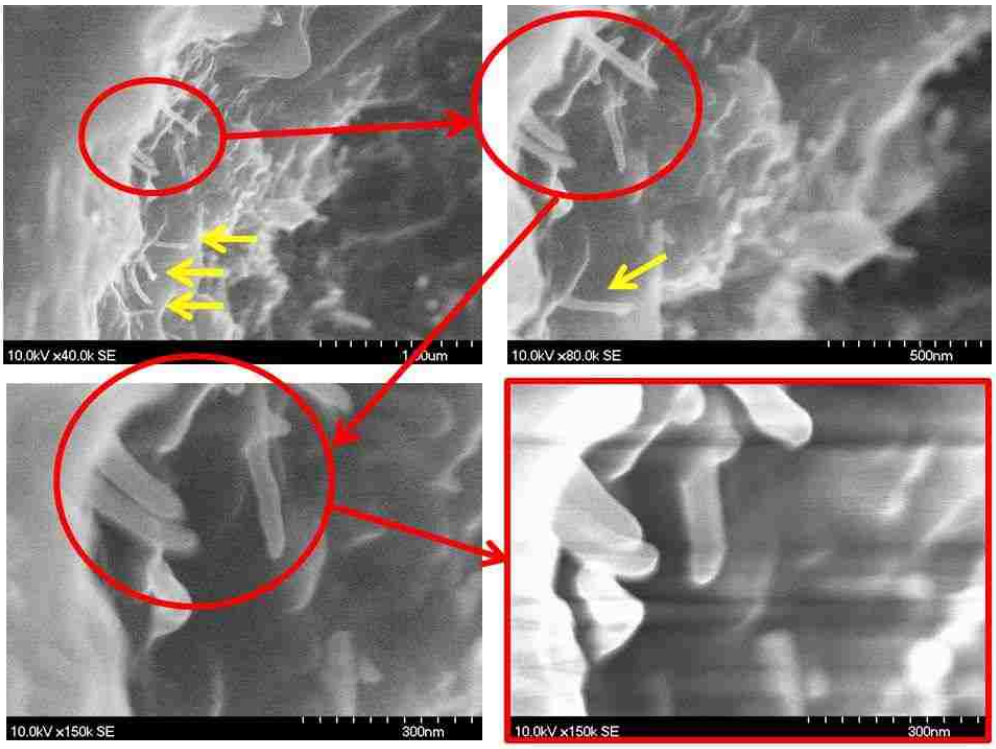

Figure 4.54: SEM images of epoxy incorporating 1.0% MWCNTs.

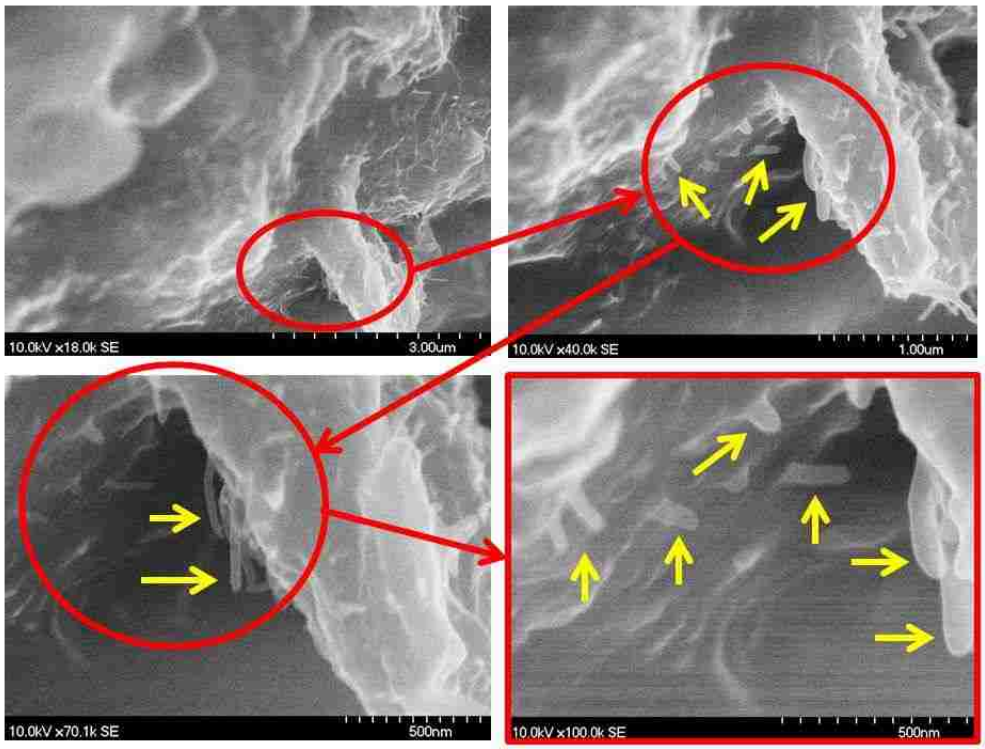

Figure 4.55: SEM images of epoxy incorporating 1.0% MWCNTs.

4.4.2 Fourier Transform Infrared Spectroscopy (FTIR)

Two samples of neat epoxy and epoxy incorporating 1.0% MWCNTs were investigated using FTIR. The intensity of reflected infrared waves was plotted at each wavenumber as shown in Figure 4.56. It can be observed that the curve of neat epoxy has higher intensity of reflected waves at each wavenumber compared with epoxy with MWCNTs. This can be attributed to adding carbon as MWCNTs to the epoxy which absorbs more waves at each wavenumber and hence reflects fewer waves. The lower shift of the curves can also prove the well dispersion of MWCNTs in the epoxy matrix.

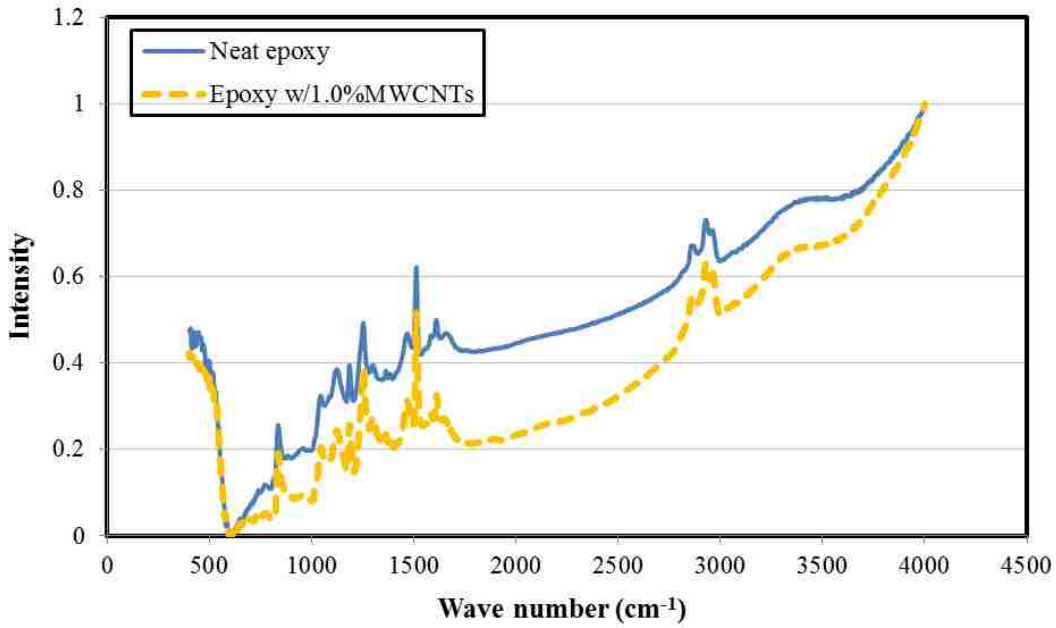

Figure 4.56: FTIR curves of reflected waves for neat epoxy and epoxy with MWCNTs.

From Figure 4.56, it can also be observed that the sharp peak at 1511 cm^{-1} is taller in the case of epoxy with MWCNTs than the case of neat epoxy. This is better shown at a close look in Figure 4.57. The peak at wavenumber 1511 cm^{-1} is a known indication of the carbon-rings and its intensity increase is attributed to the addition of MWCNTs and their strong influence on the new epoxy matrix.

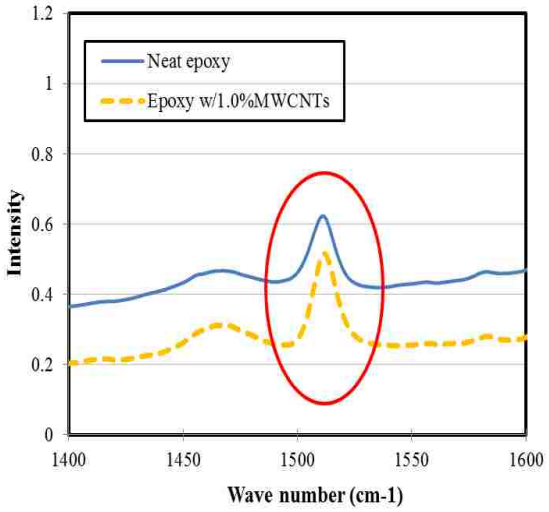

Figure 4.57: Taller 1511 cm^{-1} peak in the case of epoxy with MWCNTs.

Moreover, the most important peak for the epoxy-MWCNTs hypothesis is at approximately 1250 cm^{-1}. This peak represents the C-O bonds which prove the reaction between MWCNTs and epoxy resin as shown in Figure 4.24. Corrected to a baseline as shown in Figure 4.58, the peak height in the case of epoxy with MWCNTs was 0.192 compared with 0.138 in the case of neat epoxy with 39% increase in intensity.

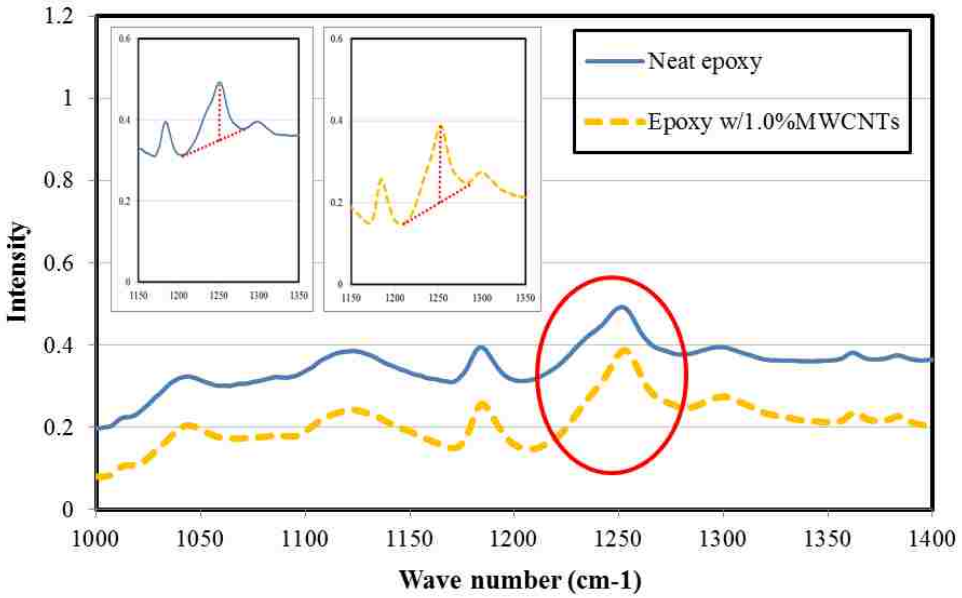

Figure 4.58: Increase of 39% at the C-O bonds peak in the case of epoxy with MWCNTs.

Furthermore, slight shifts can be observed toward higher wavenumbers along 1300 cm^{-1} (C-N bonds) and 1610 cm^{-1} (C-H bonds) peaks as shown in Figure 4.59. These peaks also indicate a higher degree of polymerization in the epoxy matrix, and may be related to the substitution of MWCNTs in the epoxy structure. There was also a large shift as shown in Figure 4.60 in the area of O-H bond at approximately 3500 cm^{-1} toward lower wavenumbers, suggesting a lengthening of the O-H bonds. All FTIR observations confined that the addition of MWCNTs changed the chemical structure of epoxy. It also confined that the use of COOH (carboxyl) functionalized groups helped making a new polymer nanocomposite with different cohesion and adhesion strengths. FTIR measurements, however, were not able to prove or disprove the effect of MWCNTs on bond of epoxy overlay to steel.

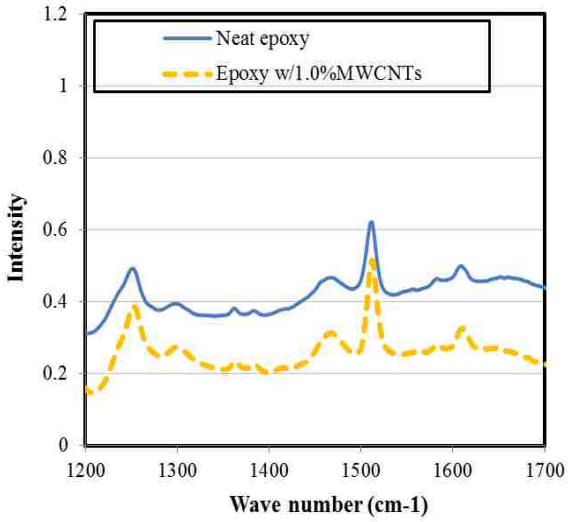

Figure 4.59: Very slight shift toward higher wavenumbers at 1250 cm^{-1} and 1610 cm^{-1}.

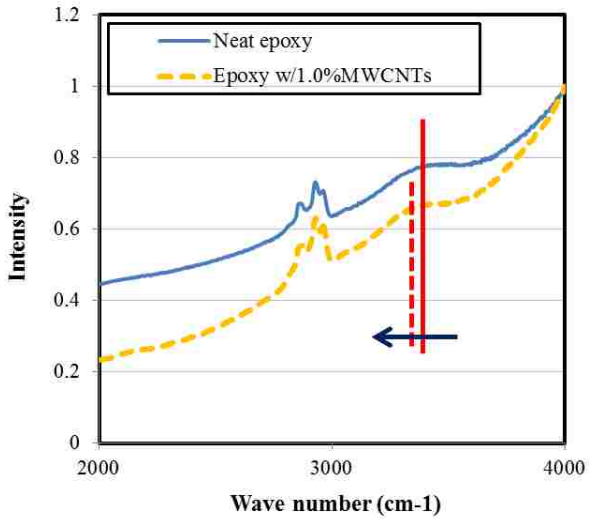

Figure 4.60: Relatively large shift at O-H bonds in the case of epoxy with MWCNTs.

4.4.3 Thermal characterization

Two samples of neat epoxy and epoxy with 1.0% MWCNTs were examined by Thermal Gravimetric Analysis (TGA) and Differential Scanning Calorimetry (DSC) to investigate the thermal stability of epoxy-MWCNTs nanocomposite. Figure 4.61 represents the TGA results of weight percentage of the samples through the variation of test temperature. It can be observed that both samples approximately experienced the same weight loss percentage at each temperature with no significant effect of adding MWCNTs on the epoxy weight loss.

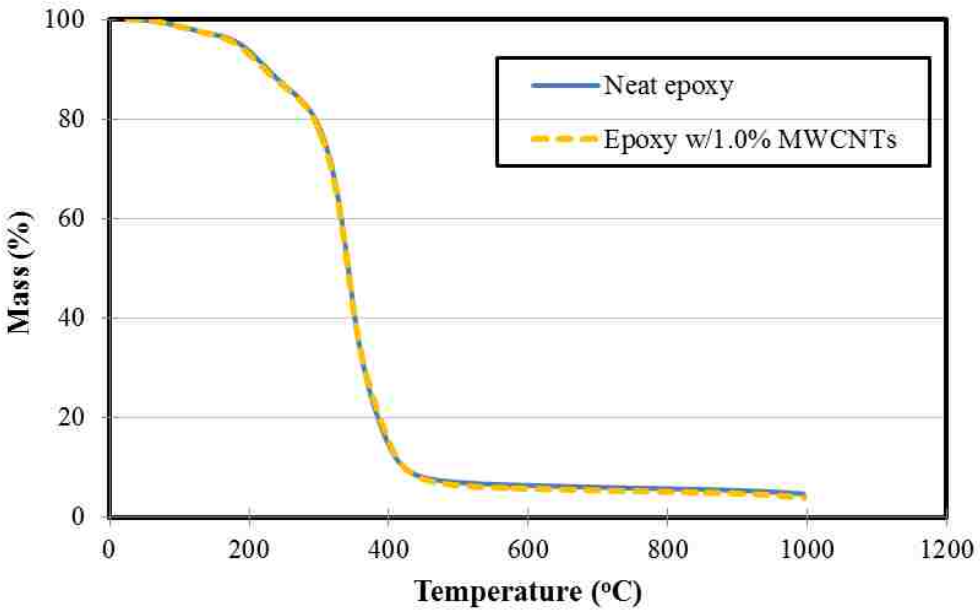

Figure 4.61: TGA results of neat epoxy and epoxy incorporating MWCNTs.

On the other hand, DSC plots showed significant difference between the curves of the two samples as shown in Figure 4.62. The plots in Figure 4.62 can be divided into three parts. The first part is the glass transition portion of the curve, the second part is the onset of decomposition, and the third part is the maximum and final decomposition. It can be observed that both samples experienced similar glass transition zone. In both cases of neat epoxy and epoxy with MWCNTs, onset decomposition occurred at 328 ^{o}C. This onset decomposition peak was attributed to the existence of eutectic impurities in the epoxy. In the case of neat epoxy, maximum decomposition, which can be defined as the characteristic peak of neat epoxy, occurred at 423 ^{o}C. In the case of epoxy with 1.0% MWCNTs, maximum decomposition took place over two peaks. The first peak occurred at 448 ^{o}C, while the second peak of maximum decomposition happened at 788 ^{o}C. However, the first peak in maximum decomposition of epoxy with MWCNTs still can be related to the characteristic peak of neat epoxy but with small shift as a result of adding

the MWCNTs. Moreover, the mentioned second peak at 788 ^{o}C in the case of epoxy with MWCNTs can be considered as the most important peak and can be attributed as the characteristic peak of epoxy influenced by 1.0% MWCNTs.

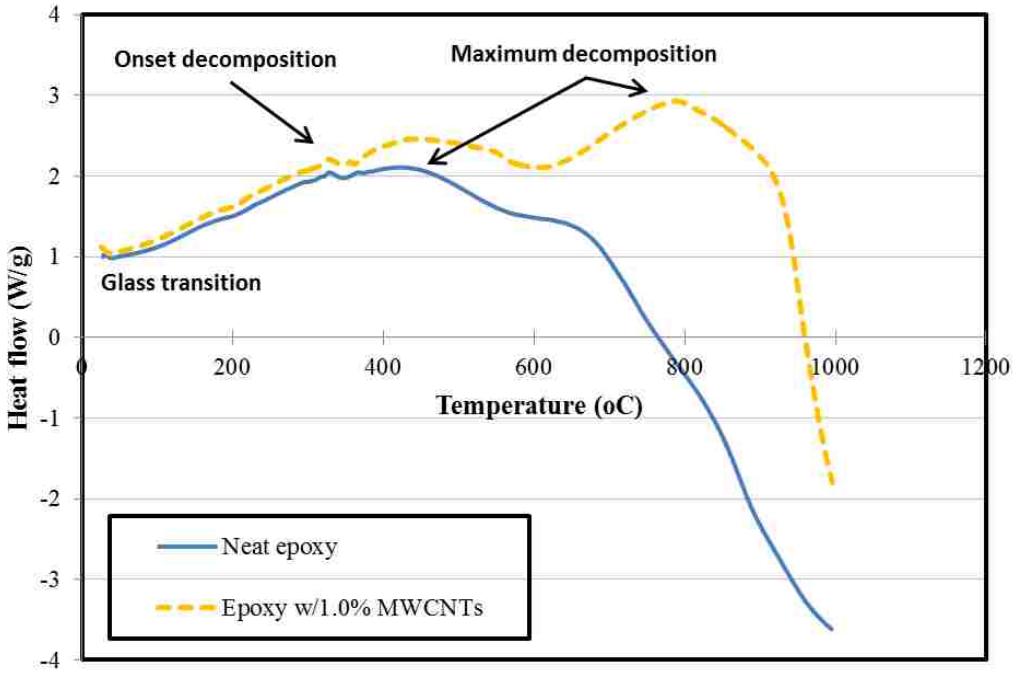

Figure 4.62: DSC curves of neat epoxy and epoxy incorporating MWCNTs.

Furthermore, the glass transition temperature (Tg), defined as the midpoint of the glass transition zone, was calculated for the two specimens as shown in Figure 4.63 following ASTM D3418 - 12 (2012). Tg of neat epoxy and epoxy with 1.0% MWCNTs was found to be 135 and 135.5 ^{o}C, respectively.

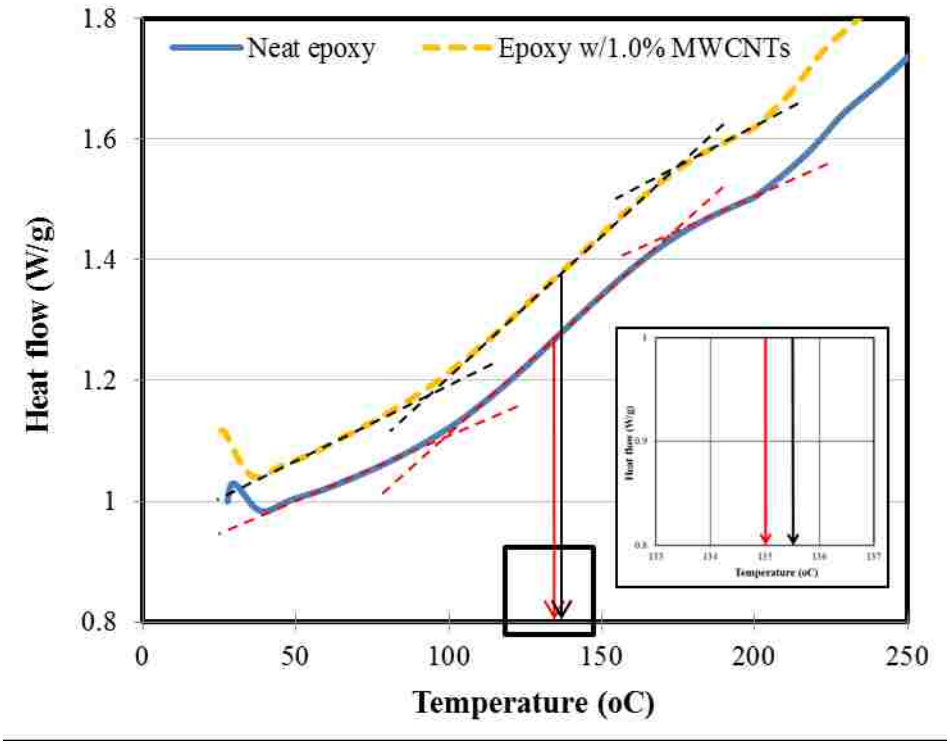

Figure 4.63: Obtaining T_g from glass transition zone.

4.4.4 Discussion of the characterization of epoxy-MWCNTs Nano-composite

Microstructural and thermal characterization of epoxy-MWCNTs nanocomposite emphasized our hypothesis that MWCNTs had altered the microstructure of the epoxy and increased the crosslinking between the epoxy groups. The new epoxy-MWCNTs nanocomposite has improved characteristics which in turn improved the mechanical properties of PC overlay. SEM images showed the MWCNTs as nanofibers capable of bridging the microcracks surfaces. The increase in the FTIR peaks proves the chemical reaction between functionalized COOH group of MWCNTs and epoxy resin creating new nanocomposite. Finally, TGA and DSC analysis showed that adding MWCNTs made the nanocomposite more thermally stable with a significantly higher maximum decomposition temperature compared with neat epoxy.

Chapter 5 Conclusions

5.1 Summary

In this research, a new generation of polymer concrete (PC) was produced and investigated. The new generation was manufactured by incorporating Multi-Walled Carbon Nano-Tubes (MWCNTs) in low modulus polysulfide epoxy and then mixed with fine and coarse aggregate or fine aggregate only to produce PC or PC overlays respectively. The research work was divided into three parts. Part Ⅰ investigated the mechanical properties of PC incorporating MWCNTs, part II investigated the bond strength between steel plates and PC overlays was performed, and part III included microstructural and thermal characterization of epoxy with MWCNTs.

PC has been utilized as structural members for a number of applications. It has also been used to produce machine foundations and as a protection for special structures. Based on this, static and dynamic mechanical properties of PC were investigated in the first part of this thesis. Investigation of the static mechanical properties of PC included compressive strength, flexural strength, and shear strength. It also included creep of PC under axial sustained stress. Dynamic mechanical tests included Charpy impact test and low-velocity impact test.

PC overlays have been used to protect steel and concrete bridge decks and are very common on orthotropic bridges. In the PC overlay mixes, no coarse aggregate was added to the mix. The bond strength between the PC overlays and steel plates was tested. This included determining the pull-off and slant shear bond strengths. Moreover, the fatigue strength of the PC overlays was investigated under cyclic loads.

Finally, the significance of MWCNTs on the microstructure of the epoxy binder system was examined. The microstructure of the epoxy resin incorporating the MWCNTs was compared with neat epoxy using the Scanning Electron Microscope (SEM) and Fourier Transform Infrared Spectroscopy (FTIR). Moreover, thermal stability of the same epoxy with MWCNTs was evaluated by Thermal Gravimetric Analysis (TGA) and Differential Scanning Calorimetry (DSC).

5.2 Conclusions

The addition of MWCNTs to the PC mixes enhanced the flexural strength, had no significant effect on shear strength, improved the flexural failure strain and made a significant improvement in the shear failure strain. MWCNTs also increased the flexural and shear toughness significantly. These improvements are attributed to the ability of the MWCNTs to produce epoxy-MWCNTs nanocomposite with improved mechanical properties. This implies the ability of the MWCNTs to alter the microstructure of PC significantly and enhance its static mechanical performance. Moreover, the functionalization of MWCNTs also allows the MWCNTs to chemically bond to the epoxy matrix and produce strong and ductile epoxy-MWCNTs. PC was proved not to be suitable for applications under axial loads. PC had relatively low compressive strength compared with conventional concrete. PC experienced fast failure in creep test in less than 24 hours. This can be attributed to the relatively high binder content (18% of total weight) in the used PC mixes compared with the conventional binder content (8-10% of total weight) typically used in overlays.

The Charpy impact test did not show any statistical difference with the recorded test energy. This can be attributed to the relatively very high impact energy used in the

test. Therefore, the Charpy impact test was not suitable to judge the energy absorption of PC. The low-velocity impact test showed significant reduction of penetration velocity with specimens incorporating MWCNTs. This indicated a slowdown of the impact target inside the PC matrix with MWCNTs. The slowdown of the impact target means that PC incorporating MWCNTs was better able to dissipate the impact energy applied to the specimen compared with the neat PC. However, no significant difference was obtained with impact force. This insignificant improvement of the impact force was attributed to the insignificant effect of MWCNTs on the shear strength of PC. The improved static and dynamic mechanical properties of PC were able to prove that the addition of MWCNTs fibres bridged the PC microcracks and significantly enhanced its cracking resistance, durability, and resistance to crack propagation.

Failure modes in the pull-off test never occurred at the bond line between the PC overlays and the steel plates. Instead, all valid failures took place inside the overlay itself indicating that the cohesion strength of the PC overlays was weaker than the direct tension adhesion strength between PC overlays and the steel substrate. However, the test results indicated that incorporating MWCNTs in PC overlays significantly enhanced the overlays cohesion strength. Failure modes in the slant shear test occurred at the bond line between PC overlays and steel, indicating that the overlay cohesion strength was stronger than the slant shear adhesion strength between the overlay and steel. Moreover, it was obvious that adding MWCNTs significantly improved the adhesion strength between PC overlays and steel and limited the failure strain. This enhancement was attributed to a chemical and mechanical effect. The chemical effect was attributed to the fact that MWCNTs already reacted with either the silane and the steel surface, or only with the

steel surface. The mechanical effect was that MWCNTs filled the rough groves on the steel surface and therefore enhanced the bond strength mechanically. Finally, limiting the bond failure strain was explained by increasing the crosslinking between the epoxy groups. This increase limits slippage of the epoxy molecules and results in limiting the shear bond strain.

In the fatigue test, incorporating MWCNTs significantly improved PC overlay resistance to damage propagation under cyclic loading. The enhancement in damage propagation resistance proved that adding MWCNTs improved the PC overlay resistance of cracks initiation under cyclic loading. Moreover, specimens with MWCNTs failed at a higher total number of cycles compared with the neat specimens. The increase in the number of cycles to failure can be explained by the ability of MWCNTs to enhance the resistance of PC overlay of cracks propagation. Therefore, incorporating MWCNTs in PC overlays is believed to improve overlay fatigue resistance which is a fundamental requirement for PC overlays.

SEM images showed the MWCNTs bridging the microcracks which allow PC to continue carrying loads. Moreover, FTIR peaks proved the reaction between functionalized carboxyl group (COOH) of MWCNTs and epoxy resin. TGA and DSC analysis showed that adding MWCNTs made the nanocomposite more thermal stable with a significantly higher maximum decomposition temperature compared with neat epoxy. As a result, microstructural and thermal characterization of epoxy-MWCNTs nanocomposite emphasized our hypothesis that MWCNTs had altered the microstructure of the epoxy and increased the crosslinking between the epoxy groups resulting in enhanced mechanical properties of PC and PC overlay.

Finally, it is important to explain that the inefficiency of a high dosage of MWCNTs can be attributed to the significant reduction of PC flowability at a high dosage of MWCNTs. While this effect on flowability is very minor in the case of 0.5 and 1.0%, it was obviously able to make an adverse effect at 1.5% due to a significant increase in viscosity. This might result in entrapping air that reduces the mechanical properties of the material.

5.3 Recommended future research

Further microstructural investigations might be performed in order to have further explanation for the chemical reaction between the MWCNTs and steel surface resulting in increasing the bond strength between PC overlays and steel. This might include Transmission Electron Microscope (TEM) and X-ray Photoelectron Spectroscopy (XPS) investigations. Moreover, further research shall be performed to obtain the optimum MWCNTs percentage in order to enhance most of the mechanical properties of PC. Furthermore, other types of nanomaterials like graphene might prove to be valuable when it is well dispersed in the PC. Finally, further testing on composite PC overlays including PC and steel plates might be necessary to prove the value of using MWCNTs.

References

AASHTO T321- 07 (2007) Determining the Fatigue Life of Compacted Hot-Mix Asphalt (HMA) Subjected to Repeated Flexural Bending.

ACI 548 committee: Polymers and Adhesives in Concrete, personal communication.

ACI 548.5R (1993) Guide for Polymer Concrete Overlays, ACI committee 548.

ACI 548.6R (1996) Polymers in Concrete—Structural Applications, State-of-the-Art Report, ACI committee 548.

ASTM C39/C39M – 12a (2012) Standard Test Methods for Compressive Strength of Cylindrical Concrete Specimens. ASTM International, PA.

ASTM C78 - 02 (2002) Standard Test Method for Flexural Strength of Concrete (Using Simple Beam with Third Point Loading). ASTM International, PA.

ASTM C109 / C109M - 08 (2008) Standard Test Method for Compressive Strength of Hydraulic Cement Mortars. ASTM International, PA.

ASTM C882/C882M – 12 (2012) Standard Test Method for Bond Strength of Epoxy-Resin Systems Used With Concrete by Slant Shear, ASTM International, PA.

ASTM C1437 - 07 (2009) Standard Test Method for Flow of Hydraulic Cement Mortar. ASTM International, PA

ASTM C1583/C1583M – 04 (2004) Standard Test Method for Tensile Strength of Concrete Surfaces and the Bond Strength or Tensile Strength of Concrete Repair and Overlay Materials by Direct Tension (Pull-off Method), ASTM International, PA.

ASTM D3418 – 12 (2012) Standard Test Method for Transition Temperatures and Enthalpies of Fusion and Crystallization of Polymers by Differential Scanning Calorimetry, ASTM International, PA.

ASTM D4475 - 02 (2008) Standard Test Method for Apparent Horizontal Shear Strength of Pultruded Reinforced Plastic Rods By the Short-Beam Method. ASTM International, PA.

ASTM E23 - 02 (2002) Standard Test Methods for Notched Bar Impact Testing of Metallic Materials. ASTM International, PA.

ASTM E1311 - 08 (2008) Standard Test Method for Compositional analysis by Thermogravimetry. ASTM International, PA.

Barbuta, M., Harja, M., and Baran, I., "Comparison of mechanical properties for polymer concrete with different types of filler." Journal of Materials in Civil Engineering, Vol. 22, 2010, pp. 696-701.

Bhutta M. A. R., Ohama Y., and Tsuruta K. “Strength properties of polymer mortar panels using methyl methacrylate solution of waste expanded polystyrene as binder”, Construction and Building Materials, Vol. 25, 2011, pp. 779–784.

Bignozzi, M.C., Saccani, A., and Sandrolini, F., “New Polymer Mortars Containing Polymeric Wastes. Part 1. Microstructure and Mechanical Properties”, Composites, Part A: Applied Science and Manufacturing, Vol.31, No.2, 2000, pp.97-106.

Bignozzi, M.C., Saccani, A., and Sandrolini, F., “New Polymer Mortars Containing Polymeric Wastes. Part 2. Dynamic Mechanical and Dielectric Behaviour”, Composites: Part A: Applied Science and Manufacturing, Vol.33, No.2, 2002, pp.205-211.

Bignozzi, M.C., Sandrolini, F., and Franzoni, E., “New Polymer Mortars Based on Unsaturated Polyester- Polyurethane Interpenetrating Polymer Networks”, Polymers in Concrete, Proceedings of the Tenth International Congress on Polymers in Concrete(CD-ROM), Department of Civil Engineering, The University of Texas at Austin ,Austin, Texas, Nov. 2001, 12p.

Chmielewska, B., Czarnecki, L., Sustersic, J., and Zajc, A., “The Influence of Silane Coupling Agents on the Polymer Mortar”, Cement & Concrete Composites, Vol.28, No.9, 2006, pp.803-810.

Choi, N.W., and Ohama, Y., “Development and Testing of Polystyrene Mortars Using Waste EPS Solution- Based Binders”, Construction and Building Materials, Vol.18, No.4, 2004, pp. 235-241.

Czarnecki, L., and Chmielewska, B., “The Influence of Coupling Agent on the Properties of Vinylester Mortar”, Proceedings of the Second International RILEM Symposium on Adhesion between Polymers and Concrete, RILEM, Cachan, France, Sept. 1999, pp.57-65.

Chung, K. H., and Hong, Y. K., "Weathering properties of elastic rubber concrete comprising waste tire solution." Polymer Engineering and Science, Vol. 49, 2009, pp. 794-798.

Dos Reis, J. M. L., "Effect of textile waste on the mechanical properties of polymer concrete." Materials Research, Vol.12, No.1, 2009, pp. 63-67.

Dowling N. E., “Mechanical behavior of materials: Engineering methods for deformation, fracture, and fatigue”, Third edition, 2007.

Ganguli S., Bhuyan M., Allie L., Aglan H., “Effect of multi-walled carbon nanotubes reinforcement on the fracture behavior of tetrafunctional epoxy”. J Mater Sci, Vol. 40, No.13, 2005, pp.3593-3595.

Gorninski, J. P., Dal Molin, D. C., and Kazmierczak, C.S., "Comparative assessment of isophtalic and orthophtalic polyester polymer concrete: Different costs, similar mechanical properties and durability." Construction and Building Materials, Vol. 21, 2007, pp. 546-555.

Ha S.K., Lee H.K., and Kang I.S., “Shear behavior and performance of rc beams with polymer mortar systems under cyclic loading.”, Journal of Reinforced Plastics and Composites, Vol. 29, No. 17, 2010, pp. 2604-2620.

Haidar, M., Ghorbel, E., Toutanji, H., "Optimization of the formulation of micro-polymer concretes." Construction and Building Materials, Vol. 25, 2011, pp. 1632-1644.

Jiang, X., Drzal, L. T., “Improving electrical conductivity and mechanical properties of high density polyethylene through incorporation of paraffin wax coated exfoliated grapheme nanoplatelets and multi-wall carbon nano-tubes”, Composites: Part A, Vol. 42, 2011, pp. 1840–1849.

Jo, B. W., Park, S. K., Kim, D. K., “Mechanical properties of nano-MMT reinforced polymer composite and polymer concrete”, Construction and Building Materials, Vol. 22, No. 1, 2008, pp. 14-20.

Jo, B.-W., Park S.K, Park J.C., "Mechanical properties of polymer concrete made with recycled PET and recycled concrete aggregates." Construction and Building Materials, Vol. 22, 2008, pp. 2281-2291.

Jo, B.-W., Tae, G.-H., Kim, C.-H., "Uniaxial creep behavior and prediction of recycled-PET polymer concrete." Construction and Building Materials, Vol. 21, 2007, pp. 1552-1559.

Joint Surface Preparation Standard, NACE No. 1/SSPC-SP 5: White Metal Blast Cleaning, October 1994.

Kaeding A.O. and Prusinki R., “Curtain Wall Panels”, ACI Special Publication, Vol. 214, 2003, pp. 151-168.

Li, W. and Xu, J., "Mechanical properties of basalt fiber reinforced geopolymeric concrete under impact loading." Materials Science and Engineering , Vol. 505, 2009, pp. 178-186.

Liu J., and Vipulanandan C., “Evaluating a Polymer Concrete Coating for Protecting Non-Metallic Underground Facilities from Sulfuric Acid Attack”, Tunneling and Underground Space Technology, Vol.16, No.4, 2001, pp.311-321.

Lopez-Anido R., Gangarao H.V.S., Pauer R.J., and Vedam V.R., "Evaluation of Polymer Concrete Overlay for FRP Composite Bridge Deck", Proceedings of the Marketing / Technical / Regulatory Sessions of the Composites Institute's International Composites EXPO '98, , Composites Institute, New York, Jan. 1998, pp.Session 13-F/1-6.

Mahdi, F., Abbas, H., Khan, A. A., "Strength characteristics of polymer mortar and concrete using different compositions of resins derived from post-consumer PET bottles." Construction and Building Materials, Vol. 44, 2013, pp. 798-811.

Maksimov, R.D., Jirgens, L.A., Plume, E..Z., and Jansons, J.O., "Water Resistance of Polyester Polymer concrete", Mechanics of Composite Materials, Vol.39, No.2, 2003, pp.99-110.

Martens R.D., and Siegel M.C., "New Low-Smoke, Low-Styrene, MMA-Free Flame-Retardant Polyester Resin Systems for Mass Transit Applications", Proceedings of the Marketing / Technical / Regulatory Sessions of the Composites Institute's International Composites EXPO '98, Composites Institute, New York, Jan. 1998,, pp.Session 14-D/1-5.

Martinez-Barrera, G., and, Brostow, W. (2010). "Effect of marble particle size and gamma irradiation on mechanical properties of polymer concrete.", E-Polymers, 2010.

Melo, V. S., Calixto, J. M. F., Ladeira, L. O., and Silva, A. P., "Macro- and Micro-Characterization of Mortars Produced with Carbon Nanotubes", ACI Materials Journal, Vol. 108, No. 3, 2011.

Mohamed, A.-M. O. and M. E. Gamal (2009). "Hydro-mechanical behavior of a newly developed sulfur polymer concrete." Cement and Concrete Composites, Vol.31, pp. 186-194.

Novoa, P.J.R.O., Ribeiro, M.C.S., Ferreira, A.J.M., and Marques, A.T., "Mechanical Characterization of Lightweight Polymer Mortar Modified with Cork Granulates", Composites Science and Technology, Vol.64, No.13-14, 2004, pp.2197-2205.

Ono S., Kawakami M., and Tokushige H., "Application of Concrete-Polymer Composites to Seismic Retrofit of Concrete Structures in Japan", ibid., 18p.

Orak, S., "Investigation of Vibration Damping on Polymer Concrete with Polyester Resin", Cement and Concrete Research, Vol.30, No.2, 2000, pp.171-174.

Oyawa W.O., "Steel encased polymer concrete under axial compressive loading: Analytical formulations", Construction and Building Materials, Vol. 21, 2007, pp. 57-65.

Oyawa W.O., Sugiura K., and Eiichi Watanabe E., “Polymer concrete-filled steel tubes under axial compression”, Construction and Building Materials, Vol. 15, 2001, pp. 187-197.

Park S. K., Jo B. W., Park D. H., and Chun B. S.. “Flexural rigidity and ductility of high-strength reinforced polyester polymer concrete beams”, Advances in Cement Research, Vol. 22, No. 2, 2010, pp. 91 –97.

Polymers Concrete-Structural applications-State of the art, ACI Committee 548, ACI 548.6R-96, January 1, 1996.

Prusinski R. C., “Study of Commercial Development in Precast Polymer Concrete”, ACI Special Publication, Vol. 58, 1978, pp. 75-102.

Rai, U.S., and Singh, R.K., “Synthesis and Mechanical Characterization of Polymer-Matrix Composites Containing Calcium Carbonate/White Cement Filler”, Materials Letters, Vol.58, No.1-2, 2004, pp.235- 240.

Rajamane N.P., Ramachandramurthy D.S., and Ravi S., “Application of Ferrocement and Polymeric Materials for Repair of Corrosion Damaged Hyperboloid Overhead Water Tank Structure”, Journal of Ferrocement, Vol.33, No.1, 2003, pp.43-54.

Rebeiz K.S., and Fowler D.W., “Flexure for reinforced polymer concrete using recycled PET”, Proceedings of the Materials Engineering Conference, Vol. 2, 1996, pp. 1037-1044, Materials for the New Millennium.

Rebeiz, K. S., and Fowler, D. W., “Shear and Flexure Behavior of Reinforced Polymer Concrete Made with Recycled Plastic Wastes”, ACI Materials Journal, special publication, Vol. 166, 1996, pp. 61-78.

Rebeiz, K.S., Serhal, S.P., and Craft, A.P., “Properties of Polymer Concrete Using Fly Ash”, ASCE-Journal of Materials in Civil Engineering, Vol.16, No.1, 2004, pp.15-19.

Reda Taha, M.M., Abdel-Wahab, M.M., and El-Dieb, A.S., “Rubber Concrete: A New Addtion to Polymer Concrete”, Proceedings of the Third International Conference on Construction Materials: Performance, Innovations and Structural Implications and Mindess Symposium (CD-ROM), the University of British Colombia, Vancouver, Canada, Aug. 2005, 11p.

Reda Taha, M.M., Kandil, U., and Soliman, E., “Generation of Polymer Concrete Incorporating Carbon Nanotubes”, Patent Filed, May 2011.

Reis, J. M. L., "Mechanical characterization of polymer mortars exposed to degradation solutions." Construction and Building Materials, Vol. 23, 2009, pp. 3328-3331.

Reis, J.M.L., and Ferreira, A.J.M., “Fracture Behavior of Glass Fiber Reinforced Polymer Concrete”, Polymer Testing, Vol.22, No.2, 2003, pp.149-153.

Reis, J.M.L., and Ferreira, A.J.M., “Assessment of Fracture Properties of Epoxy Polymer Concrete Reinforced with Short Carbon and Glass Fibers”, Construction and Building Materials, Vol.18, No.7, 2004, pp.523-528.

Ribeiro, M.C.S., Novoa, P.R., Ferreia, A.J.M., and Marques A.T., “Flexural Performance of Polyester and Epoxy Polymer Mortars under Severe Thermal Conditions”, Cement & Concrete Composites, Vol.26, No.7, 2004, pp.803-809.

Ribeiro, M.C.S., Reis, J.M.L., Ferreira, A.J.M., and Marques, A.T., “Thermal Expansion of Epoxy and Polyester Polymer Mortars－Plain Mortars and Fibre-Reinforced Mortars”, Polymer Testing, V.22, No.8, 2003, pp.849-857.

San José, J.T., and Ramirez Ortiz, J.L., “A Study of Mechanical Properties of Polyester Concrete”, Proceedings of the International Conference on Infrastructure Regeneration and Rehabilitation Improving the Quality of Life through Better Construction, A Vision for the Next Millennium, Sheffield Academic Press, Sheffield, June-July 1999, pp.477- 486.

San-Jose, J. T., Vegas, I. J., Frias, M., "Mechanical expectations of a high performance concrete based on a polymer binder and reinforced with non-metallic rebars." Construction and Building Materials, Vol. 22, 2008, pp. 2031-2041.

Sharmaa, R., and Iqbal, Z., “In situ observations of carbon nanotube formation using environmental transmission electron microscopy”, Applied Physics Letters, Vol. 84, No. 6, 2004.

Shokrieh, M. M., Kefayati, A. R., Chitsazzadeh, M., “Fabrication and mechanical properties of clay/epoxy nanocomposite and its polymer concrete”, Materials and Design, Vol. 40, 2012, pp. 443–452.

Snow R.K., “Encapsulation: Protecting Concrete Piles in Marine Environments”, Concrete International, Vol.21, No.12, 1999, pp.33-38.

Soh, Y.S., Jo, Y.K., Kim, W.K., and Choi, N.W., “Curing Shrinkage and Strength Properties of Unsaturated Polymer Mortar Added Polystyrene Resin”, Proceedings of the Sixth Japan International SAMPE Symposium, A New Perspective in Advancement of Materials -Key to the 21st Century-, Society for the Advancement of Material and Process Engineering (SAMPE), Japan Chapter of SAMPE, Business Center for Academic Society, Japan, Tokyo, Oct. 1999, pp.819-824.

Soliman, E., “New generation fiber reinforced polymer composites incorporating carbon nanotubes”, Doctor of Philosophy, University of New Mexico, 2011.

Soliman, E., Al-Haik, M., Reda Taha, M.M. “On and off-axis tension behavior of fiber reinforced polymer (FRP) composites incorporating multi-walled carbon nanotubes”, Journal of Composite Materials, Vol. 46, No. 14, 2012, pp. 1661–1675.

Soliman, E., Sheyka, M.P., Reda Taha, M.M. “Low-velocity impact of thin woven carbon fabric composites incorporating multi-walled carbon nanotubes”, International Journal of Impact Engineering, Vol. 39, 2012, pp. 39-47.

Suh, J. D., and Lee D. G., “Design and manufacture of hybrid polymer concrete bed for high-speed CNC milling machine”, International Journal of Mechanics and Materials in Design, Vol. 4, No. 2, 2008, pp. 113-121.

Sumajouw D.M.J., Hardjito, D., Wallah S.E., and Rangan B.V., “Fly ash-based geopolymer concrete: Study of slender reinforced columns”, Journal of Materials Science, Vol. 42, No. 9, 2007, pp. 3124-3130,.

Swain, S., Sharma, R. A., Patil, S., Bhattacharya, S., Gadiyaram, S. P., and Chaudhari, L., “Effect of Allyl Modified/Silane Modified Multiwalled Carbon Nano Tubes on the Electrical Properties of Unsaturated Polyester Resin Composites”, Transactions on Electrical and Electronic Materials, Vol. 13, No. 6, 2012, pp. 267-272.

Tavares, C. M. L., Ribeiro, M. C. S., Monteiro, D., Camanho, P. P., and Ferreira, A. J. M., "Experimental investigation into the static and fatigue behavior of polymer concrete reinforced with GFRP rods." Instituto de Engenharia Mecânica e Gestão Industrial, Faculdade de Engenharia da Universidade do Porto. Composites in Construtions, Figueiras et al (2001), pp. 329-333.

Ting, J. H., Lyu, J. Y., Huang, F. Y., Li, T. L., Hsu, C. L., Liu, C. W., “Synthesis of single-wall carbon nanotubes by atmospheric thermal CVD”, 17th Biennial University/Government/Industry Micro-Nano Symposium - Proceedings, UGIM, 2008, pp. 157-160.

Tokushige, H., Kawakami, M., Kurimoto, Y., Yamauchi, H., and Sasaki, T., "Porous Polymer Concrete Using Polyurethane Resin and Chipped Aggregates Made of Wood Wastes", Proceedings of the International RILEM Symposium on Environment-Conscious Materials and Systems for Sustainable Development , RILEM Publications, Bagneux, France, 2005, pp.321-328.

Van Gemert D., Herroelen B., Schueremans L., and Dereymaeker J., "Strengthening of Wooden Structural Elements by Means of Polymer Concrete", Polymers in Concrete, Proceedings of the 9th International Congress on Polymers in Concrete, Casma, Bologna, September 1998, pp.577-588.

Wahby W. S. and Prusinki R., "Precast Polymer Concrete Building Panels: Case Studies with Longevity Experience", Collaboration and Harmonization in Creative Systems, 2005, pp. 265-267.

Wang B., Chen R., Zhang T., and Jiang X., "The Application of Polymer Concrete in the Airfield Rapid Repair", Proceedings of the International Conference on Advances in Concrete and Structures(ICACS 2003) , RILEM Publications, Bagneux, France, 2003, pp.691-695.

Wheat, D. L., Fowler, D. W., Al-Negheimish, A. I., "Thermal and fatigue behavior of polymer concrete overlaid beams", Journal of Materials in Civil Engineering, Vol. 5, No. 4, 1993, pp. 460-477.

Zhao L., Karbhari V.M., Hegemier G.A. and Seible F., "Connection of Concrete Barrier Rails to FRP Bridge Decks", Composites Part B, Vol.35, No.4, 2004, pp.269-278.

Zhou, D., and Chow, L., "Complex structure of carbon nanotubes and their implications for formation mechanism", Journal of Applied Physics, Vol. 93, No. 12, 2003, pp. 9972-9976.